CORRECTION OF PHASE DISTORTION BY NONLINEAR OPTICAL TECHNIQUES

Hughes Research Laboratories
3011 Malibu Canyon Road
Malibu, CA 90265

March 1979

Contract N00014–77–C–0593
Interim Technical Report
For period 15 July 1977 through 30 September 1978
DARPA Order No. 3427

Sponsored by
DEFENSE ADVANCED RESEARCH PROJECTS AGENCY
1400 Wilson Boulevard
Arlington, VA 22209

OFFICE OF NAVAL RESEARCH
Boston, MA 02210

DARPA Order No.	3427
Effective Date of Contract	15 July 1977
Contract Expiration Date	31 May 1980
Name and Phone Number of Principal Scientist	R.C. Lind (213) 456-6411, ext. 222
Name and Phone Number of Program Manager	C.R. Giuliano (213) 456-6411, ext. 437
Contract Period Covered by this Report	15 July 1977 through 30 September 1978

UNCLASSIFIED

SECURITY CLASSIFICATION OF THIS PAGE (When Data Entered)

REPORT DOCUMENTATION PAGE

READ INSTRUCTIONS BEFORE COMPLETING FORM

1. REPORT NUMBER

2. GOVT ACCESSION NO.

3. RECIPIENT'S CATALOG NUMBER

4. TITLE (and Subtitle)
CORRECTION OF PHASE DISTORTION BY NONLINEAR OPTICAL TECHNIQUES.

5. TYPE OF REPORT & PERIOD COVERED
Interim Technical Report.
15 July 1977 - 30 Sept 1978.

6. PERFORMING ORG. REPORT NUMBER

7. AUTHOR(s)
C.R. Giuliano, R.W. Hellwarth, R.K. Jain, R.C. Lind, T.R. O'Meara, S.M. Wandzura, and V. Wang

8. CONTRACT OR GRANT NUMBER(s)
N00014-77-C-0593,
ARPA Order-3427

9. PERFORMING ORGANIZATION NAME AND ADDRESS
Hughes Research Laboratories
3011 Malibu Canyon Road
Malibu, CA 90265

10. PROGRAM ELEMENT, PROJECT, TASK AREA & WORK UNIT NUMBERS
DARPA Order No. 3427
Program Code No. NR 395-578

11. CONTROLLING OFFICE NAME AND ADDRESS
Defense Advanced Research Projects Agency
1400 Wilson Blvd.
Arlington, VA 22209

12. REPORT DATE
March 1979

13. NUMBER OF PAGES

14. MONITORING AGENCY NAME & ADDRESS (if different from Controlling Office)
Office of Naval Research
Boston, MA 02210

15. SECURITY CLASS. (of this report)
UNCLASSIFIED

15a. DECLASSIFICATION DOWNGRADING SCHEDULE

16. DISTRIBUTION STATEMENT (of this Report)
Approved for public release; distribution unlimited

135 p.

17. DISTRIBUTION STATEMENT (of the abstract entered in Block 20, if different from Report)

18. SUPPLEMENTARY NOTES

19. KEY WORDS (Continue on reverse side if necessary and identify by block number)
Nonlinear phase conjugation, Adaptive optics, Laser compensation, SBS, Four-wave mixing.

20. ABSTRACT (Continue on reverse side if necessary and identify by block number) NEXT PAGE

This report covers the first phase of a continuing program designed to explore a recently recognized property of certain nonlinear optical interactions of generating conjugate wavefronts that can be used to correct optical distortions in laser systems. These distortions include optical train aberrations, laser medium distortions, and atmospheric propagation aberrations. The program was divided into three basic areas that bridge the gap between a preliminary exploration of the

DD FORM 1 JAN 73 1473 EDITION OF 1 NOV 65 IS OBSOLETE

UNCLASSIFIED

SECURITY CLASSIFICATION OF THIS PAGE (When Data Entered)

applicable nonlinear processes and realization of their potential usefulness to laser systems. The areas were (1) to measure quantitatively the properties of phase conjugation from stimulated Brillouin scattering (SBS) at 0.69 μm, (2) to develop a theoretical understanding of nonlinear phase conjugation, and (3) to determine the applicability of nonlinear phase conjugation to various systems of interest to DARPA. We made significant advances in each of these areas during this program; these accomplishments are described in this report.

The main accomplishments of the first phase of the program are listed below:

- Demonstrated complete aberration correction by SBS for beams aberrated to 35X the diffraction limit.
- Performed detailed photographic measurements to establish spatial distribution of beam profiles to intensities down to $\sim 10^{-4}$ of peak intensity.
- Established experimentally that the fraction of nonconjugate return when using SBS for correction is below measurement limits.
- Developed systems applications exploiting novel variations of nonlinear phase conjugation techniques in the area of high-power oscillator compensation, master-oscillator power-amplifier train compensation, and systems which require correction for atmospheric turbulence with very high spatial frequency content.
- Furthered the theoretical understanding of phase conjugation by SBS in waveguides and in nonwaveguide (free space) geometries.

TABLE OF CONTENTS

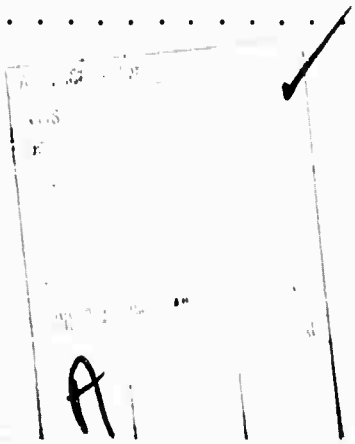

Section Page

APPENDICES

LIST OF ILLUSTRATIONS

FOREWORD

This interim technical report was prepared by Hughes Research Laboratories under Contract No. N00014-77-C-0593. It describes work performed during the 14-month period from 15 July 1977 to 30 September 1978. The program manager is C.R. Giuliano. The principal investigator is R.C. Lind, who assumed this role early in the program from V. Wang. Principal contributors to the program are T.R. O'Meara, who has been primarily involved in the systems aspects of nonlinear phase conjugation, R.K. Jain, who contributed to the acquisition and analysis of detailed experimental data; and R.W. Hellwarth, a consultant on the program; and S.M. Wandzura, both of whom made key contributions to the theoretical understanding of nonlinear phase conjugation. In addition to R.W. Hellwarth, A. Yariv also served as a consultant on this program.

The authors wish to acknowledge technical criticism and advisory support by R.L. Abrams, manager of the Optical Physics Department, and to thank T.E. Horne, who assisted in the many detailed experiments performed on this program. We also wish to thank M.B. White of ONR, the technical monitor, and Col. M. O'Neill of DARPA for their interest in this work.

SECTION 1

INTRODUCTION

This report covers the first phase of a continuing program designed to explore a recently recognized property of certain nonlinear optical interactions of generating conjugate wavefronts that can be used to correct optical distortions in laser systems. These distortions include optical train aberrations, laser medium distortions, and atmospheric propagation aberrations. The program was divided into three basic areas that bridge the gap between a preliminary exploration of the applicable nonlinear processes and realization of their potential usefulness to laser systems. The areas were (1) to measure quantitatively the properties of phase conjugation from stimulated Brillouin scattering (SBS) at 0.69 μm, (2) to develop a theoretical understanding of nonlinear phase conjugation, and (3) to determine the applicability of nonlinear phase conjugation to various systems of interest to DARPA. We made significant advances in each of these areas during this program; these accomplishments are described in this report.

A. BASIC CONCEPT

Nonlinear optical phase conjugation represents a new class of optical interactions having the potential for providing novel solutions to problems in fields such as adaptive optics for high-energy lasers (HELs), fusion laser systems, imaging systems, and laser communication systems. Traditionally, nonlinear optical interactions have been exploited to yield sum and difference frequency generation, parametric amplification and oscillation, stimulated scattering, nonlinear spectroscopy, etc. In the present context, the desired output wave from a nonlinear medium possesses the unique property of being the spatial complex conjugate, or phase conjugate, of the input wave.

To introduce the concept of phase conjugation by nonlinear optical techniques, consider the existing adaptive-optics techniques for reducing the effects of atmospheric turbulence and optical train distortions on laser beams (coherent optical adaptive techniques, COAT, for example). COAT systems adjust the phasefront of the transmitted beam to compensate for the phase distortion introduced by the optical medium. These systems sense the distortion by monitoring backscatter from the target and form a phase front that is a phase conjugate of the distortion to be corrected. The correction is accomplished by using some form of discrete, multichannel, phase-front corrector such as a deformable mirror driven by electronic servos. In contrast, the method of nonlinear optical phase conjugation directly generates the spatial phase conjugate of a distorted wavefront. This phase conjugate can be transmitted through the original distorting optical path to form a corrected beam. The nonlinear interactions automatically perform a real-time phase-front correction with high spatial frequency capability over the entire cross section of the beam without any external wavefront sensing or electronic controls.

The basic system concept of nonlinear phase conjugation for laser beam correction through the atmosphere is shown schematically in Figure 1. The process involves the following steps:

- The first transmitted pulse propagates to the target (assumed for this example to be a single unresolved glint). The purpose of this first pulse is to illuminate the glint target, which then serves as a test source at the wavelength of interest.

- The light reflected from the glint propagates through the distorting medium towards the transceiver, arriving as an aberrated wavefront.

- The phase conjugate of this distorted return wave is generated by a nonlinear optical conjugator.

- After coherent amplification to a desired power level, the phase-corrected pulse retraverses the distorting atmosphere, which now restores its phase coherence so that the entire beam is focused.

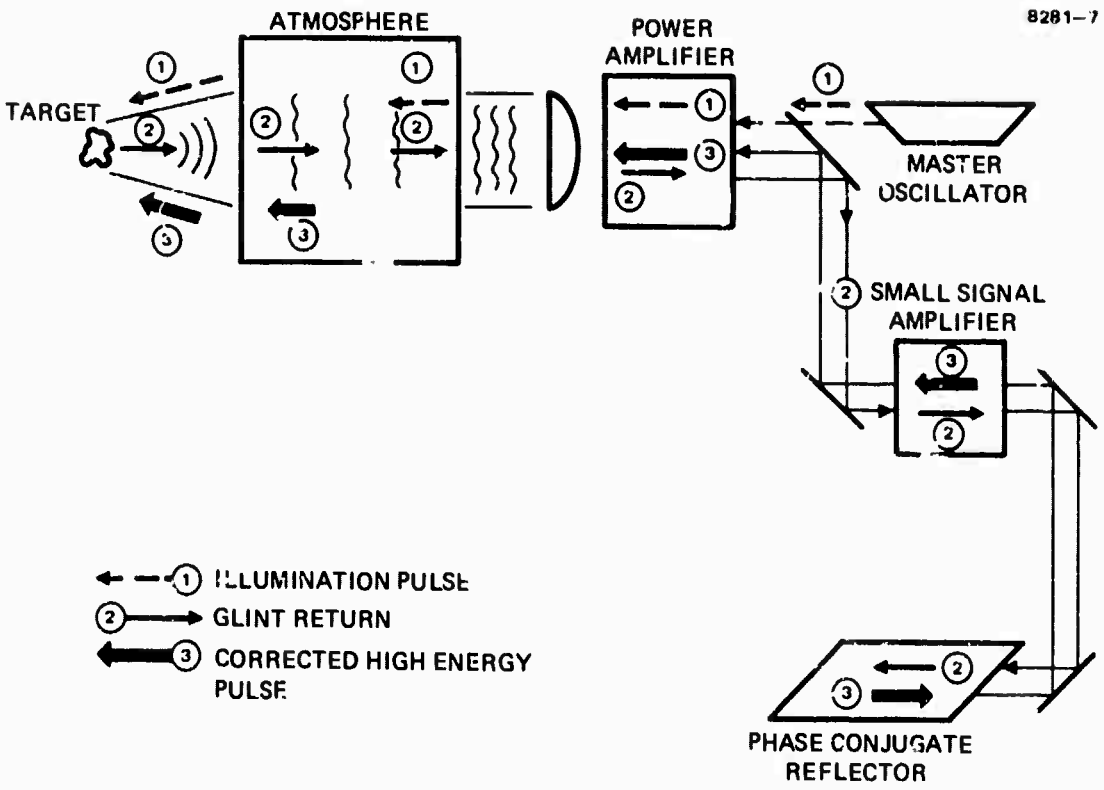

Figure 1. Basic phase-conjugation scenario.

The first demonstration of the removal of aberrations in an optical train by nonlinear phase conjugation was reported by Zel'dovich et al. (JETP Lett. Vol. 15, pp. 109-113, 1972) and Nosach et al. (JETP Lett., Vol. 16, pp. 435-438, 1972). In those experiments, the nonlinear interaction used was SBS in CS_2. In that case, the Brillouin-backscattered wave is the complex conjugate of the input signal. Recently, these experiments have been verified and o[illegible]ified at HRL (see Appendix A). This initial work led to the program described in this interim report.

B. SUMMARY OF PRINCIPAL ACCOMPLISHMENTS

The main accomplishments of the first phase of the program are listed below:

- Demonstrated complete aberration correction by SBS for beams aberrated to 35X the diffracti n l'ait.
- Performed detailed photographic measurements to establish spatial distribution of beam profiles to intensities down to $\sim 10^{-4}$ of peak intensity.
- Established experimentally that the fraction of nonconjugate return when using SBS for correction is below measurement limits.
- Developed systems applications exploiting novel variations of nonlinear phase conjugation techniques in the area of high-power oscillator compensation, master-oscillator power-amplifier train compensation, and for systems which require correction for atmospheric turbulence with very high spatial frequency content.
- Furthered the theoretical understanding of phase conjugation by SBS in waveguides and in nonwaveguide (free-space) geometries.

This report is divided into four sections followed by five appendices. Section 2 describes the experimental program on SBS phase conjugation at 0.69 μm. Section 3 discusses theoretical considerations relevant to SBS phase conjugation and describes phase conjugation by four-wave and three-wave mixing techniques. Section 4 describes potential applic[illegible]ions using the four-wave mixing phase-conjugation scheme.

SECTION 2

EXPERIMENTAL STUDIES OF SBS-PHASE CONJUGATION AT 0.69 μm

The primary objective of these experiments was to determine the amplitude of the SBS backscattered wave and the accuracy of correction for the SBS wave as a function of parameters such as the geometry of the interaction, degree of aberration, and power above threshold. Waveguides of various lengths and "free-space," or nonwaveguided, geometries were studied. In addition, image reconstruction using phase-conjugated SBS was demonstrated. The description of these experiments is preceded by a brief discussion of phase conjugation by SBS.

A. PHASE CONJUGATION BY SBS

An understanding of the physics of the SBS process is aided by recalling that light is scattered from an acoustic wave in a manner identical to the scattering from a diffraction grating. The motion of the sound waves results in a Doppler shift of the scattered light. In SBS, a strong electric field can be produced by the passage of an intense light beam. Through electrostriction, this results in periodic changes in the density of the medium and therefore in the medium index, which generates a traveling acoustic wave which, in turn, scatters (reflects) some of the input optical beam.

Figure 2 presents a simplified view of this process. The phase-aberrated beam is represented by a wavefront with a simple step. An ordinary reflection results in the doubly aberrated wavefront shown. As a result of the SBS interaction, the aberrated pump wave creates aberrated acoustic waves, which act as a moving dielectric reflector to yield the conjugate scattered wave. If the generation of sound in SBS is viewed as a collisional process in which a photon $(\vec{k}_2,\omega_2)$ undergoes parametric decay into a phonon $(\vec{k}_s,\omega_s)$ plus a photon $(\vec{k}_1,\omega_1)$, conservation of energy and momentum directly yield (as shown in Figure 3):

$$\omega_s = \omega_2 - \omega_1 \qquad (1)$$

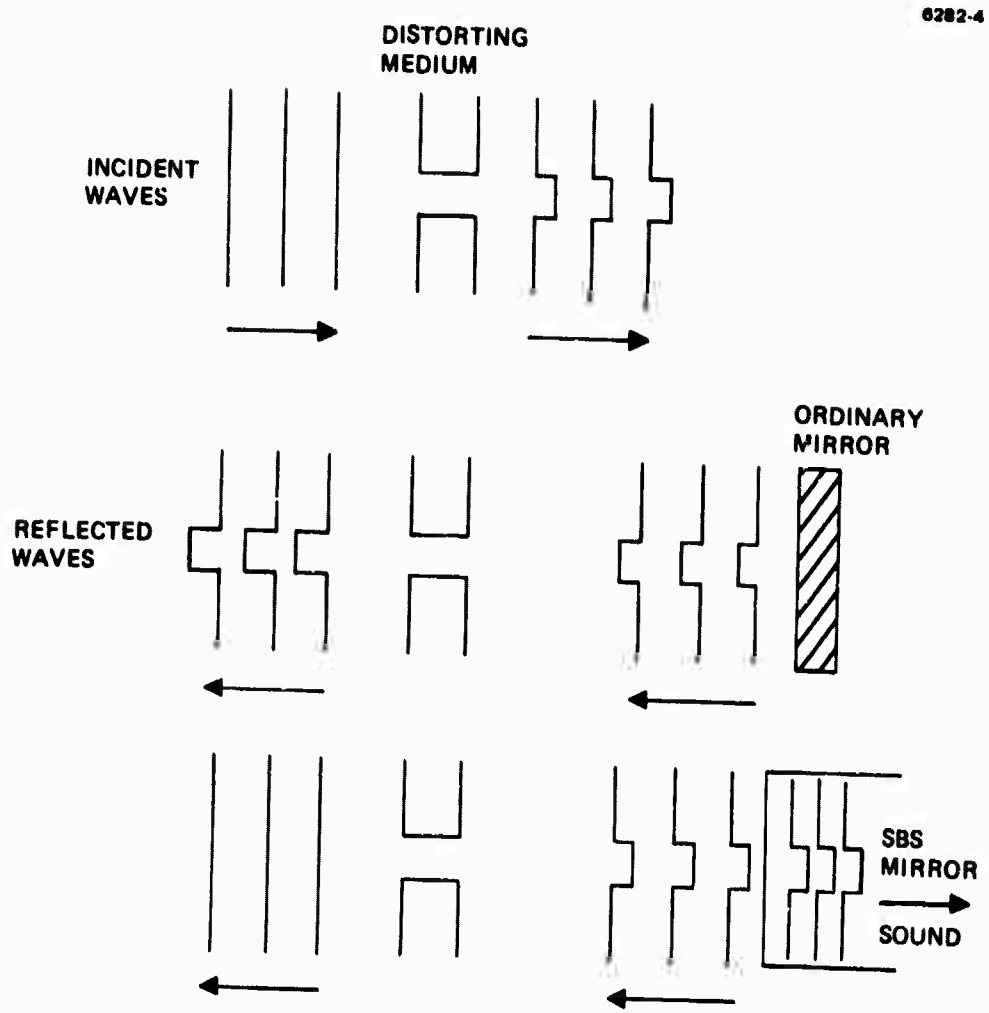

Figure 2. Simplified view of the SBS phase-conjugation process.

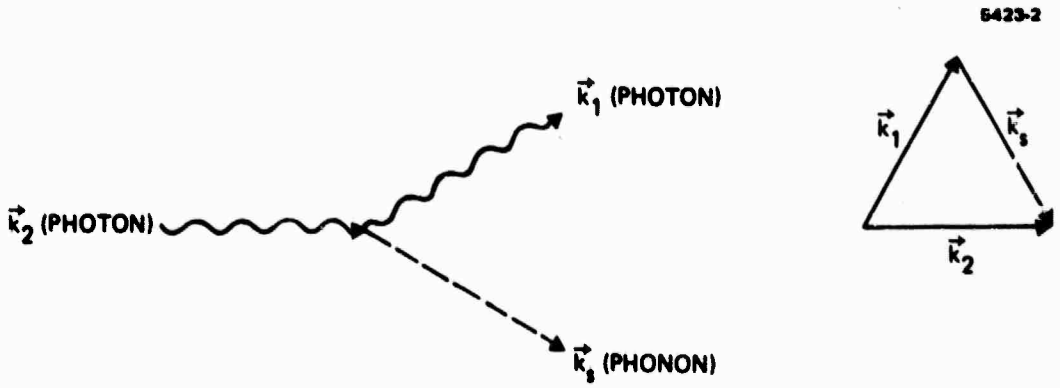

Figure 3. Generation of sound by parametric decay in SBS of light.

$$\vec{k}_s = \vec{k}_2 - \vec{k}_1 \quad . \tag{2}$$

The latter expression is known as the Bragg condition. Using Eq. 1 and $\omega_i = c_i|k_i|$, we have

$$V_s|k_s| = \left(\frac{c}{n}\right)(|k_2| - |k_1|) \ , \tag{3}$$

where n is the index of refraction (assumed to be the same for ω_1 and ω_2) and V_s is the speed of sound in the medium. Taking absolute magnitudes of Eq. 2, we have

$$|k_s|^2 = |k_2|^2 + |k_1|^2 - 2|k_1|\ |k_2| \cos\theta_{12} \quad . \tag{4}$$

For a collinear interaction θ_{12}, the angle between waves 1 and 2 is π, and $\cos\theta_{12} = -1$. Hence, we obtain

$$|k_s|^2 = |k_2|^2 + |k_1|^2 + 2|k_1|\ |k_2| = (|k_1| + |k_2|)^2 \tag{5}$$

and

$$|k_s| = |k_1| + |k_2| \quad . \tag{6}$$

By dividing Eq. 3 by Eq. 6 and rearranging, we obtain

$$\frac{|k_2| - |k_1|}{|k_2| + |k_1|} = \frac{n\,Vs}{c} \ ,$$

and, since $n\,V_s/c \ll 1$ ($\sim 10^{-5}$), it follows that $|k_2| \approx |k_1| = k$ and we obtain

$$\frac{\Delta k}{k} = \frac{\Delta\omega}{\omega} = \frac{2nV_s}{c} = \frac{\omega_{sound}}{\omega_{light}} \quad . \tag{8}$$

From the appropriate wave equations for the photons and phonons, the scattered wave (k_1,ω_1) and the acoustic wave (k_s,ω_s) can both be shown to experience gain. If the gain is greater than the loss in the medium, a growing acoustic and scattered light wave will be produced. The condition for highest gain is for collinear waves with the scattered light traveling counter propagating to the input beam. Using the condition for the gain to exceed the loss, the threshold pump intensity (I_t) is ≈ 800 MW/cm^2 for CS_2. This result is, as a first approximation, independent of the wavelength of the input photons. The frequency shift for these cases is calculated to be $\Delta\omega/\omega = 10^{-5}$, or $\sim$ 6 GHz, at 6943 Å for CS_2 and $\Delta\omega/\omega \sim 1.3 \times 10^{-4}$, or 4 GHz, at 10.6 μm for Ge.

At the high power densities necessary to reach threshold for SBS, care must be taken to avoid self-focusing. The threshold for self-focusing is dependent on total power, varies as a function of wavelength squared, and has a value of $\sim$ 20 kW for CS_2 at ruby wavelengths. These basic parameters are relevant to the experiments to be described below.

B. EXPERIMENTAL APPARATUS

A schematic of the basic experimental configuration is shown in Figure 4. A ruby oscillator/amplifier combination generates an output beam, which is focused either into a multimode waveguide of a prescribed length filled with CS_2 or into a large cell containing CS_2. The use of a waveguide results from our early experiments (see Appendix A) verifying the original results of Zeldovieh et al.[2] One of the issues addressed on this program has been to determine the effects of waveguide and nonwaveguide geometries on the phase conjugation process (see below). The SBS backward-generated wave is split off by a beam splitter and focused at the film plane with a 1-m-focal-length lens for observation. A detailed diagram of the apparatus is given in Figure 5. The ruby laser, passively Q-switched by a dye cell,

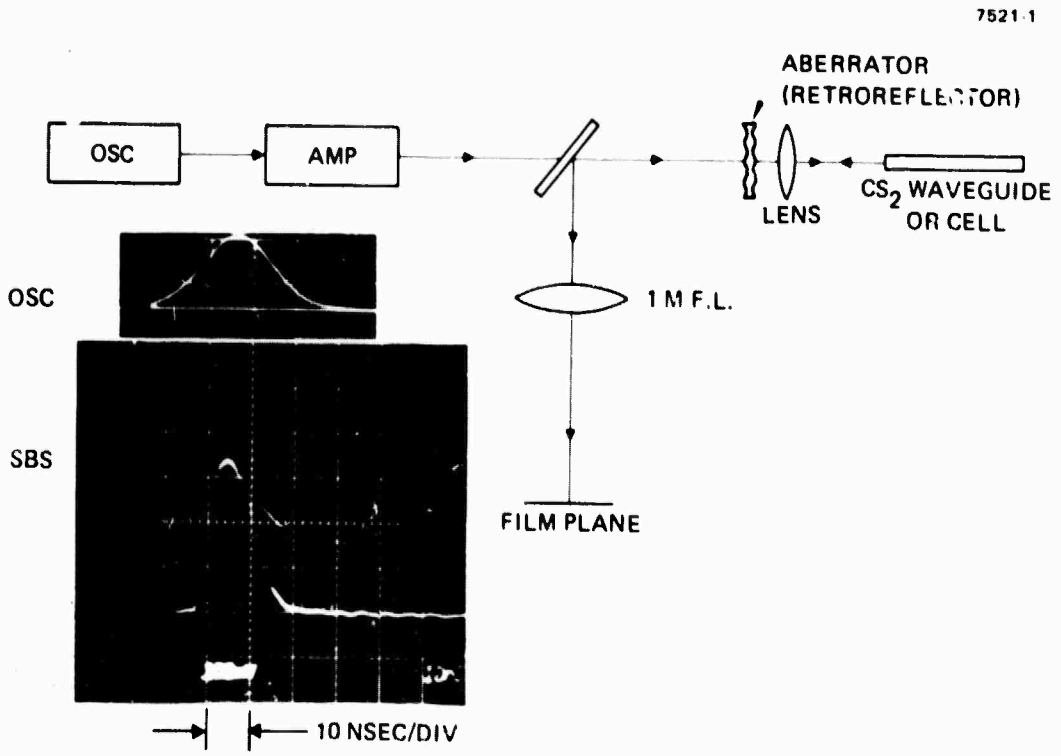

Figure 4. Experimental configuration.

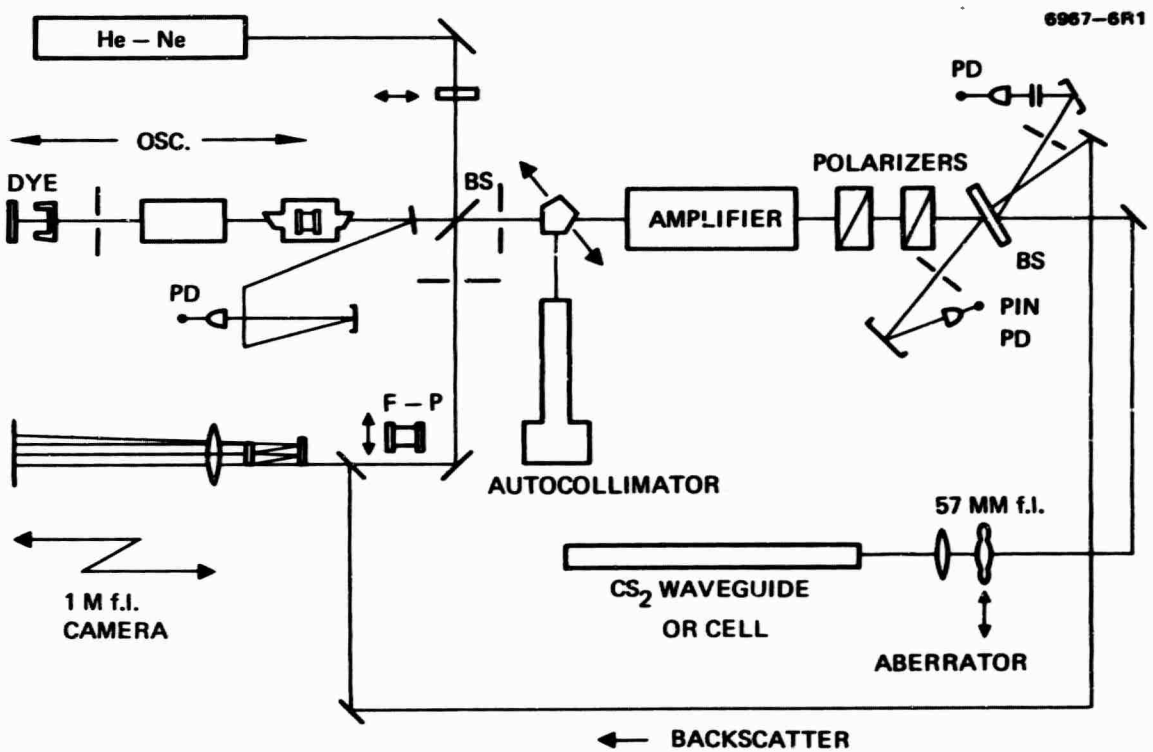

Figure 5. Detailed diagram of 0.69-μm experimental apparatus.

provides a TEM_{oo} single-longitudinal-mode output pulse of 17-nsec duration. This is amplified and controlled by an adjustable attenuator to deliver from 10 to 100 mJ to the SBS cell.

An aberration can be purposely introduced into the beam at the position shown in Figure 5 to test the corrective properties of SBS backscatter. The aberrator is a microscope slide etched in HF. The original beam quality is monitored by removing the lens-CS_2 cell combination, placing a partially reflecting mirror in that position, and reflecting a portion of the light back into the 1-m-focal-length camera through the beamsplitter. The degree of aberration introduced is then measured by placing the aberrator in front of the reference reflector, which causes the light to double-pass the aberrator. The SBS correction process is accomplished by passing the light through the amplifier and attenuator, through the aberrator shown in position in Figure 5, and into the focusing lens and CS_2 cell. For the waveguide experiments, the lens is used to focus the beam to a waist just in front of the cell entrance window, giving a divergent entrance beam. Since the index of CS_2 is higher than the glass, this diverging beam is completely internally reflected in the capillary. The waveguide SBS cell serves to increase the interaction length and percentage of light backscattered without increasing the power density to the point where laser-induced breakdown of CS_2 can occur and without increasing the total power input to the point of self-focusing. The slightly red-shifted SBS backscatter retraces the path of the original beam through the multiple bounces in the waveguide and through the aberrator, where a portion is sampled by the beamsplitter and 1-m camera. For the free-space (i.e., nonwaveguide) experiments, the waveguide is replaced by a cell filled with CS_2 (a 10-cm spectrophotometer cell is used). Various focal length lenses are used to focus the beam into this cell, taking care to avoid self-focusing.

Experiments were performed with a single aberrator (as shown) and also with two separate aberrators placed at several positions between the attenuator and the cell. The later set-up was used to simulate a distributed aberration, such as encountered in a turbulent atmosphere.

The laser pulse-shape and SBS backscattered pulse were measured on every shot using the fast photodiodes shown. In addition, the total amplified input laser energy was monitored on every shot. For measuring the SBS frequency shift beam, a Fabry-Perot etalon was used in the position shown. For these measurements, a reference beam is also provided for comparison. This was achieved by inserting a beam splitter in front of the 57-mm lens and directing the beam into the Fabry-Perot. Far-field intensity functions, or divergences of the beam, are measured at the focal point of the 1-m lens by a photographic technique using high-contrast film in a series of exposures at differing attenuations. In this way, the actual profile of the original aberrated and corrected beams can be determined independently of film linearity. Figure 6 illustrates this technique. An arbitrary beam profile is shown for various intensity levels on the film. The film threshold intensity is indicated on the figure. The procedure followed consists of exposing the film with intensity I and measuring the diameter at the film threshold D. The beam is then attenuated a known amount and the resulting smaller diameter is measured. This procedure is repeated several times (typically 10 to 15) until the intensity is reduced so that the spot is just resolvable on the film. In this manner, the entire beam profile is traced out independently of film linearity. Using this technique, we have measured the profile far out into the wings of the distribution down to intensities of $\sim 10^{-4}$ of the peak intensity (see below). Measurements were made under the following conditions: (1) laser only (the lens-waveguide combination was replaced with the 100% reflector in place), (2) SBS backscattered beam without aberrator in place, and (3) SBS backscattered beam with aberrator in place and double passed.

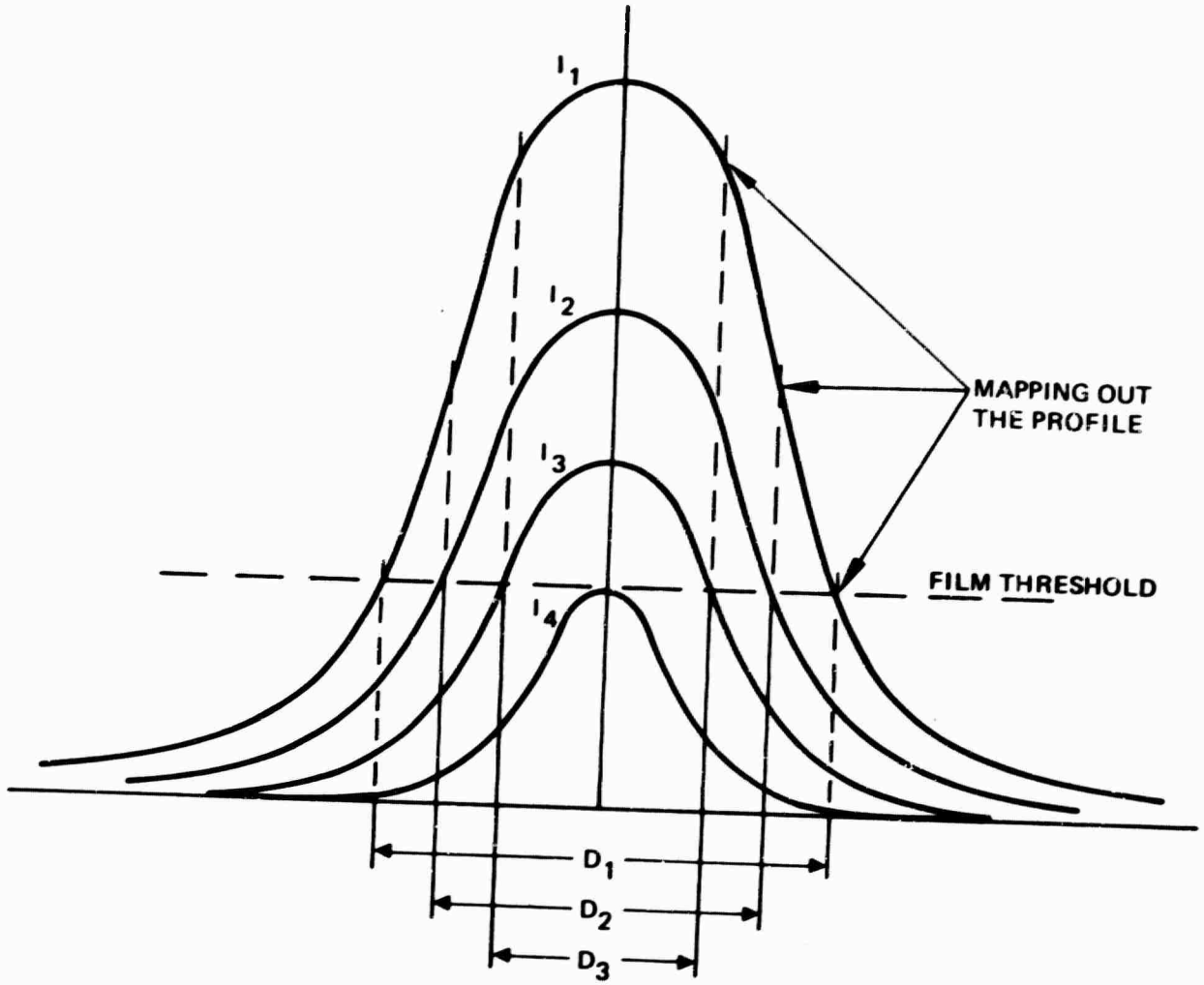

Figure 6. Determination of beam profile.

C. EXPERIMENTAL RESULTS

An example of the type of photographic data generated is shown in Figure 7. The 7(a) through 7(c) sequence is aberrator data without SBS: (a) the unaberrated beam (which is the same as the retro-reflected beam), (b) the aberrated beam passing through an aberrator labeled No. 2 (which gives a beam $\sim$ 8X diffraction limited, and (c) the aberrated beam passing through aberrators No. 2 and No. 3 (which gives a beam $\sim$ 35X diffraction limited). Figure 7(d) has the beam passing through the aberrators as before, but now the phase-conjugate SBS beam is generated, and the beam retraverses the aberrators. In this case, the spot is essentially identical with either aberrator No. 2, with both aberrators, or without an aberrator. These data imply that the SBS-corrected beam has a far-field divergence nearly equal to that of the input laser beam or a beam that is aberrated to 35X diffraction limited can be corrected.

Figure 8 gives a qualitative picture of the distortion introduced by the aberrators employed. This figure compares a photograph of a resolution chart taken through aberrator No. 3 with a photograph taken without the aberrator present. A more quantitative characterization of the aberrators used in the above experiments has also been made. The aberrators were scanned mechanically by running a stylus across the surface of each. An example of such a scan for aberrator No. 3 is shown in Figure 9. The peak-to-peak phase variation over a distance corresponding to the ruby beam diameter is typically a $\pm 2\pi$ phase shift. If the data from such scans were digitized, statistical information, rms deviations, etc. could be obtained. Also, fast Fourier transform techniques will give spatial frequency data for the aberrators. Such additional data might be useful if a detailed numerical description is required.

Using the photographic data, two methods of displaying the results can be used. First, a semi-log plot of relative intensity versus spot

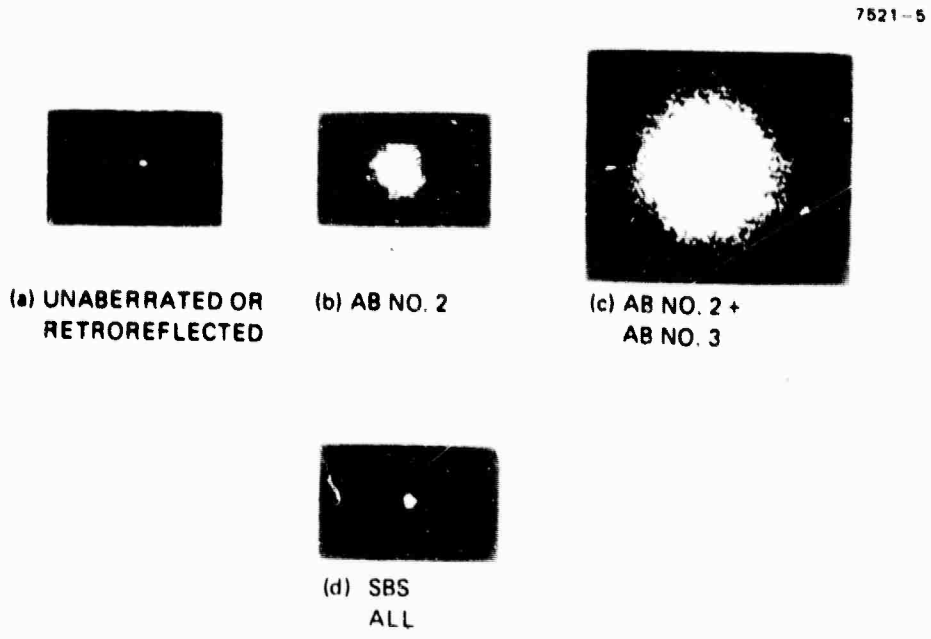

Figure 7. Photographs of aberrated, unaberrated, and SBS beams.

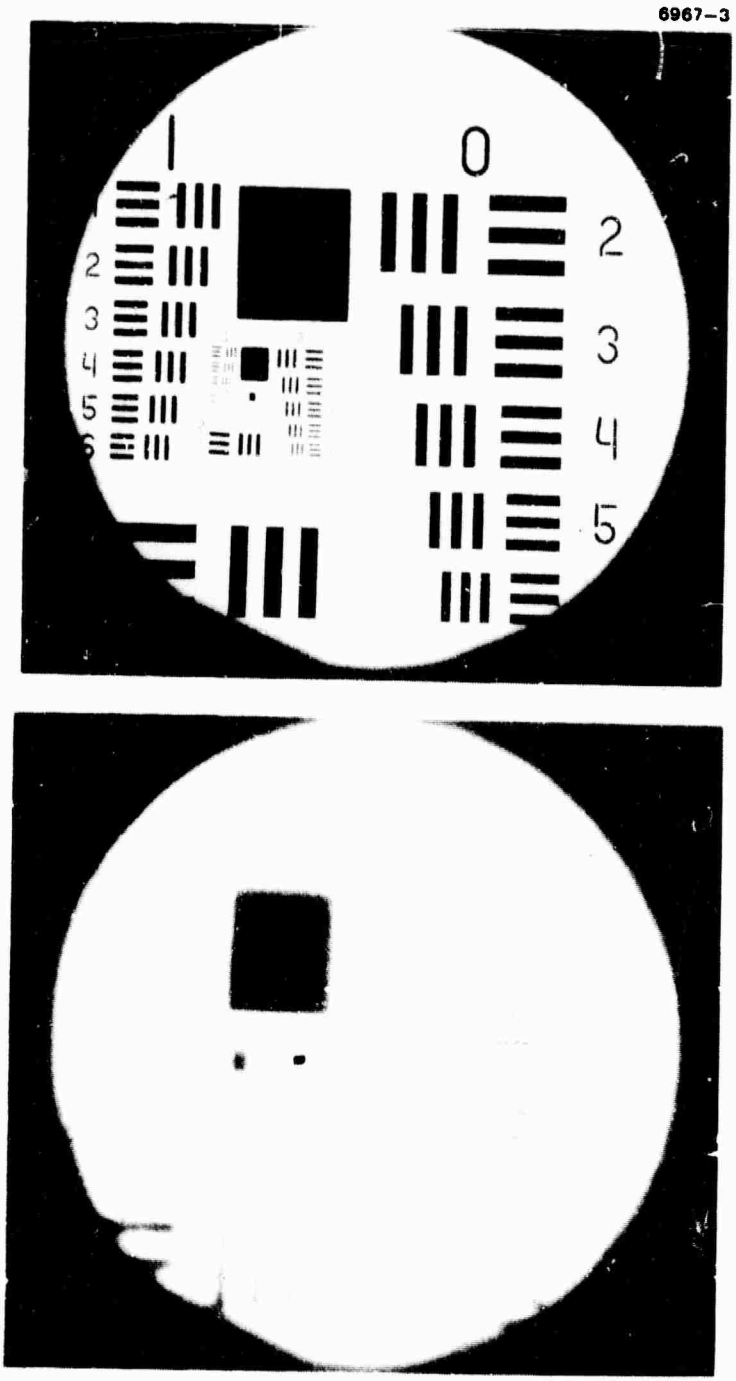

Figure 8. Degradation of resolution chart by aberrator No. 3.

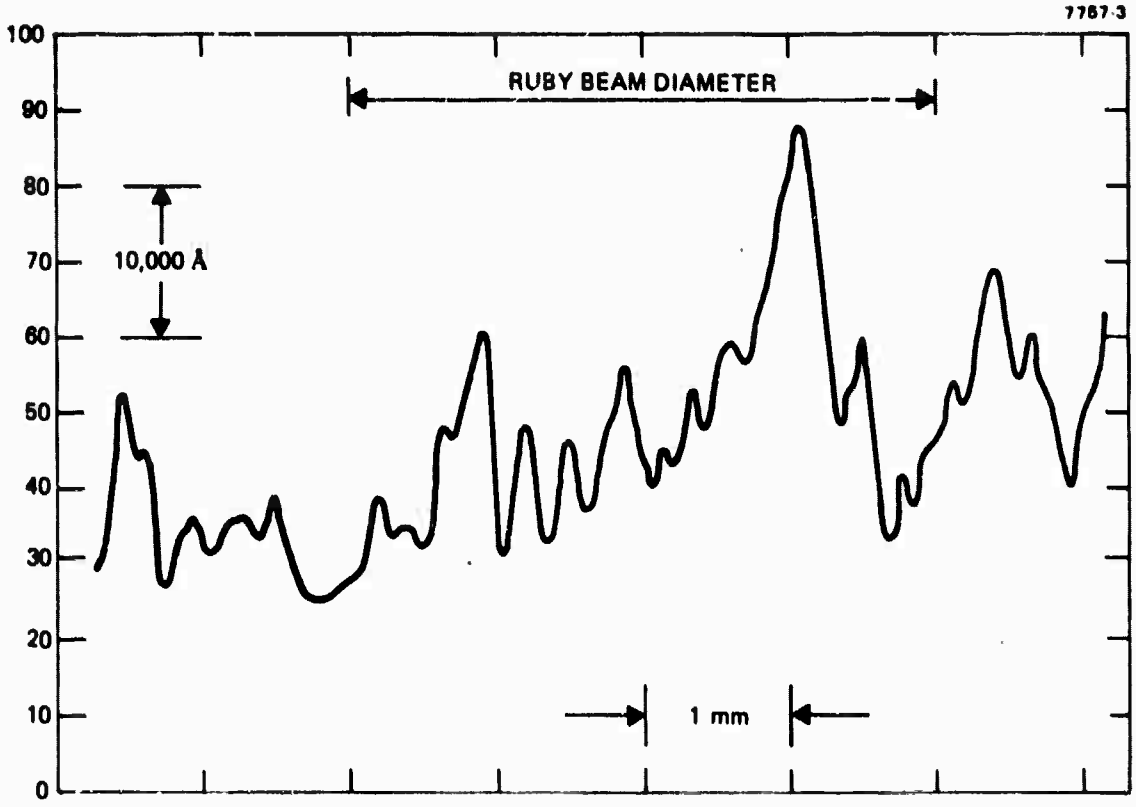

Figure 9. Scan of aberrator No. 3.

diameter squared as recorded on the film could be made. A straight-line fit will result if the beam is Gaussian with a slope proportional to the 1/e (in intensity) Gaussian beam radius. To see this, consider the following. Begin with

$$I = \frac{P_0}{\pi\delta^2} e^{-(r^2/\delta^2)} \quad , \tag{1}$$

where P_0 is the total power in the beam, and δ is the 1/e radius (in intensity) of the beam. If multiple exposures are taken, we obtain

$$\overset{\bullet}{P_{0_1}} \quad \overset{\bullet}{P_{0_2}} \quad \overset{\bullet}{P_{0_3}} \quad \overset{\bullet}{P_{0_4}} \quad \overset{\bullet}{\cdots} \quad .$$

Assume that a particular total power P_{0_1} and beam radius δ (common to all spots) give I_T (the intensity required to reach the film exposure threshold):

$$I_{T_1} = \frac{P_{0_1}}{\pi\delta^2} e^{-r_1^2/\delta^2}, \quad I_{T_2} = \frac{P_{0_2}}{\pi\delta^2} e^{-r_2^2/\delta^2} \quad , \text{ etc.} \tag{2}$$

The intensity I_{T_1}, I_{T_2} ... required to expose the film will be the same in all cases:

$$\frac{P_{0_1}}{\pi\delta^2} e^{-r_1^2/\delta^2} = \frac{P_{0_2}}{\pi\delta^2} e^{-r_2^2/\delta^2} \quad , \text{ etc.} \tag{3}$$

For each spot measured, we know P_{0_1}, P_{0_2} ... ; thus,

$$\frac{P_{0_1}}{P_{0_2}} = e^{-(r_2^2/\delta^2 - r_1^2/\delta^2)} \quad , \tag{4}$$

and we have

$$(\delta)^2 = \frac{r_1^2 - r_2^2}{\ell n \frac{\left(P_{0_1}\right)}{\left(P_{0_2}\right)}} \quad , \tag{5}$$

which is the desired result. The validity of this technique is based on the assumption that the film possesses a sharp exposure threshold and that the diameter of a given spot is equal to the beam diameter at which the intensity equals the exposure threshold. Semi-log plots of this kind are given in Figure 10. Figure 10(a) gives the aberrated beam, which is a good approximation to a Gaussian beam of about 11 times the divergence of the original beam. Similarly, Figure 10(b) plots the nearly diffraction limited SBS-corrected beam. The divergences shown are calculated from the above formula using a straight-line fit and a 1-m-focal-length lens. This type of data reduction clearly indicates that corrected beams can be achieved.

In addition to this data and all those to be shown below, many additional runs were made. These were performed using various aberrators in various combinations and locations in the beam path. In all cases, essentially perfect correction was achieved.

The analysis of these data, however, does not determine the intensity fraction of the SBS beam that is the phase conjugate of the input wave and the fraction that is not. This can only come from the detailed photographic data coupled with power-in-the-bucket measurements to be described below. To see why this is important, consider the example profiles drawn in Figure 11. Two profiles are shown: the incident beam and the SBS-corrected beam. For this example, the intensity of the SBS beam is 10% of the incident beam, a value typical of the present experiments. The dashed line corresponds to the film threshold intensity. Assume that the SBS-corrected profile follows the solid line as shown to intensities well below the film threshold. In this

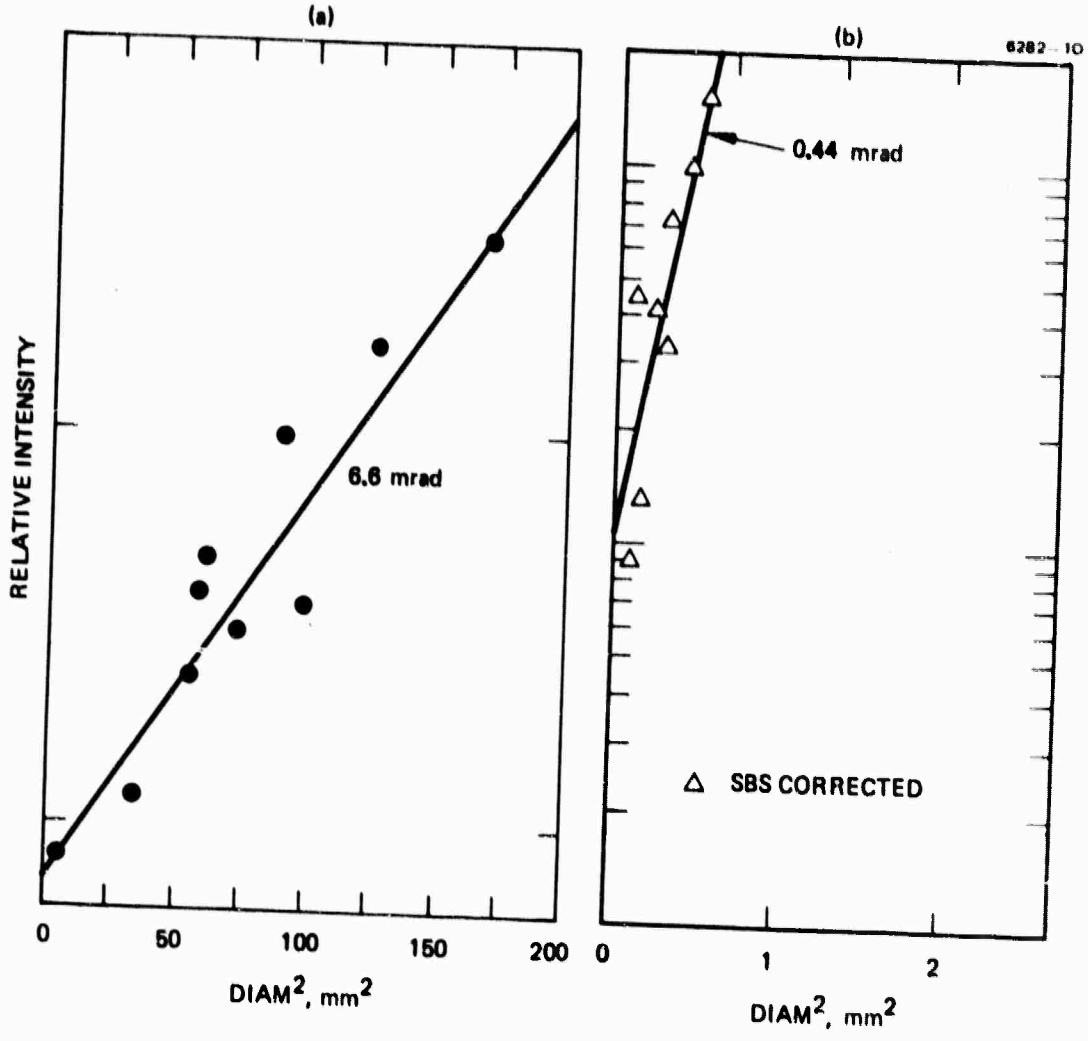

Figure 10. Semi-log plots of intensity profiles.

7621-9

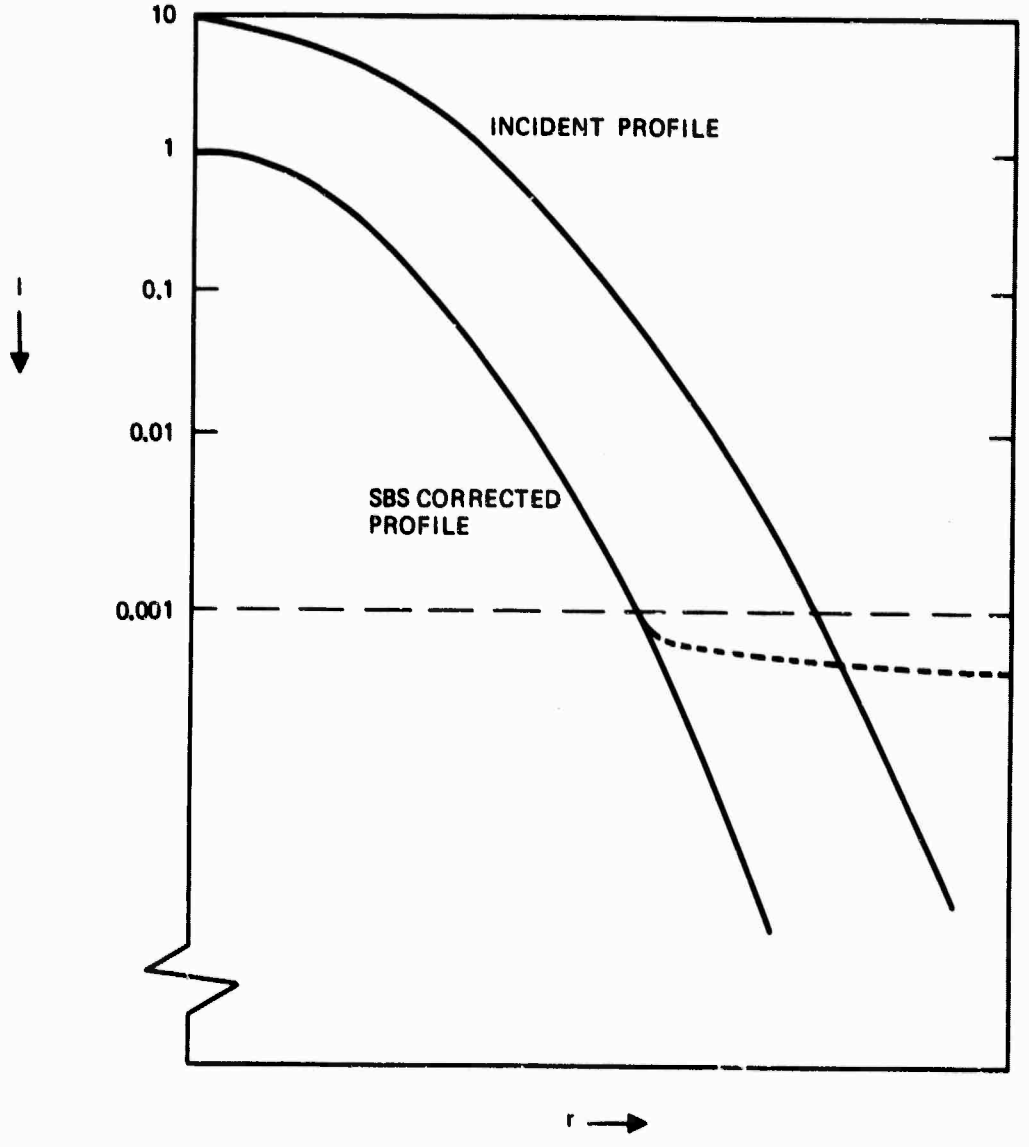

Figure 11. Example profiles.

case, two facts emerge. First, the SBS profile has a shape identical to the incident profile. Second, all of the energy in the beam is contained within this profile. This implies that the SBS-corrected beam is the phase-conjugate beam and that the fraction of conjugate return is 100%. Now assume that the SBS beam has the profile given by the dotted line, clearly the worst case possible and unlikely to occur. In this case, a large fraction of the energy could be found in the region below the dotted line (this would, of course, be non-conjugate-return energy). The objective of the detailed measurements is then twofold: to measure the intensity as far into the wings as possible and to make at least one pinhole measurement of the energy to confirm its distribution. This has been done for several experimental configurations; the detailed results are presented below.

From a complete sequence of photographic data, Figure 12 shows a normalized intensity profile as a function of beam radius for a CS_2-filled waveguide cell 81 cm long x 2.5 mm in diameter. Data are given for the retroreflected beam, SBS with no aberrator, SBS with aberrator No. 2, and SBS with aberrators No. 2 and No. 3. To plot the data in this way requires an additional data reduction technique. All sequences are normalized to the same point, which requires a common intensity value for all sequences. This value is the exposure threshold intensity. The exposure threshold is determined by plotting intensity versus diameter squared and extrapolating the straight-line fit to the point of zero diameter. This procedure is shown in Figure 13 for all the data runs shown in Figure 12 and those to follow. Figure 12 shows (as discussed previously) that the SBS-corrected beam has the same profile as the unaberrated beam down to $\sim 10^{-3}$ of the peak. Pinhole measurements were made for the conditions of Figure 12 using the pinhole diameters shown and for an additional larger diameter pinhole that collects all of the energy. (A description of the apparatus for pinhole measurements is discussed below.) By integrating the profiles shown and comparing these values to the pinhole measurements we can show that

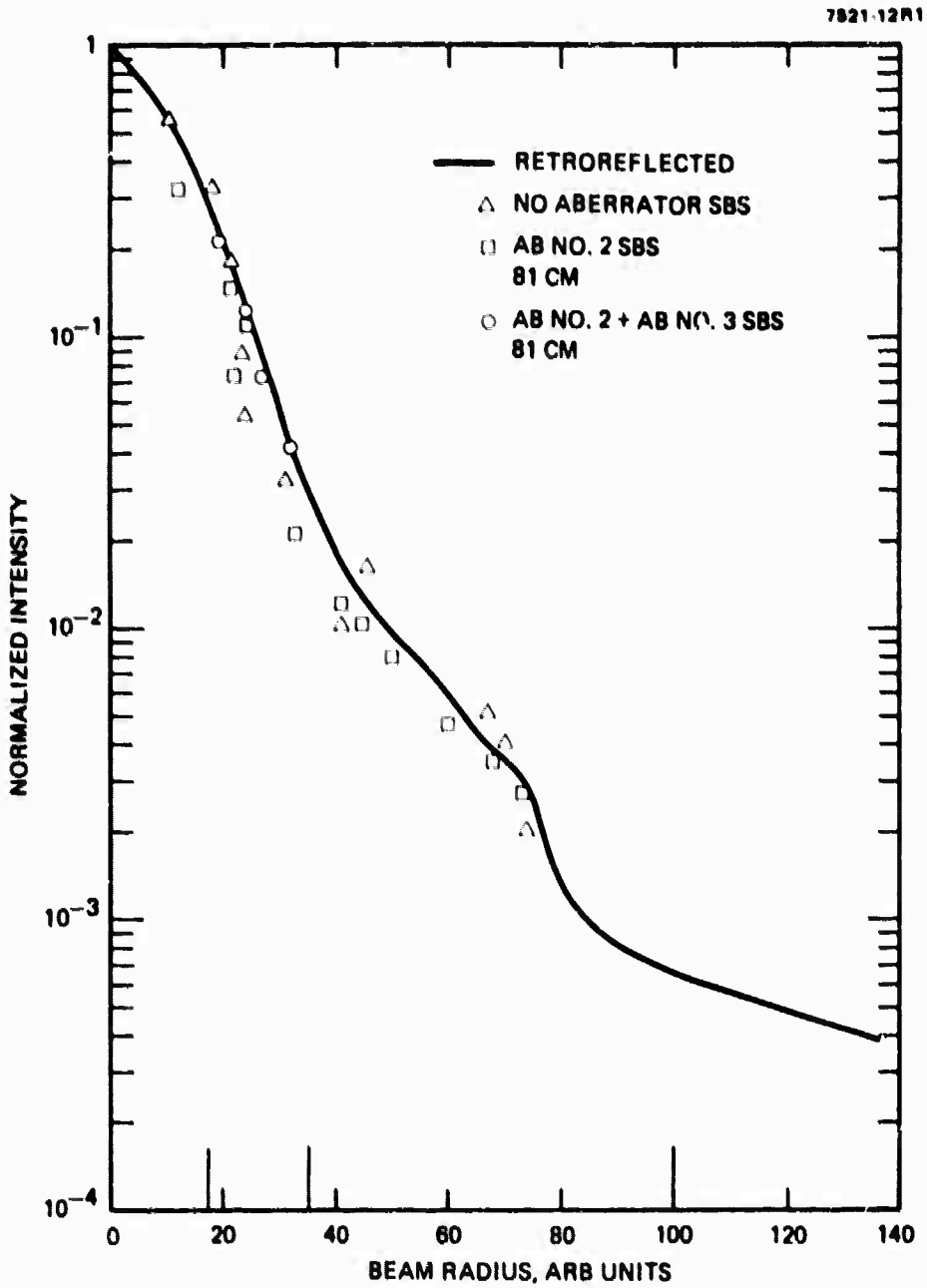

Figure 12. Intensity profiles.

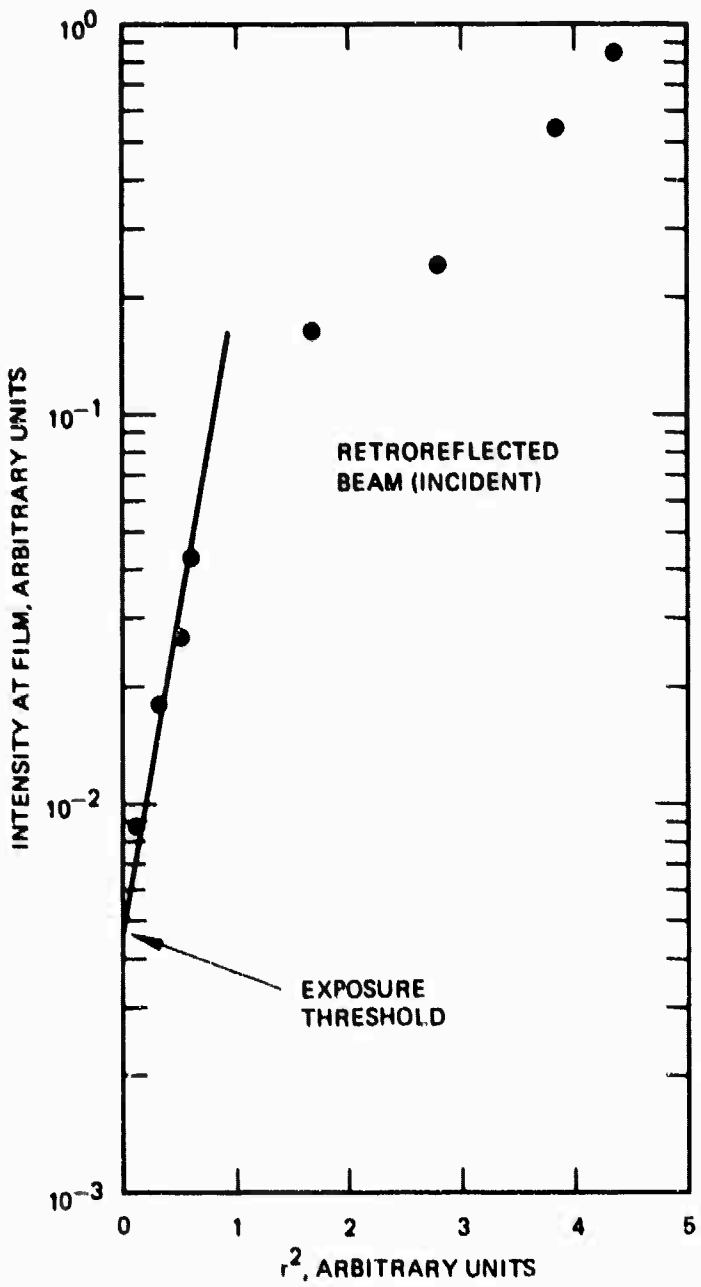

Figure 13. Determination of exposure threshold.

fraction of nonconjugated return produced is immeasurably small. That is, energy that could contribute to a return that deviates from the profile shown (e.g., non-phase-conjugate) is zero to within the experimental error (estimated to be $\sim$ 15%).

Similar results (measurements down to $\sim 10^{-4}$ of the peak) have been obtained for waveguides shorter than 81 cm. Figure 14 gives such data for an 11-cm, a 6-cm, and a 3-cm tube (the 81-cm data is also given). A comparison of these results again indicates good correction, as in the 81-cm case, but with a slight trend at the lower intensities toward larger divergences. This indicates that a larger fraction of the energy may be in the wings for the shorter tubes than for the 81-cm tube. The total SBS-backscattered energy for all waveguide lengths was measured to be $\sim$ 10% for cases without an aberrator and with aberrator No. 2 double passed.

The pinhole measurement apparatus is shown in Figure 15. Using the beamsplitter, a film plane and cross-hairs were located at the focal plane of the lens with the pinhole also at the focal plane. A photograph of the spot was taken for each datum point. This spot was compared to the cross hairs to observe if a symmetric illumination of the cross hairs can be achieved. A symmetric illumination implies that the beam is entering the center of the pinhole. These data were then recorded.

Experiments were conducted to determine the effectiveness of phase conjugation as a function of power above threshold. The 81-cm tube was used to perform the experiments. The far-field beam divergence was measured over input powers ranging from about 10% over the SBS threshold to four times the SBS threshold The far-field beam divergence obtained in these measurements was independent of pump power, indicating that, for a given waveguide geometry, the degree of conjugation is independent of power over the SBS threshold.

In addition to the experiments described above, which were conducted in a waveguide geometry, experiments were performed to study the possibility of phase-conjugation via SBS in a free-space geometry.

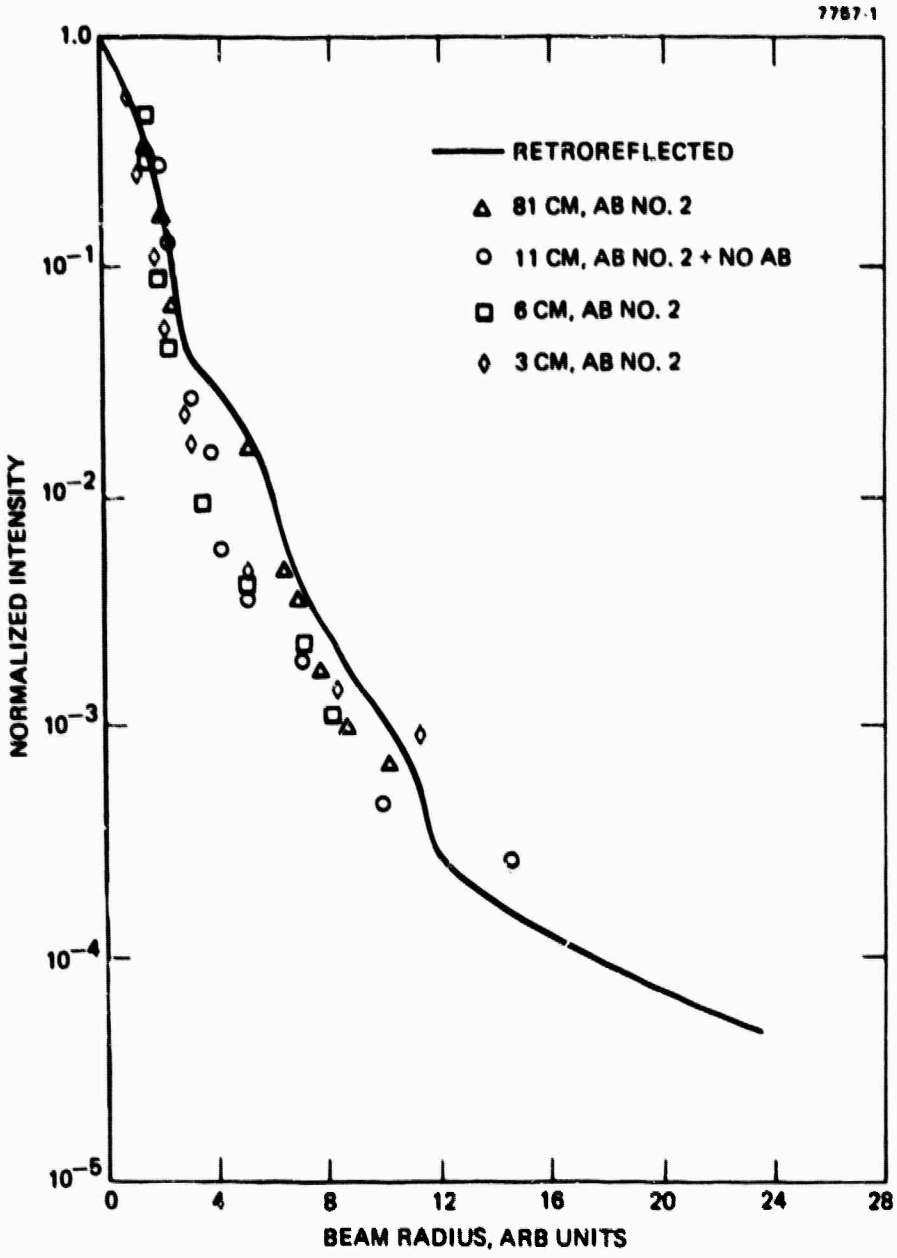

Figure 14. Intensity profiles.

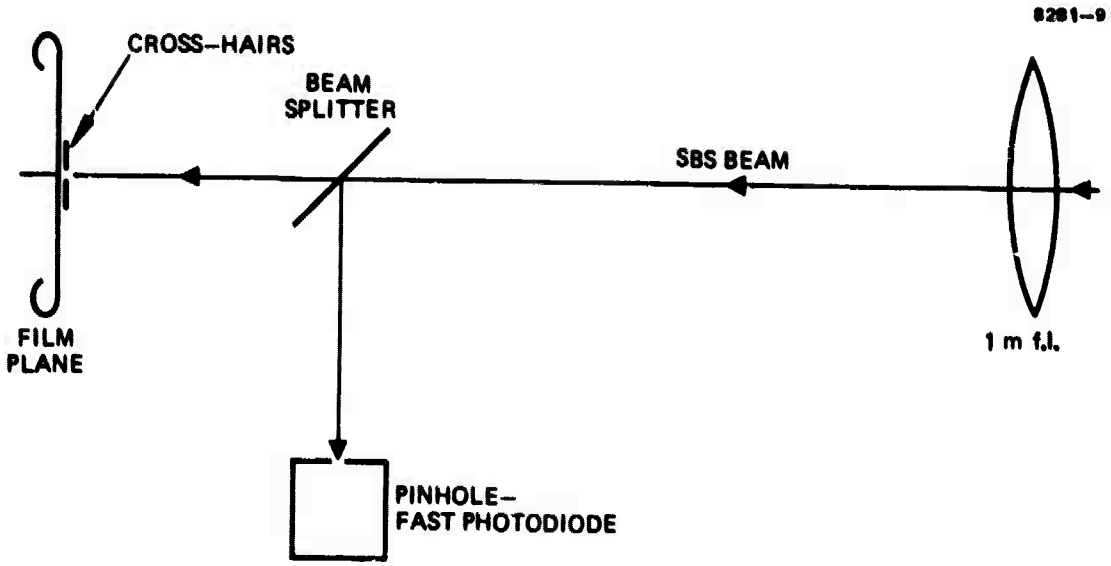

Figure 15. Pinhole measurement apparatus.

A 4.5-in.-focal-length lens was used to focus the ruby laser beam in a large cell filled with CS_2. The experimental arrangement was essentially the same as that shown in Figure 4, and the same photographic techniques as those used in the waveguide experiments were used to analyze the free-space data.

In contrast to the waveguide experiments, the backward-scattered SBS signals showed only partial wavefront correction and relatively incomplete phase conjugation when the pump power was only a small fraction above the threshold for SBS. However, the degree of conjugation was observed to depend critically on power, and every small increment in the pump power resulted in a significant improvement in the aberration removal capability of the backscattered SBS wave. In addition, the degree of phase conjugation improved significantly with the introduction of random aberrations or strong transverse random amplitude fluctuations in the beam (with the scattering of the pump laser beam into higher order spatial modes).

Figures 16, 17, and 18 illustrate the strong dependence of the degree of correction (phase-conjugation) on both the pump power and on the presence of random amplitude fluctuations (i.e., aberrations) in the pump beam. The solid lines marked R34 indicate the beam profile of the unaberrated retro-reflected beam. The data in Figure 16 correspond to a pump power level (designated as I_o) that is $\sim$5 times the SBS threshold power. At this power level, the unaberrated pump beam results in a nearly phase-conjugate backward-scattered SBS beam that has $\sim$ 30 to 40% of the incident pump power. However, as implied by the broader beam profile (R52, crosses), this backward-going beam shows incomplete reconstruction, which is evidence of incomplete phase conjugation. Introduction of the aberrator (aberrator No. 2) in the pump path results in almost complete collapse of the backward-going beam profile to that obtained for retro-reflection, implying almost complete phase-conjugation for this case. For this case, typical backward-wave returns were between 5 and 10%.

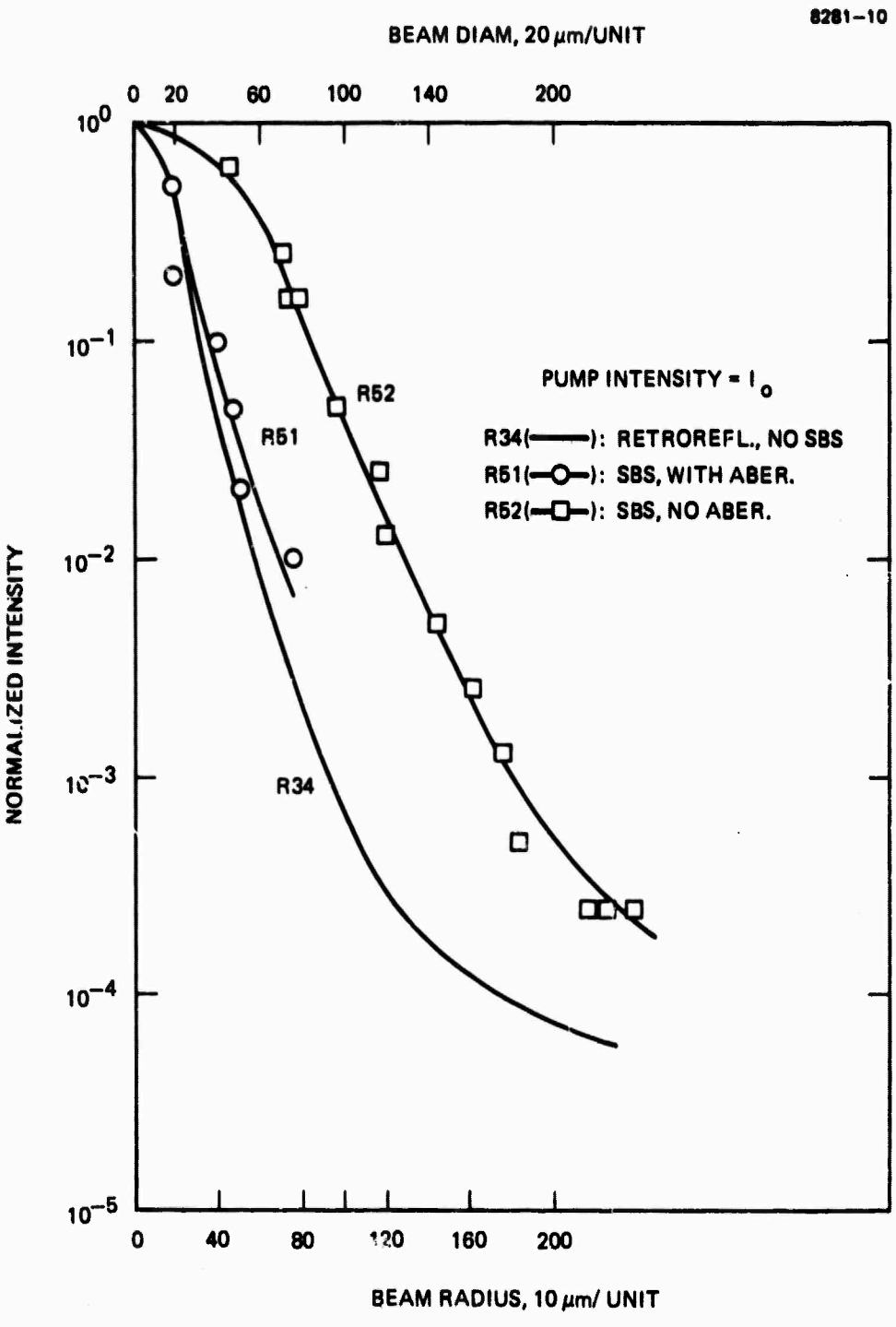

Figure 16. Phase-conjugation via free-space SBS.

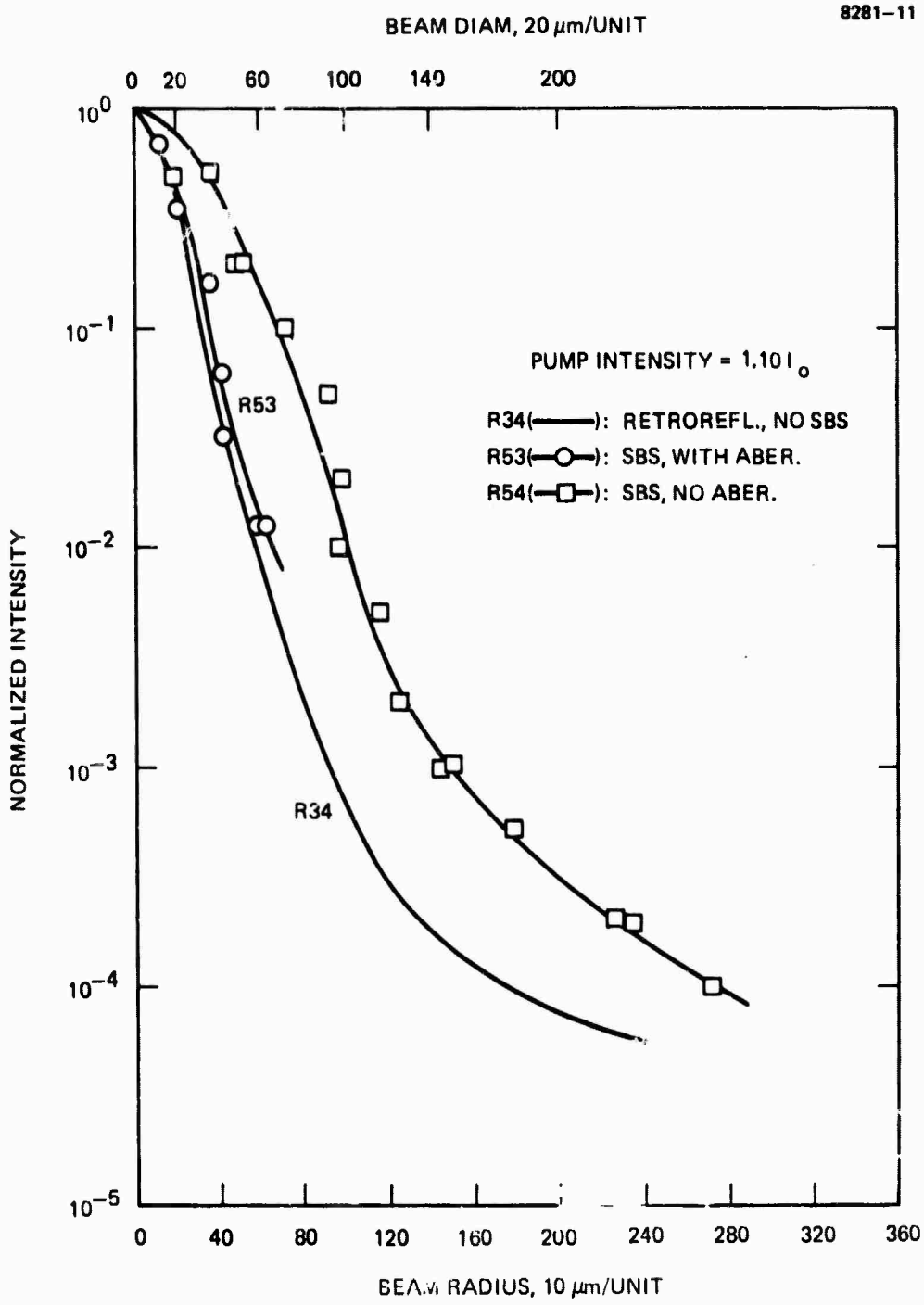

Figure 17. Phase-conjugation via free-space SBS.

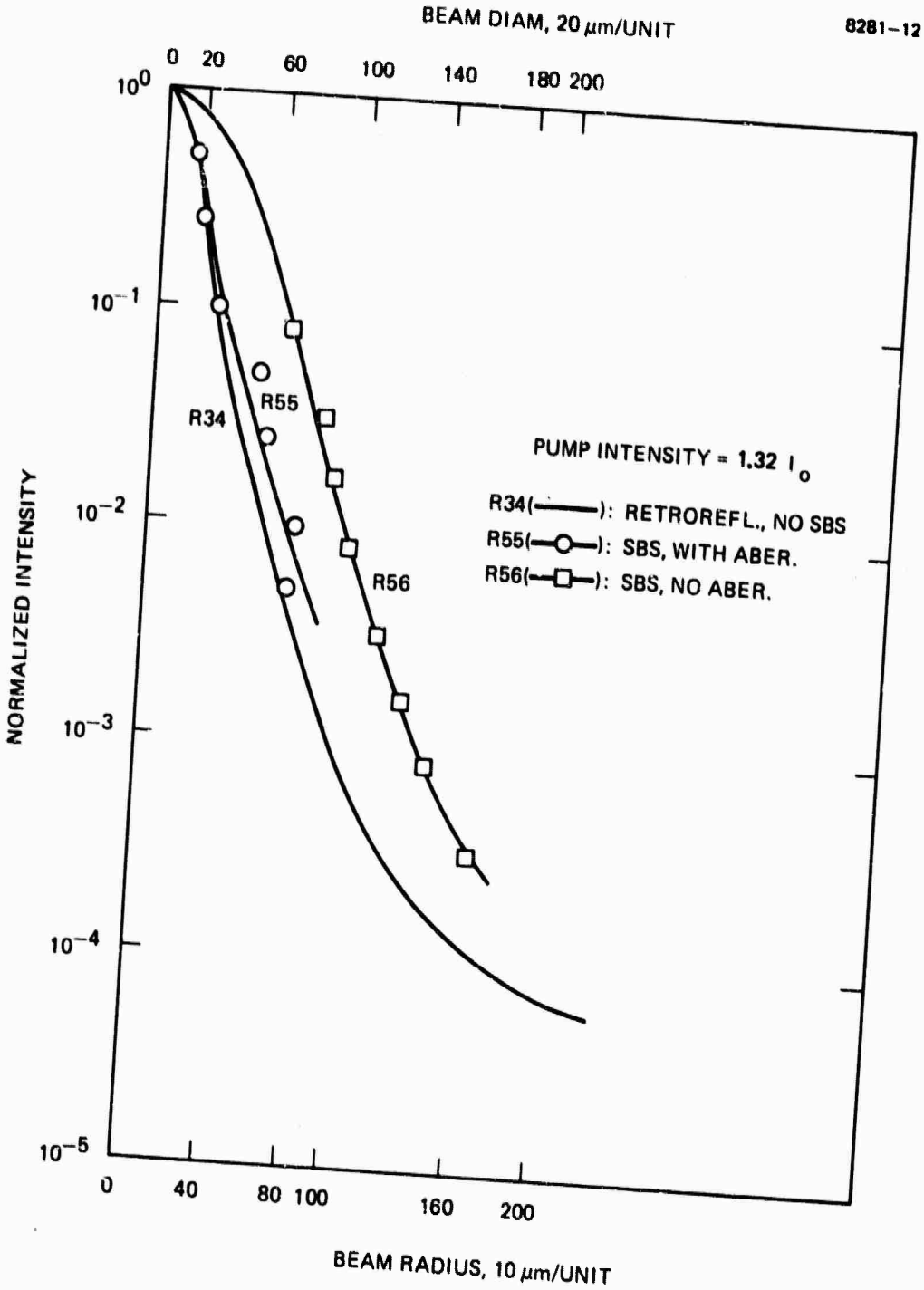

Figure 18. Phase-conjugation via free-space SBS.

As seen in Figures 17 and 18, only slight increases in power (10% and 32%, respectively) result in significant improvements in the reconstructed beam (curves R54 and R56). Higher powers were not used for fear of exceeding the damage threshold of the window of the CS_2 cell.

The results described above on phase conjugation in free space are in complete agreement with the previously referenced paper by Zeldovich et. al. on the nature of phase conjugation via SBS and are the first quantitative experimental results on this behavior. They indicate the freedom from the restraint of using a waveguide cell in situations where the lack of beam-pointing accuracy might inhibit efficient coupling into a waveguide cell.

Figure 19 shows measurements made on the frequency of the return beam. A Fabry-Perot etalon having a 3.16 mm spacing was used. The expected SBS frequency shift of 6 GHz in CS_2 was observed.

Image reconstruction via phase-conjugated SBS was also demonstrated on the present program. In these experiments, SBS is obtained by irradiating CS_2 (see Figure 20) in a waveguide cell from the Q-switched ruby laser, as in the previous experiments. The TEM_{oo}-mode ruby laser output passes through a transmitting resolution chart to acquire a well-defined spatial variation in the transverse direction (Figure 21). A 200-mm lens focuses this beam onto the 2.5-mm-diameter, 81-cm-long CS_2 waveguide cell, which acts as a "Brillouin mirror." It generates a backward-going phase-conjugated wavefront, which reconstructs the spatial profile of the resolution chart back at the original plane of the chart (Figure 21(c)). By interposing a beam-splitter between the focusing lens and the resolution chart, the backward-going (pseudoscopic) image is reconstructed at a second plane. With the use of appropriate optics, this pseudoscopic image plane is re-imaged on the film of the camera.

When a severe aberrator is placed in the path of the spatially modulated beam, it loses all its spatial information in the far field,

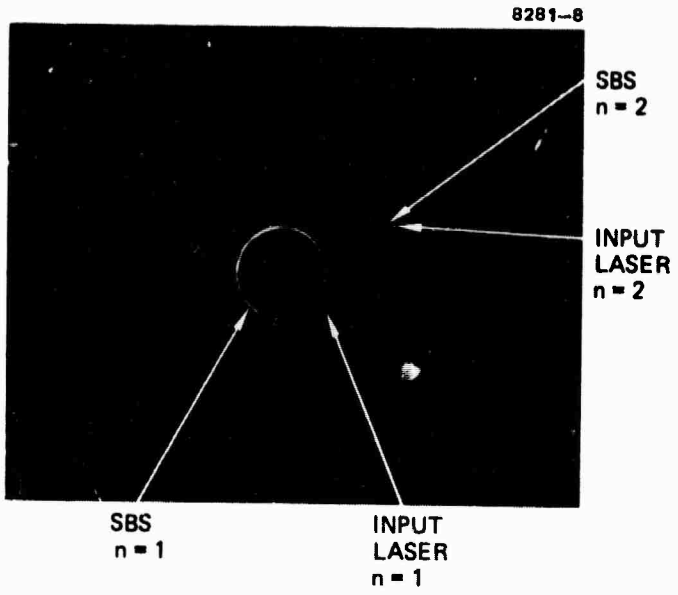

Figure 19. Free-space SBS frequency-shift measurement.

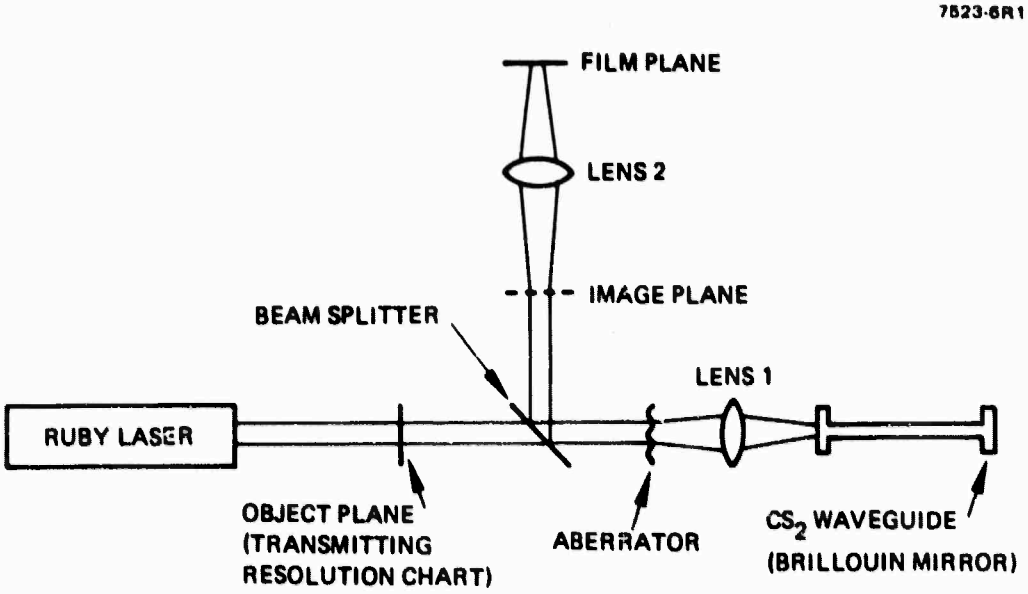

Figure 20. Experimental arrangement — image reconstruction.

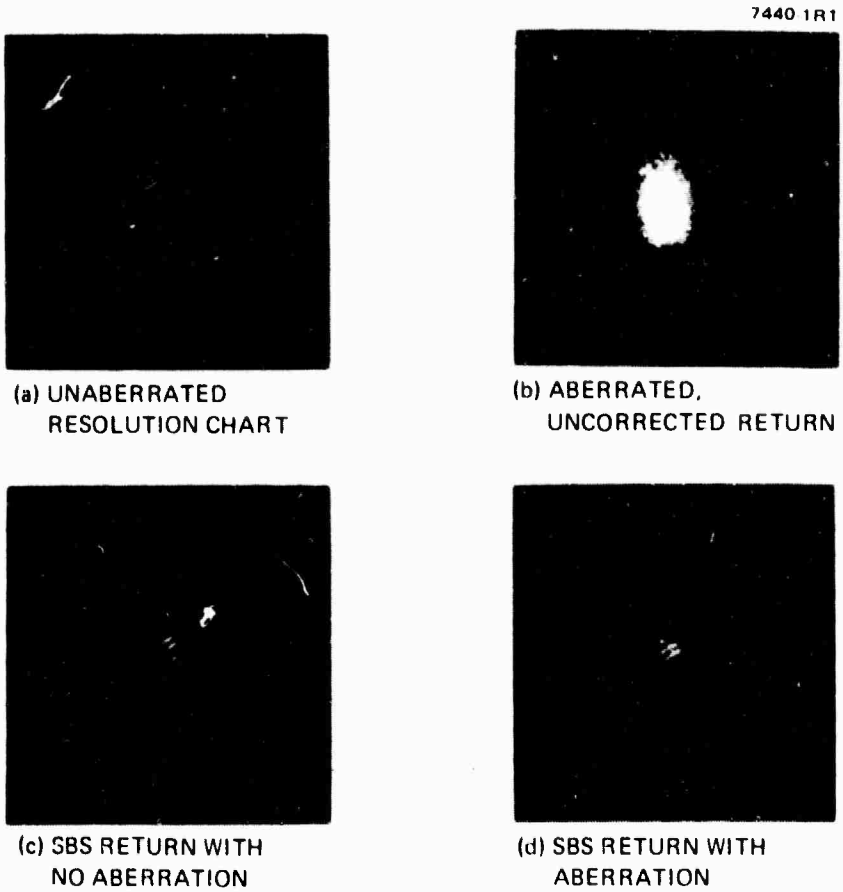

Figure 21. Image reconstruction using SBS.

as can be observed (Figure 21(b)) by replacing the Brillouin mirror with a plane reflector. However, when the Brillouin mirror is re-introduced in the experimental arrangement, it phase conjugates the wavefront of the severely aberrated beam so that the backward-going beam undoes its phase distortion as it retraverses the aberrator, thereby reconstructing the original spatial information at the pseudoscopic image plane (Figure 21(d)).

With an aberrator that results in an approximately 10-times-diffraction-limited beam in the far field, a spatial resolution of $\sim$ 5 lines/mm has been obtained with an optical system having a limiting resolution of $\sim$ 20 lines/mm. This demonstrates the potential of SBS for image reconstruction.

Although the degree of phase conjugation theoretically obtainable from SBS may suffer from limitations (see below) not present in other techniques (such as four-wave mixing), SBS does possess the advantage of experimental simplicity. As a consequence, it may be a feasible technique for phase conjugation and real-time imaging applications. The limitations in the spatial resolution obtainable with SBS phase conjugation of severely aberrated images, which are difficult to establish theoretically, were elucidated by these experimental studies.

SECTION 3

THEORETICAL STUDY OF NONLINEAR PHASE CONJUGATION SCHEMES

A. SBS AND SRS

A detailed theoretical analysis of wavefront reproduction by SBS and stimulated Raman scattering (SRS) in a waveguide was performed on this program (see Appendix B). The solution obtained was for the backward optical wave stimulated by a multimode incident optical wave in a waveguide filled with a transparent nonlinear medium. The basic conclusion from the theory is that, under many conditions (e.g., number of excited modes, phase distribution between the modes, random distribution of the amplitude of the modes), there is one back-scattered wave that has an exponential gain about twice that of any other solution and that this wave is essentially a "phase conjugate" of the incident wave. The fraction of energy that is in waves other than this phase-conjugate wave is small: it was found to be no greater than $\sim$ 7% for the arbitrary pump waves studied. For SBS, it was found that the waveguide length should be $L \gtrsim S\lambda^{-1}N^{-1}$ (where S = area of guide, λ = wavelength, N = number of excited modes) for the phase-conjugate solution to exhibit the above properties. SRS was also investigated. Here the length requirement is

$$L_{SRS} \lesssim \frac{6r_o^{1/2}S}{N|\Delta\lambda|} ,$$

where r_o is a parameter approximately equal to $\sim$ 0.1, and $|\Delta\lambda| = |\lambda_{stimulated} - \lambda_{input}|$.

The theory also suggests that SBS would yield conjugate waves in free space and in multimode waveguides. This was observed in our experiments.

In addition to understanding the basic theory of SBS, the general question of compensation of optical path difference (OPD) errors rather than optical phase errors (this distinction only appears in a frequency-shifting device) was investigated. Although SBS is likely to correct phase error rather than path error, the potential existence of a path-length-error-correcting device might be important in some applications requiring larger frequency shifts. The error $\Delta\phi$ introduced by phase correction with a frequency shift is small if $\Delta\omega/\omega < 1$ (neglecting dispersion). This criterion is easily met by SBS, where $\Delta\omega/\omega \approx 10^{-5}$ ($\Delta\phi$ is a typical relative phase error across the aperture). For SRS, where $(\Delta\omega/\omega) \simeq 10^{-2}$, apparently perfect correction has been reported in the Soviet literature for phase aberrations of $\simeq 2\pi$ (an extreme aberration in terms of reduction in on-axis intensity). When frequency shifts of 10% or greater are desired, phase aberrations of a few wavelengths would make the question of OPD correction important. It appears that nonlinear phase conjugating processes that are presently conceived are not OPD-correcting devices. If such an OPD device were possible, it would exhibit several anomalous characteristics and would not be capable of correcting all forms of phase aberration. This is traceable to the periodic nature of any phase variable. The anomalous characteristics include (1) nonuniqueness of output for a given input; (2) lack of linear superposition, giving rise to image dependent distortions; and (3) (spatially) discontinuous outputs for certain continuous inputs.

B. FOUR-WAVE MIXING

A detailed theoretical development of a second phase-conjugation scheme, degenerate four-wave mixing in a saturable absorber, was conducted on this program. With company funding, we had developed a coupled-mode theory for degenerate four-wave mixing in a two-level absorbing (or amplifying) system of motionless atoms. Here the nonlinear medium is a saturable absorber with a resonant enhancement at

each single photon step. The solutions indicate that amplified reflection, oscillation, and phase conjugation occur even in the presence of strong absorption. On the present program, this development was extended to include atomic motion.

The basic geometry for four-wave mixing is given in Figure 22. The interaction consists of two intense pump beams (E_{P_1}, E_{P_2}) and two weak signal beams (E_{S_1}, E_{S_2}). The particular case for which the theory has been developed considers all beams at the same frequency and the pumps and signals in a counterpropagating geometry as shown. The use of nondegenerate frequencies and noncollinear pumps is discussed in Section 4. Physically, the intense beam E_{P_1} interferes with E_{S_1} to form regions of high and low intensity. This interference combined with saturation in the medium spatially modulates the absorption and index of refraction. This spatial modulation leads to a dual-grating, or dual-volume, hologram picture, as shown in Figure 23. The forward pump (E_{P_1}) and probe (E_{S_1}) form a small angle (large spacing) grating, while the backward pump (E_{P_2}) and probe (E_{S_1}) form a large angle grating. In the readout process, the backward pump (E_{P_2}) scatters off the small angle grating, generating a contribution to the phase conjugate signal (E_{S_2}), and the forward pump (E_{P_1}) scatters off the large angle grating, also giving a contribution to E_{S_2}. The theory without atomic motion indicates that the magnitude of the phase-conjugate signal is a function of three parameters: the line-center absorption (gain) coefficient-interaction length product, $\alpha_0 L$; the ratio of pump intensity to line-center saturation intensity, I_p/I_{S_0}, where I_{S_0} is proportional to $(1/T_1T_2)$; and the position in frequency of the pump relative to the line-center frequency of the saturable absorber, $\gamma = (\omega - \omega_0)/\Delta\omega$, where $\Delta\omega$ = collision-broadened linewisth. For example, if $\alpha_0 L = 7$, $\gamma = 6$, and $I_p/I_{S_0} = 25$, the conjugate return wave intensity is 20X the input intensity. If the atoms move a grating period (which is of order λ) in a population relaxation time T_1, the interference pattern will be washed out, resulting in a reduction of the amplitude of the

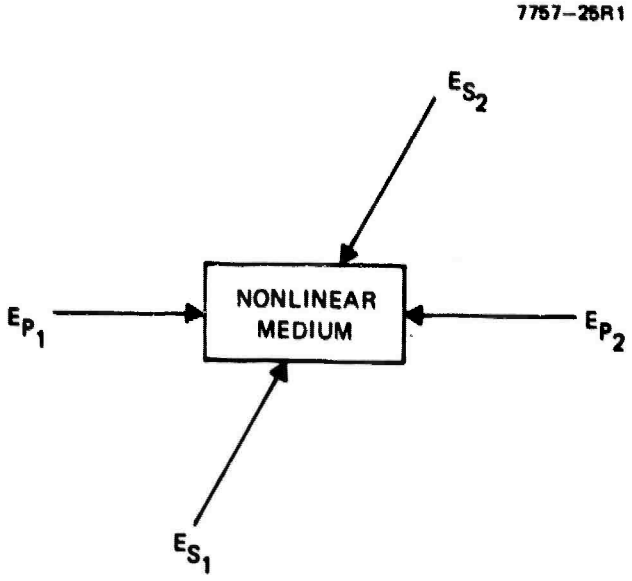

Figure 22. Four-wave mixing scheme.

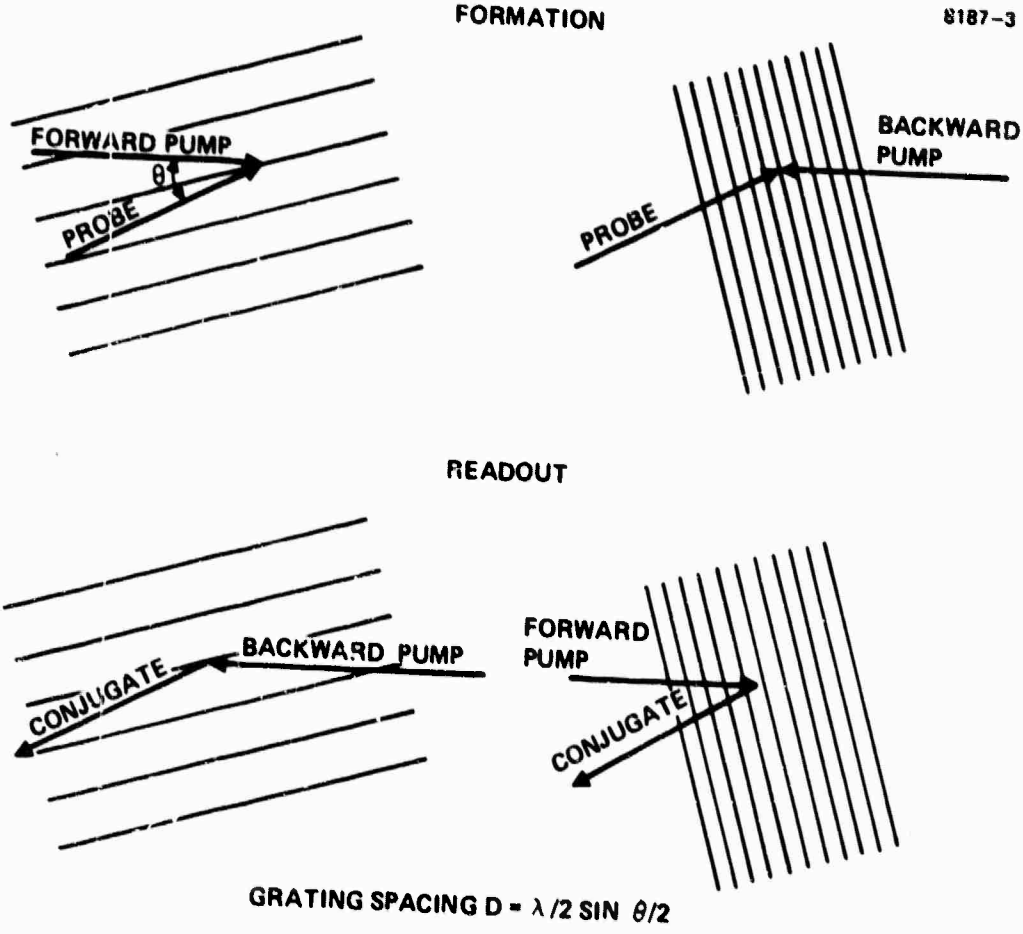

Figure 23. Dual grating picture.

conjugate wave. This diminution of the conjugate amplitude occurs even in the case of a homogeneously broadened lineshape ($1/T_2 > \Delta\nu_D$). This effect also causes a dependence of the return wave amplitude on the angle between the signal and pump beams. We have developed (see Appendix C) and applied the formalism of the "quasi-classical" density matrix to compute the relevant nonlinear couplings, thus extending the previous analysis to all ranges of the atomic motion parameter ($T_D = 1/\Delta\nu_D$). The equations have been solved exactly in third-order perturbation theory and in the "homogeneous saturation" approximation (implicit in the stationary atom results) for arbitrarily strong pump fields.

The solution for the field amplitude of the phase conjugate return beam is shown in Figure 24. The figure gives the expected reduction of the field amplitude compared to the solutions obtained previously, which did not account for atomic motion. The solution is a function of T_D/T_1 and of the angle between the pump and signal beams. For $T_D/T_1 >> 1$ (i.e., no atomic motion), the solution shows no reduction over the previous case, as expected. For angles greater than $\sim 30°$, there is a general reduction in amplitude as T_D/T_1 decreases (i.e., as atoms have time to move and wash out the grating). For small angles, the period of the grating becomes increasingly large, increasing the time it takes for the atoms to move one grating period and thus minimizing the Doppler motion reduction. This is exhibited in the solutions obtained. For small angles (such as $T_D/T_1 << 1$), the reduction in amplitude approaches a factor of two. This is because the large angle grating (smaller period) is becoming completely washed out and can no longer contribute to the return.

We have also studied polarization effects in four-wave mixing systems. The various nonlinear optical media in which four-wave mixing is observed will exhibit different relationships between the polarizations of the signal and pump waves and the polarization and amplitude of the reflected (phase conjugate) wave. This is because, even

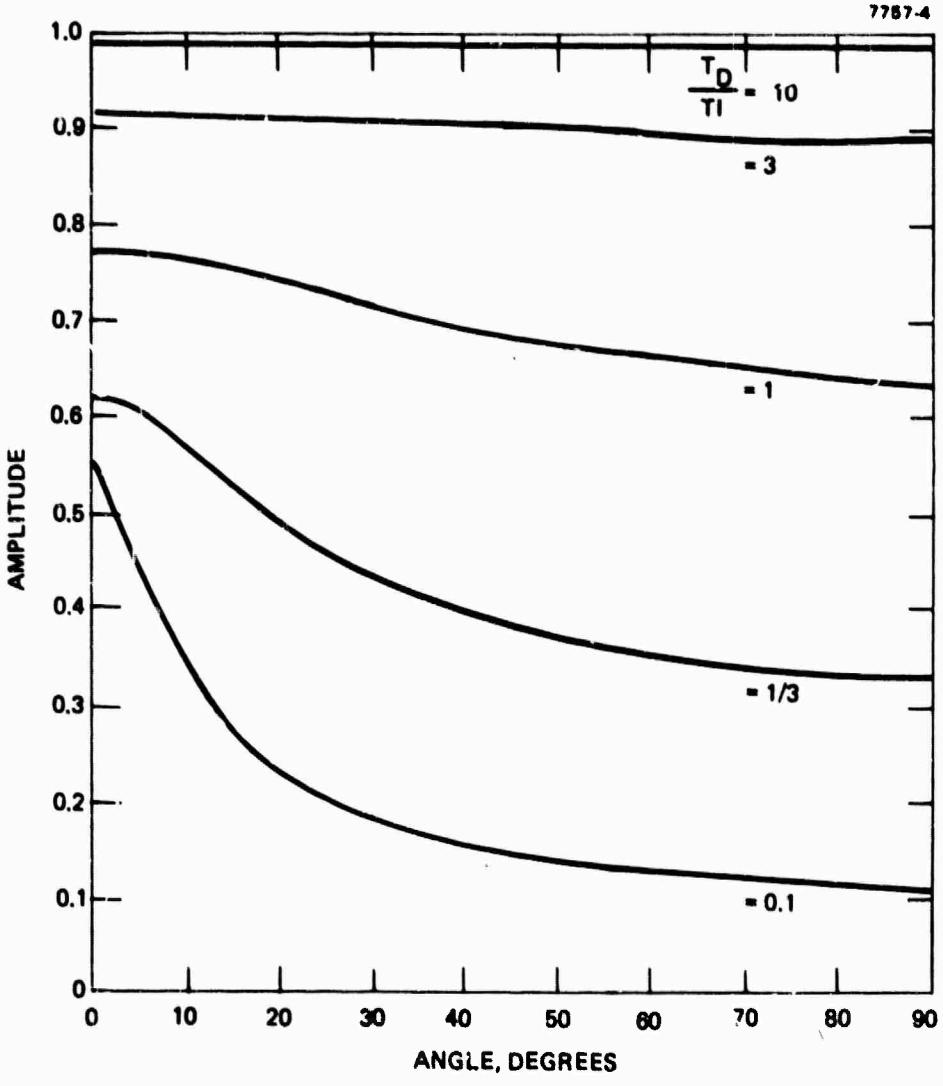

Figure 24. Reduction in amplitude.

In isotropic materials such as gases and liquids, the third-order polarizability contains two different types of tensor structures, giving rise to induced polarizations of the form

$$\vec{P} = \beta_1 \vec{E}_s (\vec{E}_1 \cdot \vec{E}_2)$$

$$+ \beta_2 \{\vec{E}_1 (\vec{E}_s \cdot \vec{E}_2) + \vec{E}_2 (\vec{E}_s \cdot \vec{E}_1)\} \quad .$$

(In crystal media, even more tensor structures can appear.) For example, only the β_2 term dominates in the single photon resonant process. In the two-photon resonant case, β_1 probably dominates. In a nonresonantly enhanced process (CS_2, for example), β_1 and β_2 can be of comparable magnitude.

Table 1 gives examples of the expected output polarizations, relative efficiency of conjugation, and angular dependence of the conjugate signal. The examples are for nonresonant, single-photon resonant, and two-photon resonant interactions. The arrows and dots indicate all the nonredundant directions of the linear polarization states of the appropriate beams. The efficiencies indicate which terms contribute to the output, and the subscripts S and T indicate single- and two-photon cases. For the nonresonaat case, the first column gives all beams copolarized. In this case, since the dot products are all nonzero, each term contributes to the conjugate output, giving an efficiency of $\beta_1 + \alpha\beta_2$. In the second column, the pump and signal are cross polarized, giving a zero dot product, but the pumps are copolarized, giving a nonzero dot product in the first term. Thus, the β_1 term is the only term remaining. The remaining columns are determined in the same manner. (The absolute efficiency is larger in the resonant cases.) The angular dependence arises in the third columns. In this case, under the assumption of molecular dipole scattering, when the beams are at 90°, the playback pump polarization is oriented parallel to the probe propagation vector, and hence the scattered fields vanish in the direction of the conjugate wave (retro direction). Thus operation is not possible at this angle.

Table 1. Effect of the State of Polarization on the Conjugate Output

	Nonresonant			Single-Photon Resonance			Two-Photon Resonance		
Pump one	↑	↑	↑	↑	↑	↑	↑	↑	↑
Pump two	↑	↑	⊙	↑	↑	⊙	↑	↑	⊙
Signal	↑	⊙	⊙	↑	⊙	⊙	↑	⊙	↑
Conjugate output	↑	⊙	↑	↑	0	↑	↑	⊙	0
Relative efficiency	$\beta_1 + 2\beta_2$	β_1	β_2	$2\beta_{S2}$	0	β_{S2}	β_{T_1}	β_{T_1}	0
Angular dependence	No	No	$\cos^2\theta$	No	NA	$\cos^2\theta$	No	No	NA

NOTE: ⊙ = in plane.
↑ = perpendicular to plane.

6306

C. MATERIALS FOR FOUR-WAVE MIXING

In this part of the program, we have investigated candidate materials for four-wave mixing. Materials suited to the blue-green were of particular interest, and some are listed below.

The general classes of nonlinear materials useful for four-wave mixing can be described under two major categories:

- Those that are nonresonant (i.e., show a very weak spectral dependence in the nonlinearity $\chi^{(3)}$ that results in the phase-conjugate signal).

- Those that are resonant or show a pronounced increase in the nonlinearity versus wavelength, as might occur in the vicinity of an allowed transition in a two-level system.

In both cases, four-wave mixing might occur as a result of:

- A temporal modulation of the polarization at 2ω that scatters the signal wave.

- A spatial modulation of the real part of the refractive index (i.e., via a light-induced pure phase volume hologram).

- A spatial modulation of the absorption or gain coefficient (imaginary part of the refractive index), i.e., via a light-induced amplitude hologram.

- A combination of the above.

In any of the three cases, the resonant media generally require lower power densities (at appropriately chosen wavelengths) than the nonresonant media for comparable reflectivity of the conjugate wave. Examples of nonresonant media include:

- Materials with high nonlinear refractive indices, such as CS_2 (in the visible), germanium (in the infrared), and conjugated polymers (such as diacetylenes).

- Materials that are near a phase transition that may be induced locally in space by the interference pattern of the light field, such as ferroelectrics (e.g., KDP) near their critical magnetic fields.

- Materials in which free-carrier refractive-index profiles can be easily induced, such as semiconductors (Si, CdS, GaAs, etc.) near and above their band edges.

Resonant media — both single- and two-photon transition media — might exhibit enhancements of their nonlinearity over broad or extremely narrow spectral ranges, depending on the width of the relevant resonances. For laser pulses longer than a few nanoseconds, the single-photon transitions appear more promising and generally require extremely low power densities for phase-conjugate returns of a few percent. The volume holograms in such media occur via the nonlinear saturable absorption of the transition, which results in high conjugation efficiencies at power densities comparable to the saturation intensity I_{sat}. Since I_{sat} is inversely proportional to σ (the absorption cross section) and τ (the recovery time for the absorption), phase conjugation at extremely low power densities ($\sim$ mW/cm^2) may be possible with a choice of slowly recovering highly absorbing media. An example of such a material is Na-fluorescein (in orthoboric acid), which exhibits remarkable saturation properties at optical power densities of less than 500 mW/cm^2 at 488 nm (Ar^+ laser) and at slightly higher powers ($\sim$ 2 W/cm^2) at 501 nm (HgBr laser). Efficient (a few percent) backward-wave generation has already been demonstrated at relatively low power levels ($\sim$ 1 to 10 kW/cm^2) of Ar^+ laser radiation (at all lines from 488 nm to 514.5 nm) using a 1.5-cm-long ruby crystal, which acts as a broad-band, three-level, blue-green saturable absorber (similar to Na-fluorescein in orthoboric acid). Dye molecules in the fluorescent state, as used in liquid solutions for lasers, also act as excellent fast-recovery-time (10 nsec) saturable absorbers, as might be required for several high-data-rate, large-bandwidth phase-conjugation applications. However, the price for speed is a higher operating power density resulting from the correspondingly larger saturation intensities ($\sim$ 100 MW/cm^2 to 10 GW/cm^2).

Similar considerations applied to a preliminary search for nonlinear materials at 2.7 μm (HF laser) indicate that Ge, polydiacetylenes, $LiIO_3$, and CS_2 are promising nonresonant candidates, whereas an appropriate HF medium, absorbing or amplifying, could be used as a resonant four-wave mixing material.

Certain specific examples of lasers and candidate materials in the visible and at 2.7 μm are summarized in Table 2. An important factor in the figure of merit is the damage threshold of each material. This is particularly true for the case in which conjugate returns at high efficiencies are desired from a nonresonant material since in this case the efficiency is generally a monotonically increasing function of the power density. If high efficiencies are attainable at power densities much below the damage threshold (as seems to be true for several of the resonant nonlinear materials), high-power phase conjugation will be demonstrated by magnifying optics that will reduce the power density of such beams (to optimal levels) at the phase conjugator.

D. THREE-WAVE MIXING

In addition to SBS and four-wave mixing, a third conjugation scheme using a parametric difference frequency generation process was briefly examined. This process was first suggested by Yariv as a phase-conjugation scheme to correct for the modal dispersion introduced in a multimode fiber optic waveguide used for image transmission. This process makes use of the quadratic nonlinearity of the $\chi^{(2)}$ nonlinear susceptibility present in non-centro-symmetric crystals.

A schematic of the basic phase-conjugation scheme is shown in Figure 25(a). In the three-wave scheme, a pump wave at frequency ω_3 is mixed in a nonlinear crystal with a signal wave at frequency ω_1. From this mixing, a new wave (idler) at the difference frequency $\omega_2 (\omega_2 = \omega_3 - \omega_1)$ is generated that is the phase conjugate of the signal wave. That is, the mixing results in growing coupled waves with amplitudes E_1 and E_2, each of which is proportional to the conjugate of the

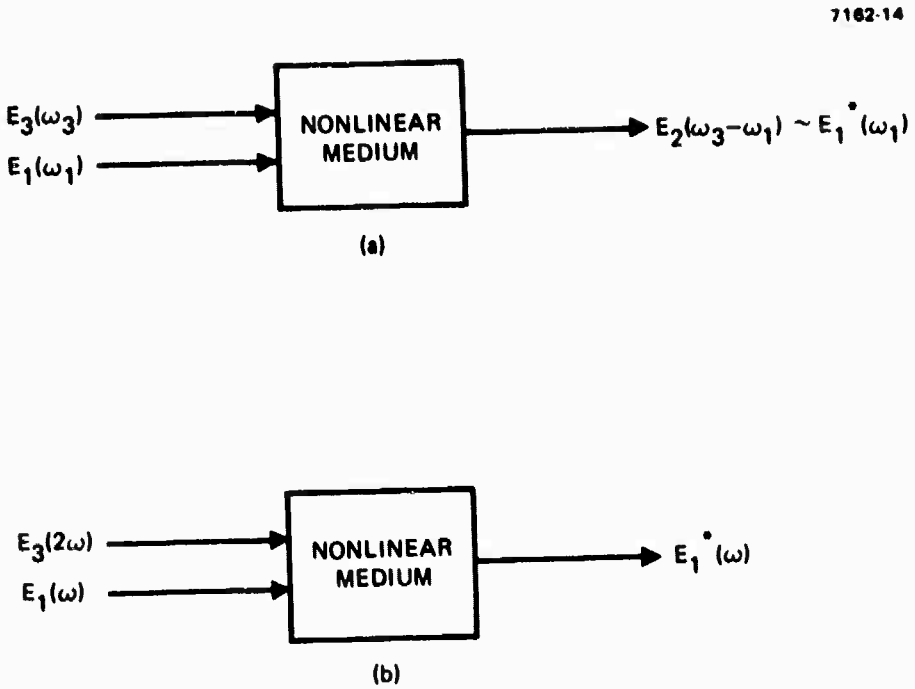

Figure 25. Three-wave mixing schemes.

Table 2. Candidate Materials

Laser (Wavelength)	Material	Typical Power Densities[a]
Dye lasers (e.g., Rhodamine 6G at 590 nm)	Dye solutions (e.g., 10^{-4}M Oxazine in ethanol)	∿100 MW to 1 GW/cm^2
Doubled-YAG (532 nm)	Ruby (0.05%)	∿1 to 10 kW/cm^2
	Si ($\rho \geq 100$ Ω-cm)	∿1 MW/cm^2
HgBr (501 nm)	Na-fluorescein	≲1 W/cm^2
	Ruby (0.05%)	∿1 to 10 kW/cm^2
Ar^+ (488 nm/ 514.5 nm)	Na-fluorescein	≲1 W/cm^2
	Ruby (0.05%)	∿1 to 10 kW/cm^2
Ruby (694.3 nm)	Rubrocyanine in methanol	∿1 kW/cm^2
	CdSe, CdS	∿1 to 10 MW/cm^2
	Cryptocyanine in methanol	∿50 MW/cm^2

[a]For conjugate returns of a few percent.

other. Thus, if E_1 is the input signal wave, a wave E_2 emerges at the exit of the medium where $E_2 = KE_1^*$. If the pump wave E_3 is an intense field, the wave E_2 may exhibit amplification ($K > 1$). This is a result of conservation of energy. Here the energy of the pump wave is coupled through the polarization generated at frequency $\omega_2 = \omega_3 - \omega_1$ by the nonlinear mixing to the field E_2. If the pump wave frequency ω_3 is set equal to $2\omega_1$, then ω_2, the down-converted wave, will have the same frequency as the input wave ω_1 and will be the phase conjugate. The latter

process (shown in Figure 25(b)) is of primary interest for most applications. From an examination of the solution of the differential equations given by Yariv describing three-wave mixing, one observes that for multimode fields (general aberrated beam), each mode of the signal field, $E_1(\omega_1)$, interacts only with its counterpart mode at ω_2. This is a result of the need to "phase match" in the transverse direction (across the beam) and in the propagation direction. This "three-dimensional" phase matching will ensure exact phase conjugation. The need to phase match each mode to achieve exact phase conjugation is a serious limitation on three-wave mixing. This implies that only a narrow bundle of rays or a few modes that are nearly phase matched on alignment of the beams will have sufficient amplitude to be observed and are the only modes phase conjugated.

Since the three waves in this example are traveling in the same direction through the crystal, there exists a need to be able to distinguish the input wave from the conjugate wave. This is done by making the polarization of the generated wave $E_2 = KE_1^*$ orthogonal to the signal wave E_1 (waves E_1 and E_3 have the same polarization). This requires a material that satisfies the type II phase-matching condition. Such crystals might be Te, Ag_3AsS_3, CdSe, or KDP.

An experimental demonstration of phase conjugation by three-wave mixing was done by Avizonis et al. (Appl. Phys. Lett. Vol. 31, pp. 435-437, Oct. 1977) at 1.06 μm. The crystal used was lithium formate. Conjugate signals 0.5% of the input signal were observed to be limited by the ability to phase match ($\Delta k = k_3 - k_1 - k_2 \neq 0$). These experiments showed that the conjugate signal observed was an extremely sensitive function of the alignment.

Figure 26 shows a conceptual realization of this process for a HEL using a shared aperture. An illumination pulse is initiated in the same manner as in Figure 1 to obtain a glint return. The glint return passes through the parametric amplifier to generate the conjugate waveform, which is selected by the polarizer. This wave is further amplified

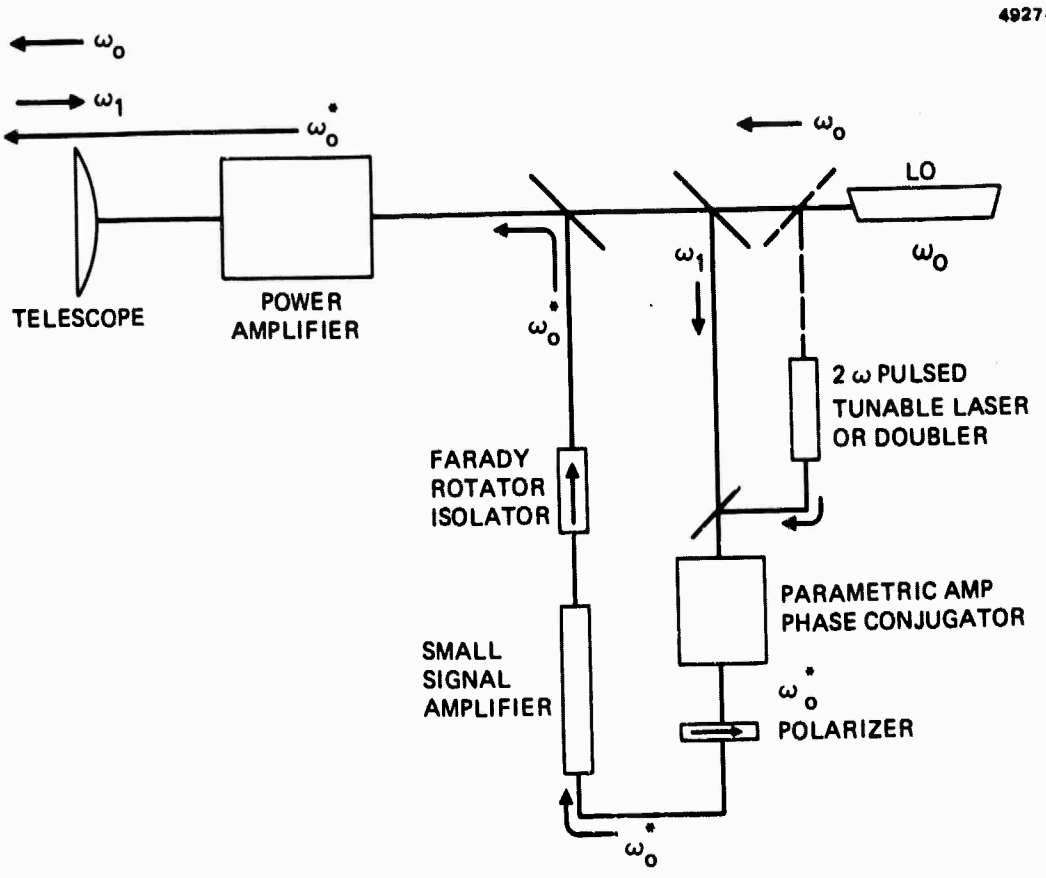

Figure 26. Phase conjugation scenario using three-wave mixing.

and sent back through the power amplifier to the target. One advantage of this process is the free choice of the frequency shift of the conjugate wave with respect to the input wave. A major disadvantage of this scheme is that the path containing the Faraday rotator isolator is not included in the conjugation process and is not corrected.

SECTION 4

SYSTEMS APPLICATIONS

A. SYSTEMS OVERVIEW AND SCOPE

We have tentatively examined several possible applications for nonlinear phase conjugation (NPC) systems. These applications fall basically into three categories: (1) local corrections for optical defiguring or local aberrating paths (e.g., laser media), (2) relay mirrors for path distortions up to but not including the relay mirror, and (3) target-referencing systems (for all classes of distortion). The basic objectives are (1) to identify any systems limitations that may occur because of the inherent nature of NPC and (2) to identify new techniques for using NPC that could have a major impact on systems design.

We have emphasized operation at visible wavelengths for two reasons. First, assuming that the required laser development is forthcoming, visible operation offers a major potential for improved overall system operation in future long-range systems. More explicitly, excepting turbulence-induced problems, the shorter wavelengths both offer reduced diffraction spreading and appear to be less susceptible to atmospherically induced nonlinear effects because of lower absorption. Second, it is only at visible wavelengths that the path compensation advantages of NPC systems strongly dominate those of conventional adaptive-optic systems. Specifically, a 4-m aperture operating at visible wavelengths through the atmosphere will require about 3,000 control systems and deformable mirror actuators or control points. Hence, NPC offers the potential of replacing a very complex system with a single NPC correcting device.

In summary, we believe that operation at visible wavelengths offers major advantages for ground-to-space missions, and that a large NPC system offers potential for compensating the substantial loss in performance produced by atmospheric turbulence and its secondary effects

(amplitude scintillation) that occur at visible wavelengths. That is, we believe that amplitude preservation (of the reference wave field) in the retransmitted wavefront may be essential for optimium correction at visible wavelengths and that NPC offers a promising way of achieving it.

Although we have high confidence, based on our experimental work, that NPC will achieve excellent compensation for laser beams that share a fully common path with the reference (or probe) wave, such a path is not easy to achieve in operational systems. For example, the point ahead angles required when operating against orbiting targets (although only tens of microradians) appear to cause sufficient lack of path commonality to degrade system performance badly. This effect, commonly called the point-ahead isoplanatic problem, is more fully discussed in Appendix D. Since no solution to this problem (at visible wavelengths) appears to exist, we have excluded this class of system from explicit consideration in this report.

The relay systems offer appreciable advantages in this respect. Specifically, one can position or fly a reference ahead of the relay* and thereby, in principle, fire the laser back over substantially the identical propagation path taken by the reference.** However, practical considerations associated with reference size motivate consideration of operational modes that do not employ a fully common laser and reference path, as discussed below.

Although isoplanatic effects provide the key argument against long-range target referencing systems, there are others. In many respects, the NPC system shares the same problems as the conventional phase-conjugate adaptive optical systems: (1) convergence time is limited by

---

*This concept (as far as is known) was independently conceived and proposed to NASA by Hughes and Rockwell International in 1974 proposals to transmit laser power from a ground station to a cooperative satellite.

**The surface and associated air mass of the Earth move a bit during the transit time from the top of the atmosphere to the surface and back, but this produces only a minor perturbation from path commonality.

(typically*) four or five round-trip propagation times and (2) with static targets, the (nearly diffraction limited) focused beam forms on the dominant glint or highlight as a reference, a reference that may "burn off" as operation proceeds, shifting the aim point to the next glint, etc. The generally proposed solution to this latter problem is to offset the laser beam from the reference by electronic override techniques (such techniques have been experimentally demonstrated). At the beginning of this contract, it was not self-evident whether such an offset could be achieved in an NPC system since its natural operation is to focus the laser beam directly on the dominant glint, and simple electronic tilt override is not possible. We have found, however, that it is possible to achieve an electrooptic tilt override by several techniques. One approach is to employ a four-wave mixer NPC by perturbing the pump angles and/or frequencies somewhat (this is discussed below).

Another problem that carries over from conventional phase conjugation systems is target-motion-induced Doppler shifts. These are generally removed in a conventional adaptive optical system by either a Doppler tracking local oscillator or electronically by a second (tracking) local oscillator downconverting the i.f. output of the optical heterodyne detector. Again, we have found that appropriate frequency and angle offsets of the pumps can achieve a frequency shift adequate for Doppler compensation. In fact, it is possible to achieve simultaneous pointing offset and Doppler compensation and yet maintain perfect phase matching in the four-wave mixer. (This is also discussed below.) Thus, although we do not explicitly consider target referencing systems in this report, we do consider two of the key problems associated with them since they share these problems with the relay systems.

System applications to local correction systems can be further broken down into the following categories for more detailed examination:

---

*Assuming that multiwavelength conjugation is feasible, multiwavelength operation decreases convergence time. However, if the amplitude distribution in the reference return wavefront must be preserved, this will considerably increase convergence time.

(1a) oscillator compensation, (1b) MOPA compensation, (1c) satellite-based optical train compensation. Likewise, several approaches to relay systems applications are considered. These systems employ NPC compensation for a ground-based system operating to an orbiting relay. The scope of the attempted wavefront correction progressively increases through this sequence. In applications 1a and 1b, the aim is primarily to correct for the laser medium distortions and, in some cases, for some of the intracavity optical elements. In application 1c, the key compensation is for an orbiting primary mirror and the lasing medium. In relay applications, the aim is to compensate the entire ground-based optical train, including the laser medium and the atmospheric portion of the propagating path.

We have included several structurally different approaches in each application; in particular, we have attempted to examine both oscillator and MOPA alternatives when they could be found. Further, we have included systems appropriate for both short pulse and cw (or long pulse) operation to best accommodate future development in laser technology. Although our major emphasis is on visible systems, we believe that the basic concepts are applicable at any wavelength.

While investigating the relay systems, we found that it is extremely desirable (perhaps essential) to provide both a tilt override capability (as previously discussed for target referencing) and a focus override (to prevent the conjugated wavefront from being simply retroreflected with a convergence equal to the divergence of the incident beam). This requirement comes about because the geometry of the transmitted beam and the reference beam may not be the same. In particular, it is decidedly convenient to use a reference that is much smaller than the relay mirror. At the extreme, we could have a situation in which the transmitted beam was essentially collimated and the reference beam was generated by a point source located (by approximately the point-ahead angle) ahead of the relay mirror. The geometrical difference in the paths taken by these two waves leads to both a focus offset requirement in the NPC system and to additional isoplanatic problems not present when the transmitted and reference waves have similar geometries.

B. SYSTEMS INVESTIGATED

1. Local Correction Systems

A limited, but nevertheless very important, application of nonlinear phase conjugation is to the internal compensation of oscillators and master-oscillator power-amplifier (MOPA) systems. The potential advantages over conventional intracavity adaptive-optics systems are (1) simultaneous correction on N laser lines, each with its own distortion, appears feasible; (2) much higher spatial-frequency distortions can be corrected; (3) very much higher bandwidth corrections can be achieved; and (4) ultimate cost should be lower because the system is intrinsically simple.

a. Oscillator Compensation

One basic approach to oscillator compensation is illustrated in Figure 27. In a general sense, three key elements are included: (1) a plane wavefront generator, (2) a lasing medium, and (3) a nonlinear phase conjugator. In the system illustrated, the plane wavefront is produced by a pinhole spatial filter, and the phase conjugator is an SBS system. To facilitate the discussion of these systems, we will use transmission optics and low-power implementations. In some cases, we will also discuss implementations and problems appropriate to high-power applications.

There are several fairly basic problems with the system depicted in Figure 27. First, there is a problem with pinhole burnout. Second, because the pinhole transmission with badly distorted wavefronts may, during initial start-up, reduce the ensemble gain below SBS threshold conditions, there is a problem with threshold start-up. Third, there are two problems with the beam splitter: a large portion of the plane wavefront returning from the pinhole is lost* by the splitter, and,

*The lost energy can of course be largely recovered by adding a mirror which redirects the beam back in the direction of the output wavefront. Such a recovery system must act like an interferometer so the correct phasing and angular orientations must be carefully maintained.

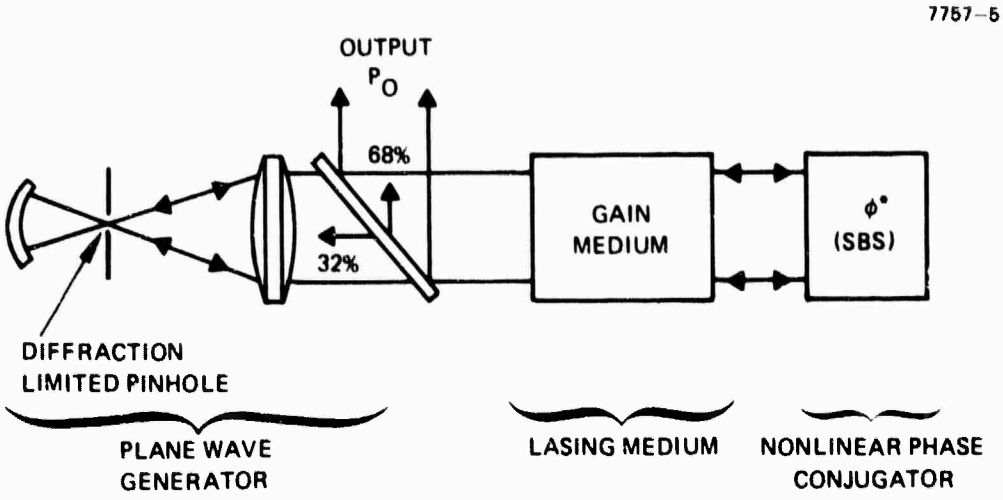

Figure 27. A basic approach to oscillator compensation. The beam splitter would be replaced by a diffraction grating at high power levels and the illustrated splitter ratio gives about 10% feedback.

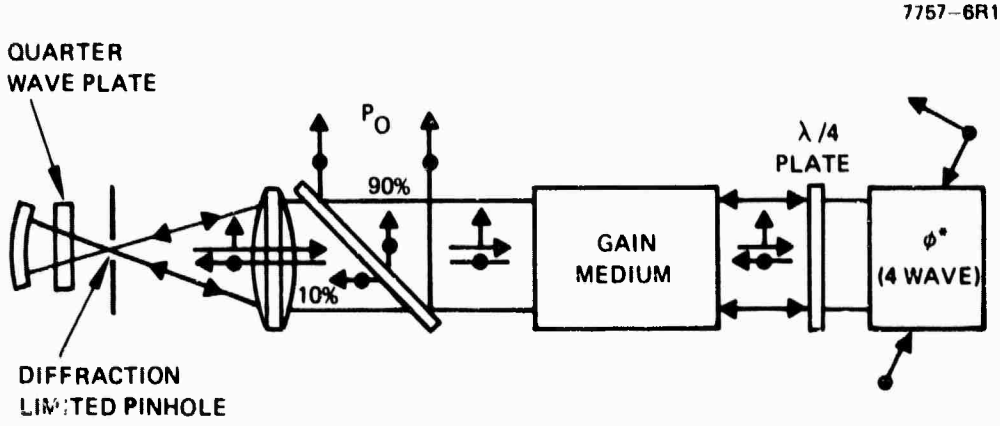

Figure 28. A more efficient approach to oscillator compensation. By employing a phase conjugator which rotates the plane of polarization and a polarization-sensitive beam splitter, the power lost by the splitter is largely avoided and the power density on the pinhole is reduced by a factor of three (for the same feedback).

consequently, the power density on the pinhole is higher than need be. Fourth, the frequency offset produced in a basic SBS conjugator progressively accumulates and eventually walks off the gain profile line width of the lasing medium.

In Figure 28, we have corrected some of these defects by incorporating a polarization switching phase conjugator using the polarization rotation schemes discussed in Section 3. Thus, the wavefronts reflected off the conjugator are polarized parallel to the splitter (normal to the plane of the paper), and the polarization of the wavefront transmitted back via the pinhole system is rotated by 90° by a double pass through a quarter-wave plate. The polarization plate is chosen to pass this polarization substantially without reflection. For example, it may be an interference filter operated near Brewster's angle for the filter, or it may be a diffraction grating chosen to give high efficiency at this polarization. Thus, for 10% feedback, for example, the beam splitter can be designed to transmit 10% of its incident energy to the pinhole, as contrasted to the 33% transmitted by the system shown in Figure 27. Further, the "lost" energy from the second pass of the splitter in Figure 27 is eliminated. To avoid the frequency walk off problem, we have replaced the SBS conjugator with a four-wave conjugator in Figure 28.

Figure 29 shows a pump supply to the system shown in Figure 27 wherein the sustained pump is achieved via oscillator feedback. Since the pump supply will not function during initial start-up, we have added a one-pulse pulsed oscillator, which supplies the required pump power during the start-up. We have taken advantage of the degeneracy of the four-wave mixing system to isolate the two types of pump by angular separation.

In addition to the technology problems presented by the phase conjugator, the pinhole, and the splitter elements, there are basic problems associated with the confocal resonator configuration associated with mode volume filling.

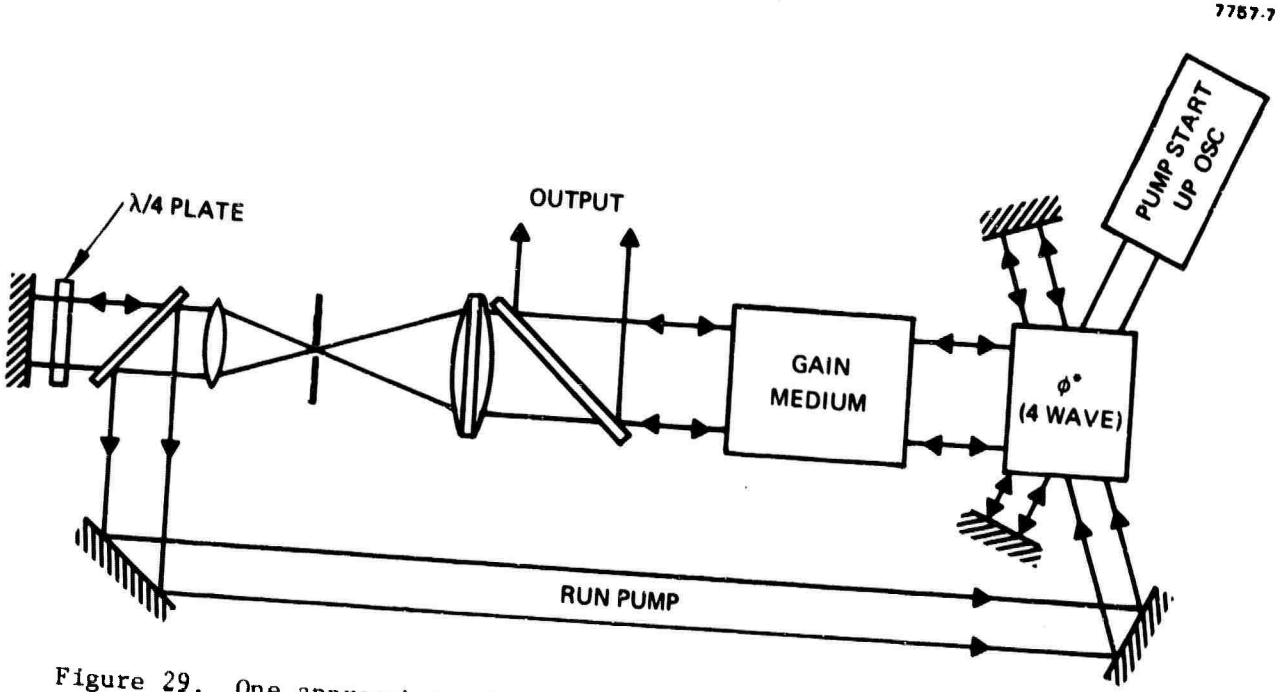

Figure 29. One approach to obtaining the pump waves. A pump start-up oscillator initially supplies the pump source. Once strong oscillations are initiated, the pump oscillator shuts off and the pump is supplied by feedback from the oscillator itself.

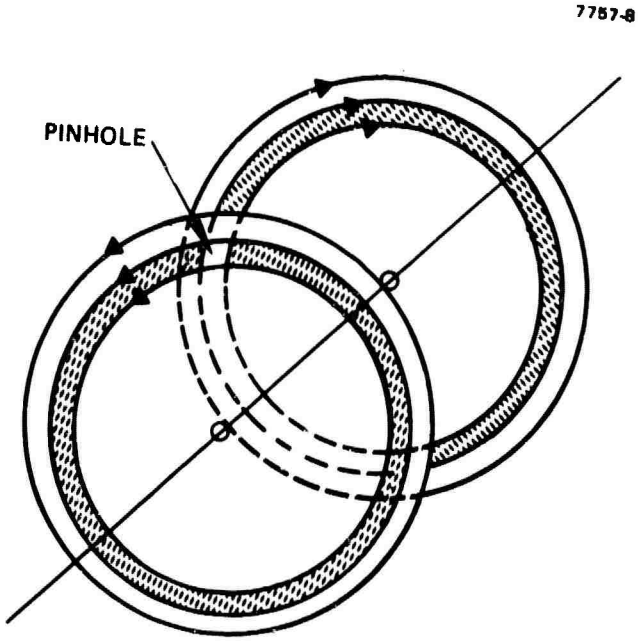

Figure 30. The "rotary" pinhole system. A pair of rotating wheels with an annular hole in each wheel forms a pinhole with rotary edges. In this way, heating at the pinhole edges is distributed over an area hundreds of times greater than with a conventional pinhole.

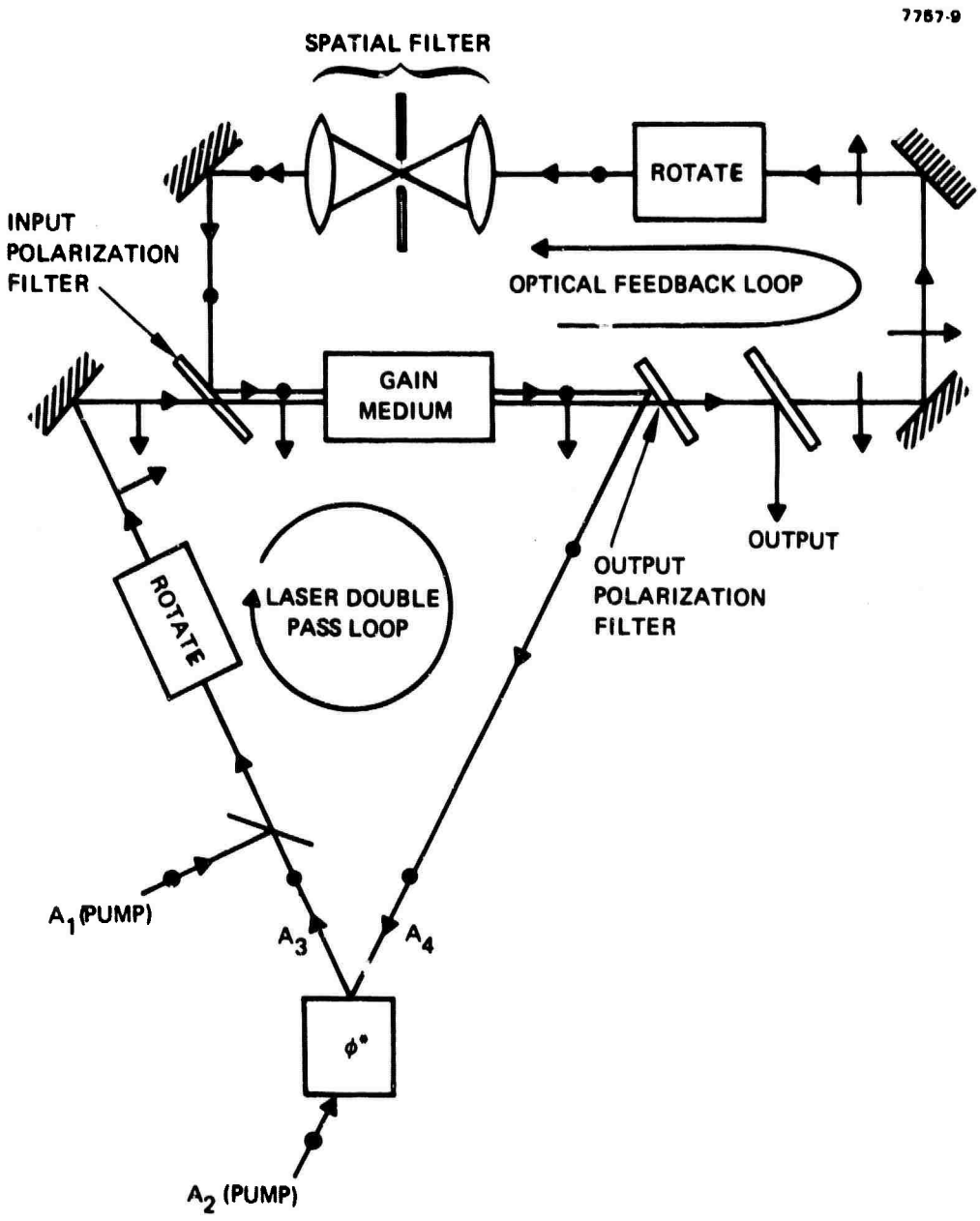

Figure 31. A "figure eight" ring laser oscillator with a phase conjugator for gain medium compensation. The gain medium is double passed in the same direction in two differing polarization states before exiting the output polarization separation systems.

We have explored alternatives (such as Fabry-Perot resonators) to the pinhole spatial filters without finding anything of strong promise. Currently, it appears that the best approach would be to use rotary metal disks to distribute the pinhole peripheral heating over a much wider area, as illustrated in Figure 30. The pinhole system should be somewhat canted such that reflected energy from the periphery of the pinhole does not re-enter the oscillator.

We have also explored several possible ring-resonator oscillator configurations; the most promising one to date is illustrated in Figure 31. Basically, the feedback follows a figure eight path. The upper loop of the "8" is the usual optical feedback loop, while the lower loop is a double-pass loop in which the polarization state of the wavefront transmitting the amplifier is first normal to the plane of the loop. The wavefront reflects off the output polarization filter to the phase conjugator, reflects as a conjugated wavefront, has its polarization state rotated to the plane of the loop, passes the amplifier once more, and then exits through the exit polarizer. Two optically active rotators are required to set up the double pass of the lasing media. Note that the phase conjugator is operating off-axis in a mode contrary to its natural functioning. This operation can be obtained in a four-wave conjugator, as described in Appendix E.

Another approach to the "plane-wave-make" element of the basic oscillator system is illustrated in Figure 32. This approach employs a four-wave mixer with pumps derived from the probe or signal wavefront as was the case in the oscillator system of Figure 29. In the present case, however, the distortions present in the probe wavefront are retained on the pump. For example, consider a wavefront distortion that is essentially a one-dimensional distortion with variation in the y direction. This distortion maps into a z-direction distortion in the pump field, thereby destroying the regular spacing in the gratings that reflect the probe wave. Thus, the grating efficiency is reduced by the dephasing of the scattered probe signal, and the reflected signal is accordingly

reduced. Accordingly, the single-pass gain for undistorted wavefronts is much greater than for distorted wavefronts, and the system will oscillate with modes that correspond to such wavefronts. Distortions in the orthogonal direction can produce corresponding reductions in gain by operating in tandem off a second four-wave mixer whose pump direction is normal to the original set.

b. MOPA Compensation

Because of the double-pass nature of phase conjugation correction systems, we have found that amplifiers are more natural candidates for correction than are oscillators. One approach to MOPA compensation is illustrated in Figure 33. In this figure the oscillator and amplifier are separately compensated. The oscillator system is basically the same as previously illustrated in Figures 27 and 28 with the mirror M_1 and the four-wave mixing conjugator forming the resonator system. A portion of the oscillator's circulating power is split out by splitter S_1, passes through the amplifier, is conjugated and rotated in polarization on reflection, and again passes through the amplifier, where the power level is increased and the amplifier distortions cancel in the second (output) pass through the amplifier. In order to improve

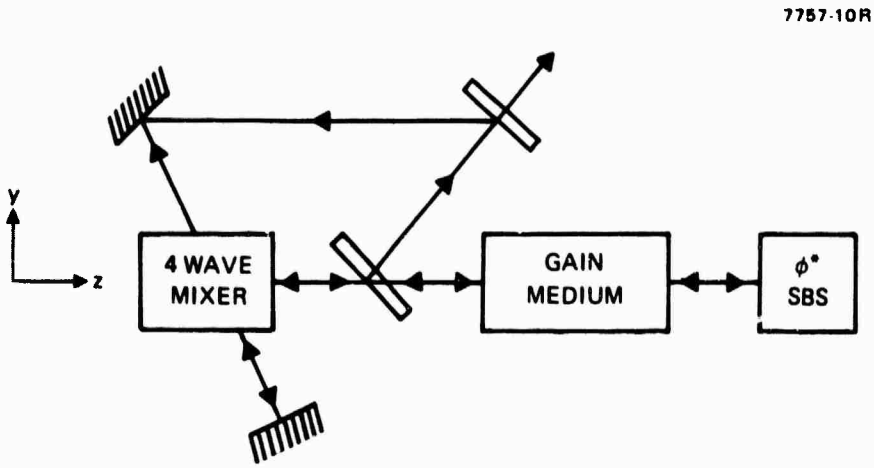

Figure 32. Oscillator with a nonlinear plane-wave generator. Functionally the four-wave mixer substitutes for the pinhole element of Figure 27.

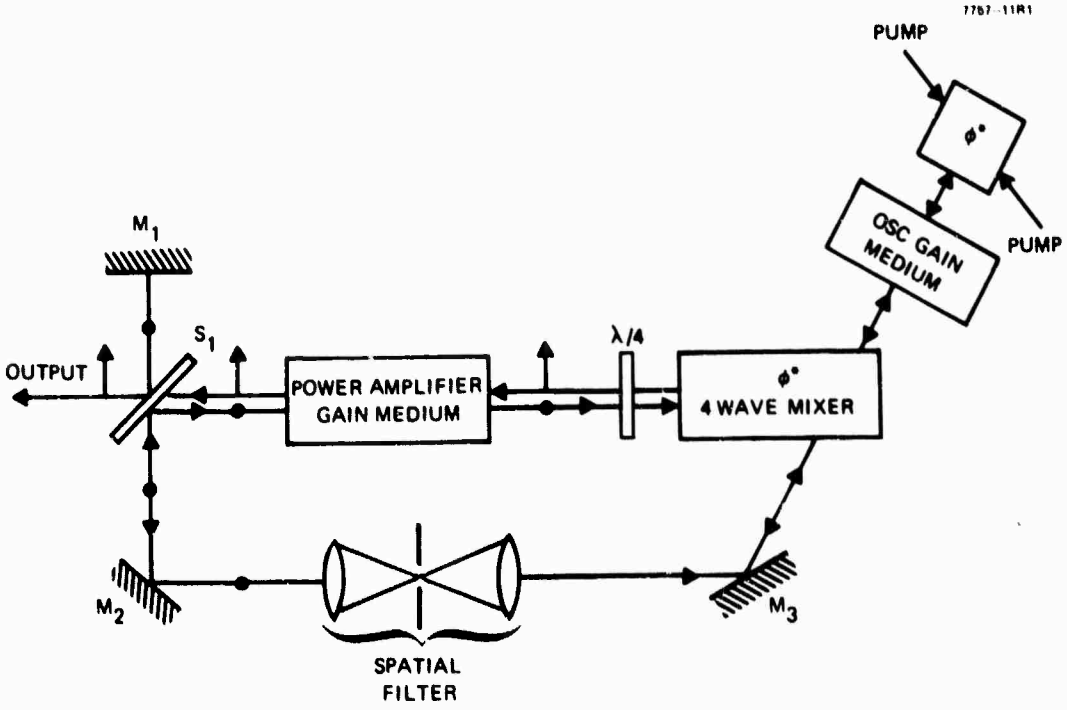

Figure 33. A MOPA system with separate phase conjugators to control the wavefront of the oscillator and the wavefront of the amplifier output.

coupling efficiency. The splitter S_1 is a polarization filter designed to pass substantially 100% of the wave that impinges on it polarized in the plane of the paper. Thus, polarization isolation minimizes the likelihood that feedback from the amplifier will capture the oscillator system. Note that the amplifier-compensating four-wave mixer is arranged in such a way that its pump fields are supplied by the circulating fields within the oscillator.

Many other MOPA configurations are feasible. However, since MOPAs are used exclusively in the systems that follow, we defer further discussion to the discussion of those systems.

c. Satellite Optical Train Compensation

This general systems concept is illustrated in Figure 34. Basically, this is a MOPA system in which the oscillator is injected into the power amplifier via a low-efficiency diffraction grating coupler embossed on the primary mirror. In this way, both the primary mirror and secondary mirror (and additional optical-train elements (not illustrated) as well as the gain medium of the amplifier are double passed. Thus, all these elements have their OPD distortions (largely) compensated by the familiar double-pass operation of the phase conjugator.

In more detail, the oscillator wavefront, which we assume to be of high quality, is focused* to a spot, most likely in the obscuration hole of the secondary, and diverges to fill the primary. A nominal percentage, say 1%, of this wavefront is diffracted off a shallow diffraction grating to a direction that is collimated with that of an undistorted feed source for the telescope. The remainder reflects in the zero order of the grating in the output direction. The grating is circularly symmetric, and its period is a function of radius because the required diffraction angles are a function of radius.

The diffracted component exits the telescope as a collimated beam if the primary and secondary are well figured, traverses the amplifier

*We have examined the feasibility of focusing to a diffraction-limited spot in a space environment on other programs. It appears that this can be accomplished without breakdown.

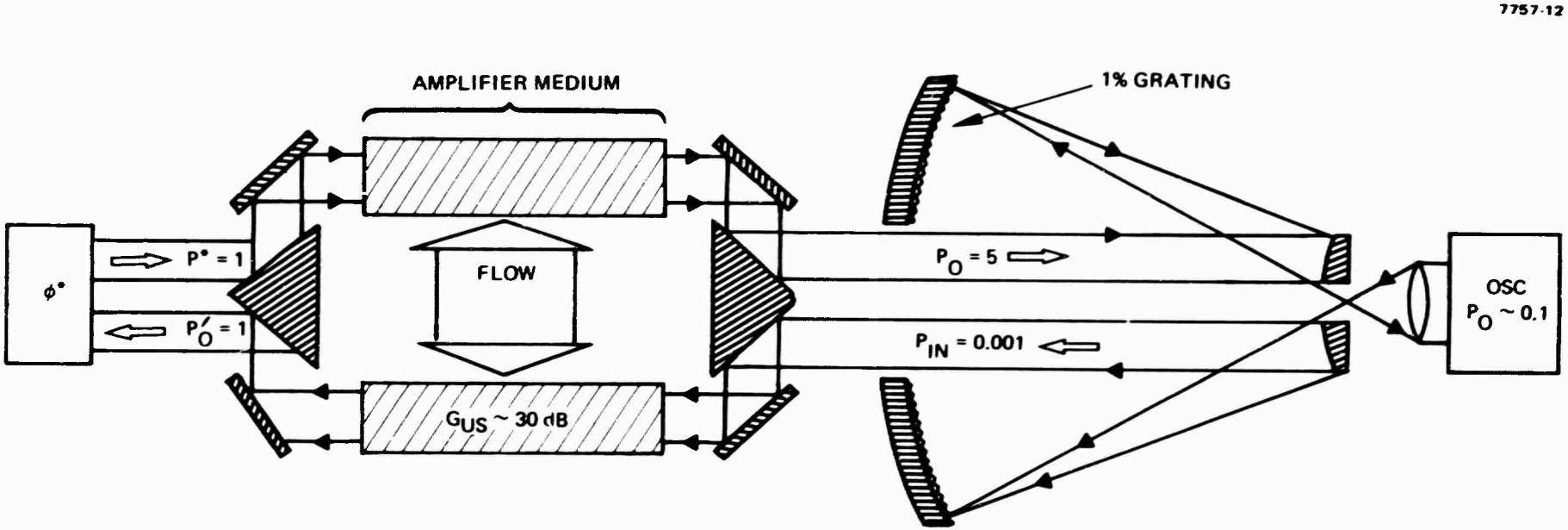

Figure 34. Satellite-based system. Although the power levels and flows are illustrated from right to left in the lower half and reversed above it will be understood that the actual power flows are two way over both paths.

and thereby picks up any media path distortions, is conjugate-reflected, again passes through the amplifier, and exits it with the amplifier distortions stripped off. The majority (99%) of the output power is reflected in the zero order off of the primary mirror and exits the system as a high-quality wavefront.

If the primary is distorted, then the double-pass system will also result in a very substantial primary compensation. However, with very large distortions, the angular differences between the reflected and injected wavefronts cause some deterioration in performance.

Although we have greatly relieved much of the requirement for precision optical figuring on the main telescope, the price has been a requirement for precision injection of the oscillator reference. More specifically, any distortions in the injected wavefront impinging on the primary are directly mapped onto the output wavefront. For example, if the injection focus is shifted a distance D, as illustrated in Figure 35, a change in optical path difference from the outer edge of the mirror to the inner (obscuration) edge will be produced; from the geometry of Figure 35, this change can be shown to be

$$\Delta\overline{OPD} = D(\cos\theta_{min} - \cos\theta_{max}) \quad ,$$

where θ_{max} and θ_{min} are the angles measured to these two edges, as illustrated in the figure. For typical values ($\theta_{max} = 30°$, $\theta_{min} = 6°$), this gives

$$\Delta\overline{OPD} = (0.13)D \quad .$$

Thus D must be held to a tolerance* of about plus or minus one wavelength to hold this class of induced error within reasonable tolerances; this is not an easy objective to achieve. Although this is only a focus

*This tolerance is not unique to NPC-type systems. It is a typical problem with all local referencing wavefront-error-sensing/compensation systems.

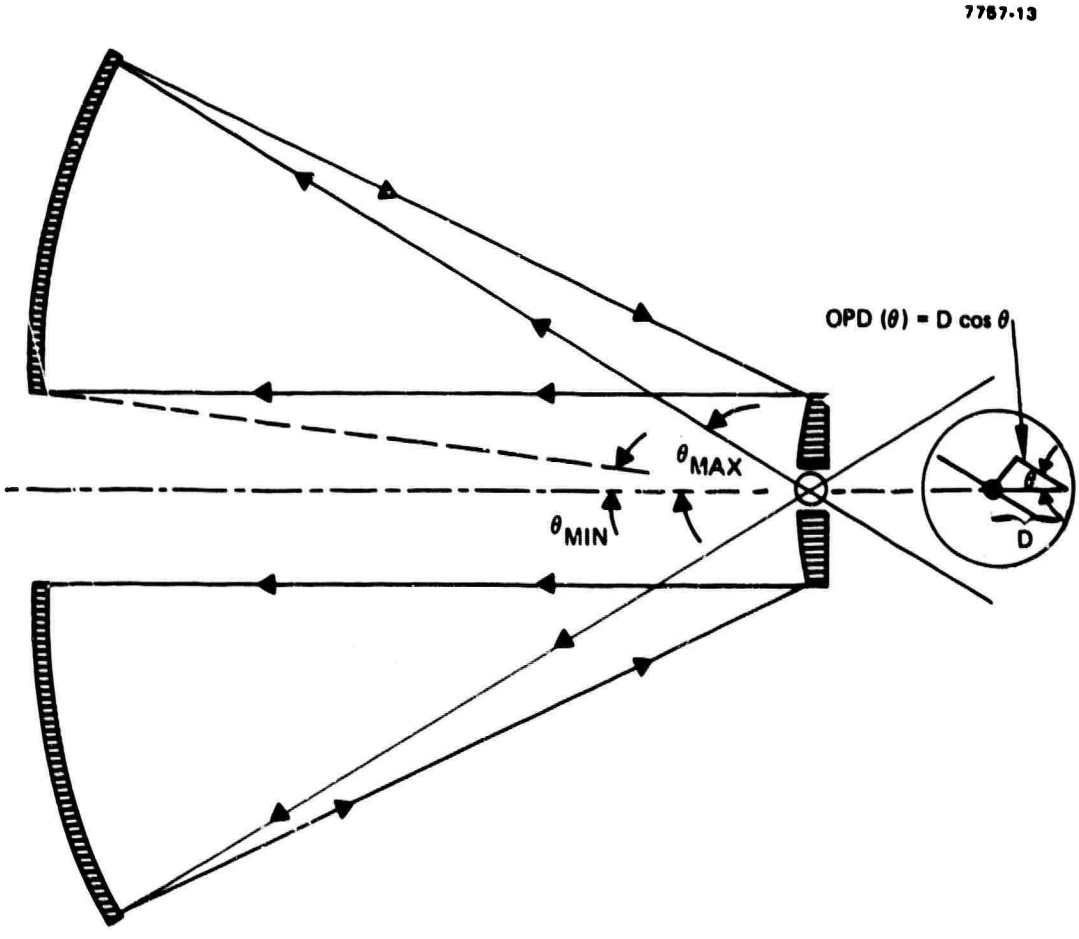

Figure 35. Geometry for tolerance investigation of the injected focus position.

error to first order, it is not clear how one could obtain the information to compensate it.

A small amount (nominally 1%) of the power radiated from the primary is diffracted back into the oscillator system, where (at higher levels) it presents a problem in its potential for capturing the oscillator. It is this feedback problem that has forced us to employ a low-efficiency grating and concomitant high-power oscillators. We discuss more sophisticated approaches to feedback suppression below.

If high oscillator power levels must be used, then the nominal oscillator of Figure 34 may become a MOPA system (as in Figure 33, for example). One way of implementing an intermediate power amplifier is to "reflex" or iterate the basic concept, as illustrated in Figure 36.

Another method of attacking the feedback problem is to use a quarter-wave plate ahead of the conjugator to rotate the plane of polarization in the second pass. The grating coupling could now be increased to 5 to 7% with a decrease in required driver power by a factor of five to seven. The 5 to 7% feedback power is suppressed by a polarization filter between the primary and the oscillator.

2. Orbiting Relay Systems

a. Basic System Configurations

Basically, we have considered three classes of satellite systems in which we are transmitting power to a satellite relay, as illustrated in Figure 37. In all three systems, a four-wave mixer called ϕ^* is used to compensate the propagation path distortions introduced by the atmosphere, the ground-based optical train, and an aberrating laser medium.

All three systems employ MOPA laser configurations, in which a well-controlled wavefront (generated by a reference oscillator) is used to probe the path distortions. For the moment, we take the satellite to be frozen in orbit for conceptual purposes. System A is a cw or long-pulse system that locates the oscillator on the satellite. The reference

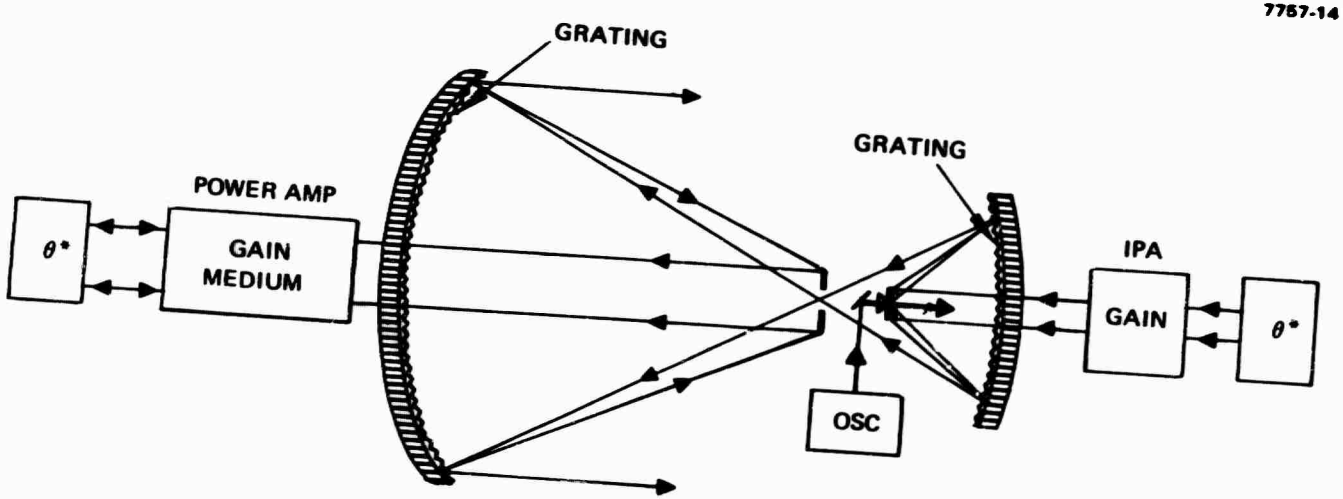

Figure 36. A reflex system in which the oscillator of Figure 34 is replaced by an intermediate power amplifier (IPA) which is again decoupled from the oscillator by a second diffraction grating.

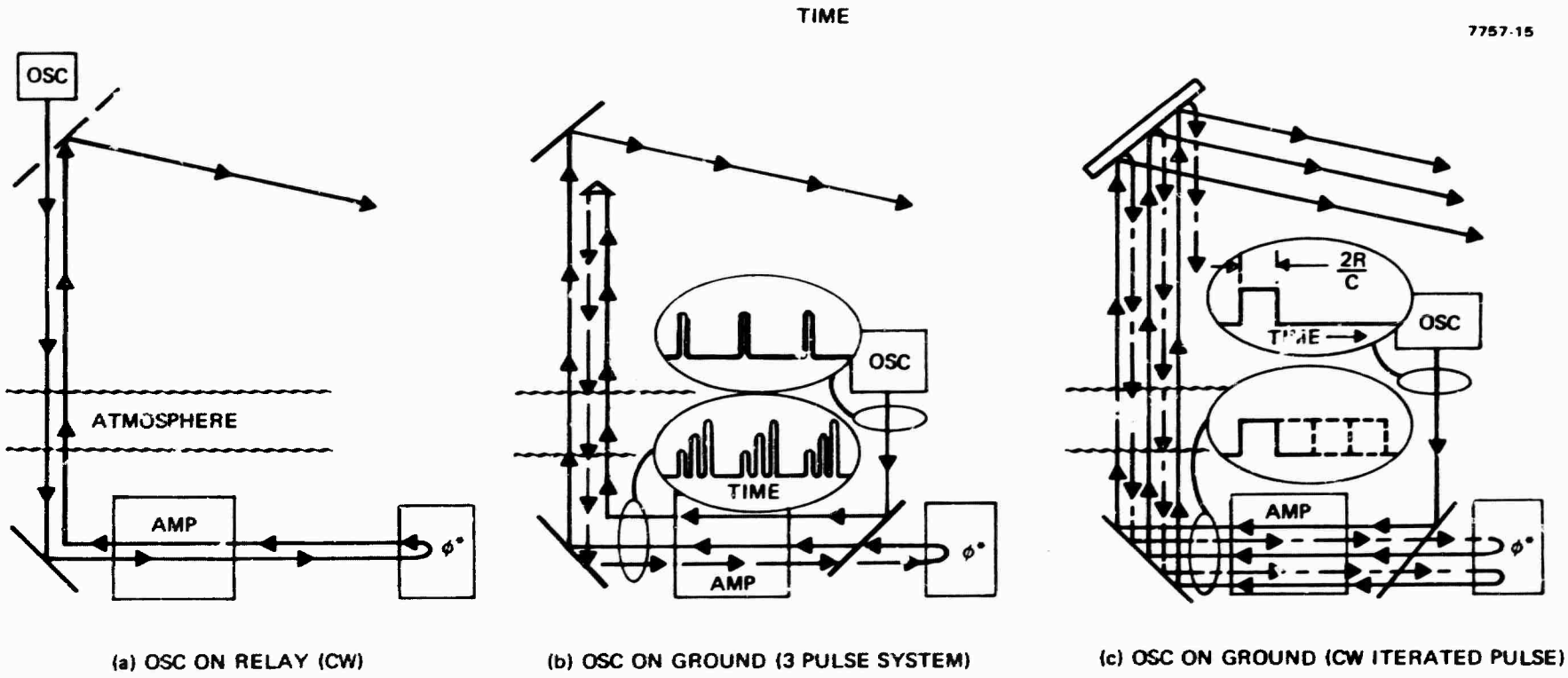

(a) OSC ON RELAY (CW)

(b) OSC ON GROUND (3 PULSE SYSTEM)

(c) OSC ON GROUND (CW ITERATED PULSE)

Figure 37. Propagation path diagrams for three classes of relay system.

oscillator output wavefront, which is assumed to be undistorted, transmits downwards "through" the relay mirror, picks up (probes) the atmospheric and amplifier distortions, "reflects" from the phase conjugator, is again amplified, retransmits through the beam director and the atmosphere, and exits the atmosphere as an undistorted beam.

System B employes a ground-based reference and injects a train of short pulses (nominally about 1 μsec) at a desired pulse repetition frequency. Each injected oscillator pulse generates a triplet of pulses (as illustrated in Figure 37), spanning (roughly) the round-trip propagation time in duration. The first pulse of the triplet reflects off a corner reflector or other retro system, returns after the round trip delay as a second pulse with superimposed atmospheric/amplifier distortions, is conjugated and reamplified, and returns to the satellite relay mirror as the higher-power and wavefront-compensated third pulse of the triplet. The conjugator or amplifier is then temporarily deactivated such that no further iterations occur before the next oscillator pulse is injected into the system.

System C is similar except that a longer oscillator pulse (equal to the round trip time) is employed and the oscillator is shut off after the initiating pulse. The system gain is controlled such that the system iterates indefinitely on the initial pulse, giving a system operation that is effectively cw (i.e., a system that transmits continuously for several seconds or more). For conceptual purposes, we have shown the retro-reflector in this case as a number of mini-retros embedded in the relay mirror; however, in fact it would be a more conventional retro-reflector located in front of the relays, as discussed below.

We have identified three basic classes of functional problem that occur in all of these systems. First, during the round trip propagation time, the reference moves from its old position in such a way that the system points behind. That is, it refocuses back at the old, rather than the current, reference retro or oscillator position. Second, each

received pulse is generally Doppler shifted in frequency from that of the oscillator, as illustrated in Figure 38. In fact, with the System C, the Doppler shift progressively accumulates such that the return pulses will eventually have their line center shifted off of the gain line profile, and the system will cease to amplify (and to operate). Third, with small references, the conjugator system refocuses to the dimensions of the retro or reference oscillator, or as closely as it can subject to diffraction limitations, whereas the desired focus on the laser beam corresponds to a full illumination of the relay mirror.

The best solution to the "point-behind" problem is to locate the reference oscillator or retro system in front of the satellite relay mirror by a distance corresponding to the point-ahead angle (thereby minimizing the isoplanatic problems associated with point-ahead systems). Further, it avoids the problem of having to operate "through" or "around" the relay mirror. We will call this the "carrot-on-the-stick" approach, as illustrated in Figure 39. The required angular separation between the reference and the relay (centers) is

$$\theta_p = \frac{2v_o}{c} \cos\theta \quad , \tag{1}$$

where v_o is the orbiting tangential velocity, c is the velocity of light, and θ is the azimuthal angle. Unfortunately, since the required exact spacing is a function of the azimuthal angle, it varies with overhead position and time. Specifically, the stick distance (Figure 39) is

$$x_{stick} = \frac{\Delta\theta_p}{\cos^2\theta} = \frac{2H}{\cos\theta}\left(\frac{v_o}{c}\right) \quad . \tag{2}$$

Thus, we believe the most practical approach will be a fixed stick spacing together with minor (time-varying) point-ahead/behind. We have examined the residual isoplanatic degradation resulting from choosing

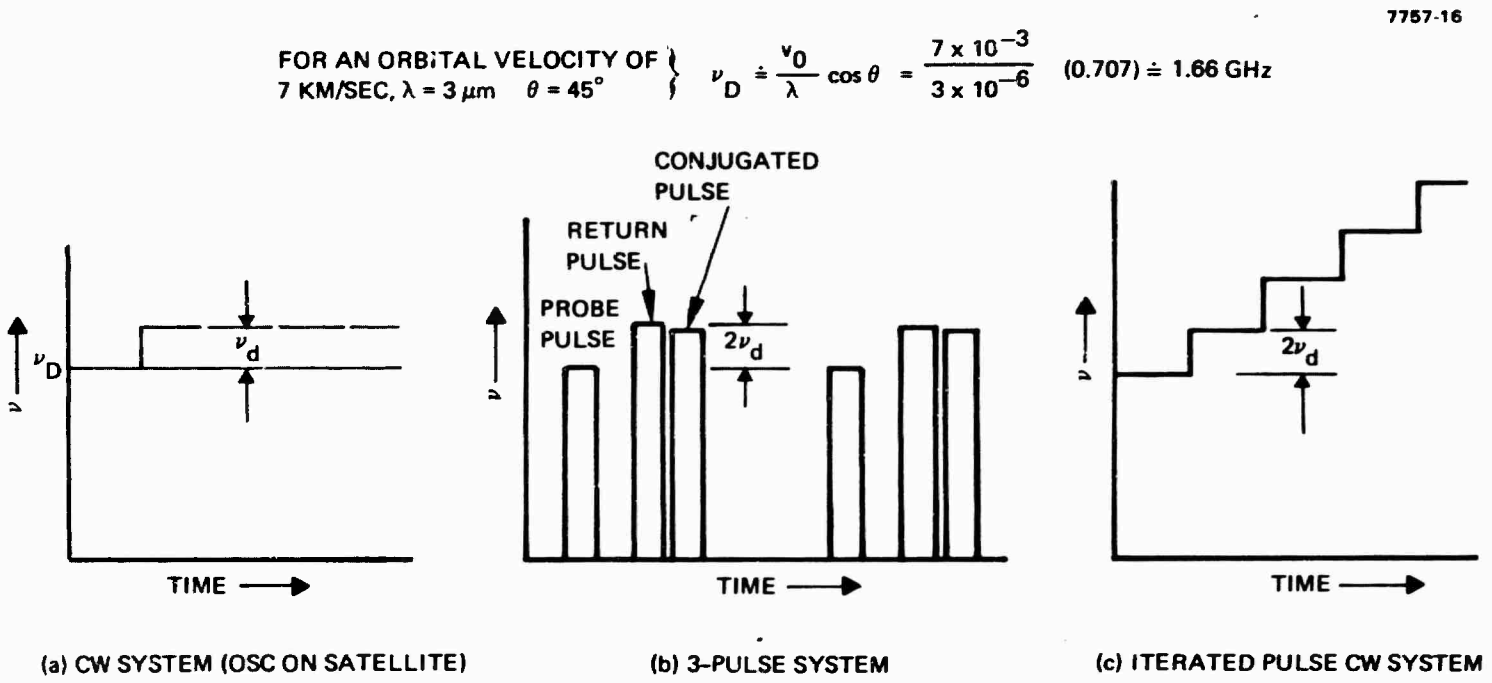

Figure 38. Doppler offset dynamics in three classes of systems.

x_{stick} at compromise θ angles of 22.5° and 30°, at λ = 3 μm, and found it to be small. It will be more serious at visible wavelengths, but we have yet to quantify it.

In any event, given a fixed stick length, one is faced with the combined problem of generating angular and frequency offsets in a system that generally does not accommodate them in the elementary forms illustrated in Figure 37. However, we have found that it is possible to generate these offsets by several approaches (as discussed below). We call these subsystems "override" systems since they override the natural tendency of the conjugator.

In spite of the Doppler and point-ahead problems, which are incurred as a consequence of the orbital motions, there are offsetting benefits. Since the reference oscillator or corner is well ahead of the relay mirror by the time the high-power phase-conjugated beam arrives at the relay mirror (Figure 39(d)), the feedback coupling into the oscillator (system A) or the reference corner (system B) is minimized. If this angular spatial separation is not adequate to suppress the main beam feedback to the desired levels, the polarization separation techniques previously discussed in the OSC/MOPA compensation sections can be used. Note, however, that this decoupling presents a problem to the cw iterated pulse system (system C of Figure 37). In particular, we desire to form a well-collimated, mildly converging beam centered on the relay mirror, yet we must simultaneously illuminate the reference with sufficient energy to return a pulse of adequate strength to the ground system to establish the next iterated pulse. A rough calculation suggests that there is not adequate energy in the sidelobe structure of the main beam to give the feedback desired for the system (typically we would design for 2% total feedback with 10% of the main beam being extracted for the reference retro). We have identified two possible solutions to this problem. One approach is to extract a portion of the beam from the vicinity of the relay mirror and to transfer it to the reference site by a mini relay system. The other approach is to split the override

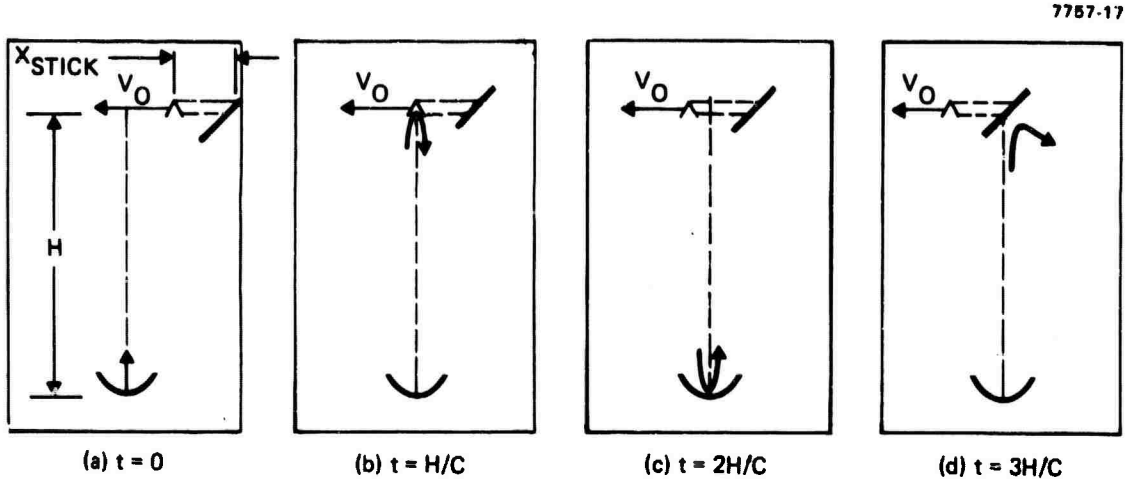

Figure 39. Time progression of a pulsed wavefront in a carrot-on-a-stick retro system. In the ideal system the initial pulse is launched to point ahead of the corner reference (a), intercepts it and is retro reflected. (b), is reflected and conjugated at the ground station (c), and intercepts the relay mirror on axis (d). Since the conjugated wavefront retraces exactly the same path the isoplanatic problem is minimized.

system in such a way that it generates two beams, one (90% of the energy) centering on the relay and the other (10% of the energy) centering and focusing on the retro. Either approach extracts the reference with high efficiency. With the simpler split beam approach, the beam centered on the retro will be pointed ahead and thus will traverse a somewhat different atmospheric path (i.e., it will be subject to isoplanatic effects). This does not matter for small retros.

Systems B and C can obtain improved oscillator injection efficiency by means of a polarization-sensitive beam splitter and a polarization rotator on the satellite. For this purpose, a quarter-wave plate backed by a cats-eye retro system could replace the corner reflector. In this application, the phase conjugator should be designed to reflect with the inci. ' polarization state.

C. FOCUS, TILT, AND DOPPLER OVERRIDE SYSTEMS

As discussed in the previous section, the natural tendency of a basic nonlinear phase conjugator is to return the energy at the effective frequency of the reference to an aimpoint centered on the reference, with a focus corresponding to the divergence exhibited in the radiated wavefront of the reference. For those cases where the reference is moving and is not located on the target, the basic system may miss the target as well as one or more additional key system objectives. More specifically:

- The motion of the target or of a relay satellite in a relay system during the reference pulse transit time may provide a complete miss.
- For systems like the relay systems where the reference is not on the target, the natural focus provided by the conjugator is generally incorrect for focusing on the target. Even with target referencing, the target motion during the reference propagation time may produce some focusing error.
- The Doppler shift of the reference or the target may cause the returning wavefront and the conjugated wavefront to be sufficiently shifted in frequency to fall outside the gain profile of the lasing medium.

Since these problems would significantly degrade the performance of our projected system, we believe that some type of "override" on the basic conjugator operation will be required to compensate for them. We have identified two basic approaches to such override systems. First, the outgoing and return paths can be effectively separated such that tilt, focus, and frequency changes can be introduced on only the outgoing path.* As discussed below, the path separation may be either temporal (limited to short pulse systems) or spatial (via polarization separation). Second, an appropriate perturbation can be introduced in one or more pump angles and frequencies such that the retro wavefront retains its conjugated properties but has a shifted frequency, tilt, or focus as a consequence of the pump perturbations.

1. Override by Path Separation

This subsection discusses temporal and spatial techniques for focus and tilt override. Frequency override can in principle also be incorporated by including a frequency-shifting unit (such as an accounts optic cell), but this will not be discussed in detail.

Temporal techniques require short pulse operation, and we will use the three-pulse satellite system discussed above as an example. We have added a gated override box to the system in Figure 40(a), and in Figure 40(b) we have illustrated one approach to constructing the gated override. Basically, just following the passage of the tail end of the return probe pulse through the electrooptical element, a high-speed switch (such as a thyratron) transfers a fixed voltage (and charge) onto the electrooptical electrodes via a capacitor precharged to a voltage appropriate to a prescribed tilt and focus override. The tilt system consists of cascades of prisms with alternating directions of the transverse electric field on successive prisms. A one-dimensional focusing element that uses the alternation principle is also illustrated. The

*The outgoing path is conceptually the more natural location for the override system, but the incoming path will serve equally well with inverted (reversed) override perturbations to those actually required.

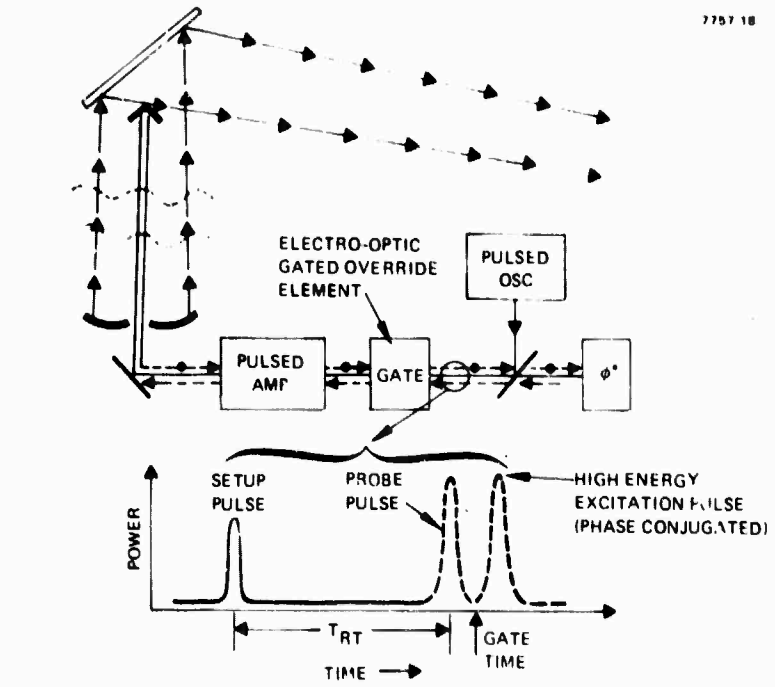

(a) THE GATED OVERRIDE ELEMENT, APPLICABLE TO SHORT PULSE (< 1 μSEC) SYSTEMS

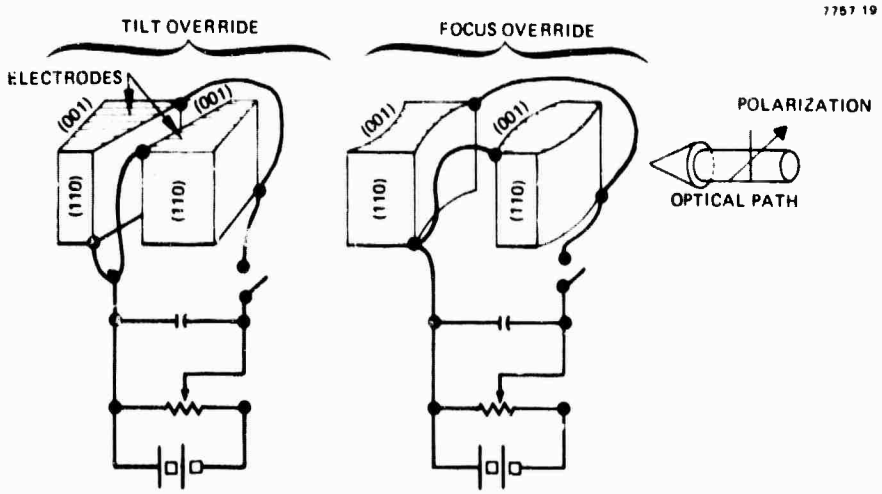

(b) ELECTROOPTIC TILT AND FOCUS OVERRIDE SYSTEMS. THE BLOCKS WOULD BE CONSTRUCTED OF CdTe FOR IR WAVELENGTHS.

Figure 40. Time gated override techniques.

extension of the focus system to two dimensions involves some complexity, which takes us beyond our present scope, but solutions have been worked out.* The electrodes of the system are discharged following the transit of the third, or high-energy, excitation pulse. The discharged process is allowed to be more leisurely since it need only be completed before the onset of the next oscillator initiation pulse of the next three-pulse sequence. If the corner movement does not quench the potential fourth pulse, the deflection potential of the electrooptical element, possibly with an associated pinhole, can be used to quench the fourth pulse return to the conjugator. For example, this could drive it below the threshold of an SBS conjugator.

In the second class of path-separation systems, illustrated in Figure 41, a four-wave-mixer conjugator is used. It switchees the (linear) polarization state of the incident signal wavefront. This permits the outgoing and returning wavefronts to be effectively separated with high efficiency. The polarization state reflected off of the reference retro system is similarly switched in this instance by a double-pass through a quarter-wave plate. Thus, the outgoing wavefront is everywhere horizontally polarized, and the return wavefront is everywhere vertically polarized. The brewster-angle multiplayer filter is only one of several possible techniques for achieving polarization separation. At 3 μm or longer wavelengths, diffraction grating systems will undoubtedly be the preferred approach.

2. Pump Perturbation Override Systems

We have found that it is also possible to perturb the wavelengths and angles in the pump source of a four-wave mixing conjugator in such a way that: (1) the Doppler shifts are cancelled in the phase-conjugated wavefront by the pump frequency perturbations, (2) the conjugated wavefront is returned with the desired small angular offset to yield the

*For example, see J.F. Lotspeich, U.. Patent No. 3,892,469, "Electro-optical Variable Focal Length Lens Using Optical Ring Polarizers," July 1, 1975.

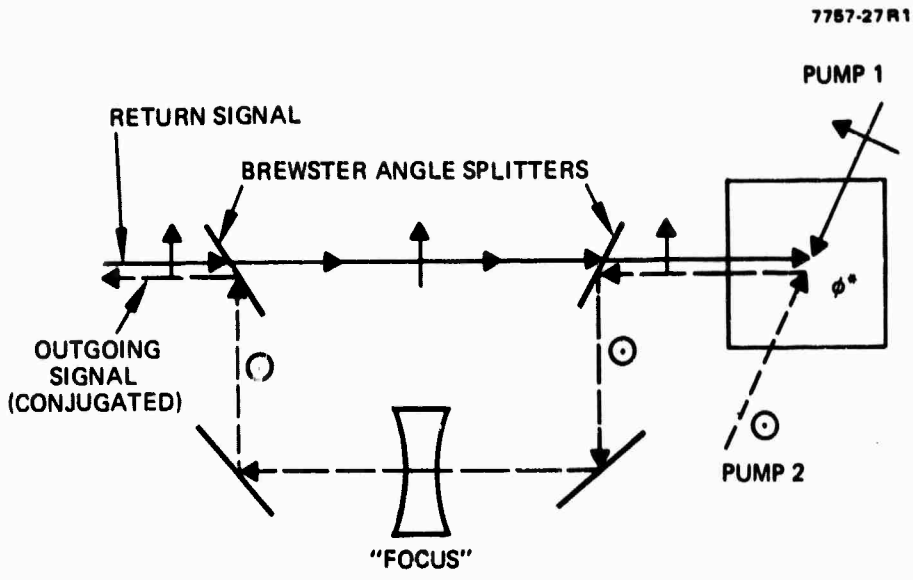

Figure 41. Focus override by path splitting by polarization rotation via pump manipulation.

point-ahead adjustment, (3) exact k-vector matching (for efficient mixing) is retained, and (4) at least a partial focus override correction can be incorporated. The system configurations that permit these overrides of the basic conjugator operation are discussed in Appendix D. In addition, the sizes of the required pump perturbations are quantified in the appendix. The approach will accommodate either a full point-ahead correction or a partial correction with the carrot-on-the-stick approach.

D. ISOPLANATIC EFFECTS ASSOCIATED WITH THE EXTENT OF THE REFERENCE

As mentioned in the introduction, even when the reference is moved ahead of the relay by exactly the point-ahead angle, there are additional isoplanatic problems that occur with a relay system operating in low orbits. These problems are associated with the fact that it is generally impractical to make the reference with an extent comparable to that of the relay mirror. In particular, as illustrated in Figure 42, it is advantageous to use a reference that has a small aperture to hold down system cost and to minimize OPD errors associated with the reference optics (which would be impressed on the main laser output with any type of conjugation system). As illustrated, from a ray optics viewpoint, there is an angular shift θ_F between the reference rays and the beam rays that is typically 10 to 20 μrad at the outer rays for low-altitude orbits. A broad comparison of these numbers to the results given in Figure D-4 of Appendix D strongly suggests that this class of isoplanatic effect, which we call "focus mismatch," will be troublesome at visible wavelengths. There does not appear to be a significant focus mismatch problem, even for point source references, for the synchronous orbit problem since the offset angles are too small.

Although we believe this is an important problem deserving of further study, it appears to be a basic problem associated with referencing from relay systems at visible wavelengths and one that is independent of the adaptive optics system employed, be it an NPC or a conventional system.

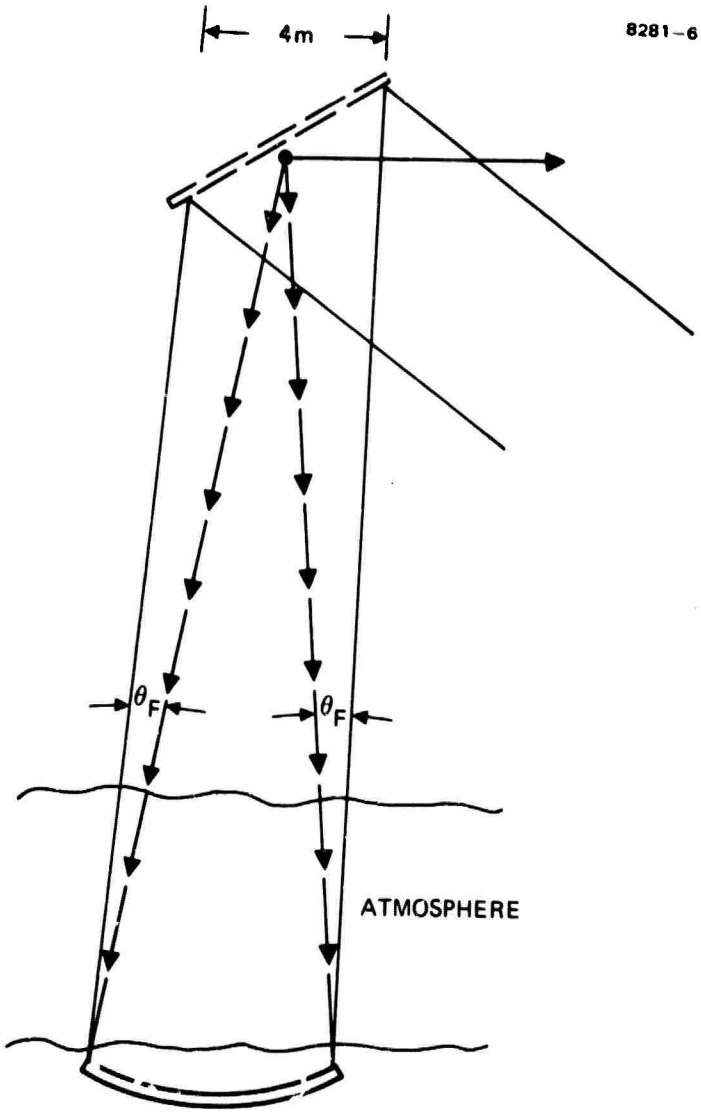

Figure 42. The focus-mismatch isoplanatic problem. In this system, a point reference files ahead of a relay mirror such that the reference beam and the laser beam are coaxial in space. However, because the laser beam is not focused on the reference, there is not an exact overlap on the reference and laser paths.

REFERENCES FOR APPENDIX C

1. A. Yariv and D. M. Pepper, Opt. Lett. 1, 16 (1977).

2. R. L. Abrams and R. C. Lind, Opt. Lett. 2, 94 (1978); 3, 205 (1978).

3. F. W. Block, Phys. Rev. 70, 460 (1946).

4. A. Yariv, Quantum Electronics, Second edition (Wiley, New York, 1975).

5. R. P. Feynman, F. L. Vernon and R. W. Hellwarth, J. Appl. Phys. 28, 49 (1957).

6. This procedure seems to be justifiable only when the lower of the two resonant states is the true ground state. I am indebted to M. Sargent for clarification of this point.

7. A. J. Palmer, "Radiatively Cooled Vapors as Media for Low Power Nonlinear Optics" (to be published).

8. R. P. Feynman, Phys. Rev. 76, 769 (1949).

9. B. D. Fried and S. D. Conte, The Plasma Dispersion Function (Academic Press, New York, 1961).

10. P. F. Liao, D. M. Bloom and N. P. Economou, Appl. Phys. Lett. 32, 813 (1978).

APPENDIX A

Reprinted from OPTICS LETTERS, Vol. 2, page 4, January 1978

Correction of phase aberrations via stimulated Brillouin scattering

Victor Wang and Concetto R. Giuliano

Hughes Research Laboratories, 3011 Malibu Canyon Road, Malibu, California 90265
Received August 16, 1977

We have obtained quantitative measurements on the correction of severely aberrated laser beams using stimulated Brillouin scattering (SBS) at 0.69 μm. We have shown that under certain conditions SBS can be used to restore an aberrated optical beam to its original unaberrated condition. When an optical beam double passes an aberrating region after reflecting from an "ordinary" mirror (i.e., a plane mirror) the aberration is twice that obtained from a single pass. However, when the aberrated beam enters a medium that allows SBS to occur, it emerges from its second pass through the aberrating medium in the same condition as that in which it originally entered. Quantitative experiments are described in which a single-mode ruby laser beam is intentionally aberrated by passing it through an etched plate. When the beam is allowed to double-pass the plate using an ordinary reflector (i.e., plane mirror), the beam divergence is more than 10 times the diffraction-limited divergence. However, when we replace the ordinary reflector with a cell in which SBS can take place, the SBS reflected beam is restored to diffraction-limited divergence when it is allowed to pass back through the aberrating medium. Applications of this time-reversal or phase-reversal technique for correcting aberrations in optical trains and atmospheric turbulence are discussed.

The correction of aberrations introduced by the atmosphere or by optical components in the propagation of laser beams is of great interest and current activity.[1,2] Adaptive optics techniques currently under development for reducing the effects of atmospheric turbulence and/or optical train distortions on laser beams [e.g., coherent optical adaptive techniques (COAT)] involve systems that adjust the phasefront of the transmitted beam to compensate for phase aberration by monitoring backscatter from the target. The correction is accomplished by using some form of discrete, multichannel, phasefront corrector driven by electronic servos, such as a deformable mirror.

In contrast, certain nonlinear optical interactions can generate the spatial phase conjugate of a distorted wavefront, which then can be transmitted through the original distorting optical path to form a corrected beam (the return beam from a glint upon a target contains all the necessary information to correct for the atmosphere's distortion). These nonlinear interactions automatically perform a phasefront correction that is spatially continuous over the entire cross section of the beam without any external wavefront sensing or electronic controls and may well have an economy, speed, and simplicity beyond conventional adaptive optical schemes.

The work described here represents the first report of a quantitative experimental evaluation of phase conjugation derived through a nonlinear optical effect. We also describe a concept where this effect can be used to correct the aberrations of a laser transmitter propagated through a turbulent atmosphere.

The basic concept of nonlinear phase conjugation for laser beam correction through the atmosphere is shown schematically in Fig. 1. The process may be described as occurring in the following steps:

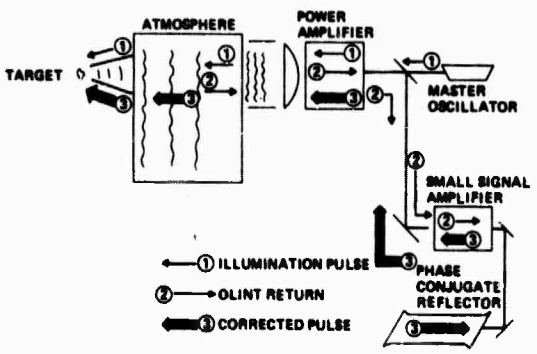

Fig. 1. A conceptual pulsed laser system using SBS for correction of atmospheric and laser-induced distortions.

1. The first transmitted pulse propagates to the target, assumed for the purpose of this example to be a single unresolved glint. The purpose of this first pulse is to illuminate the glint target, which then serves as a test source at the wavelength of interest.
2. The light reflected from the glint propagates through the distorting medium toward the transceiver, arriving as an aberrated wavefront.
3. The phase conjugate of this distorted return wave is generated by a nonlinear optical conjugator.
4. After coherent amplification to a desired power level, the phase-corrected pulse retraverses the distorting atmosphere, which now restores its phase coherence so that the entire beam is focused.

The weak backscatter to be expected from a distant target would suggest that a very-high-gain amplifier would be necessary to overcome the losses. In the last few years the technology for this high gain has been developed for 1.06- and 10.6-μm laser-fusion systems.

0146-9592/78/0100-0004$0.50/0

A gain of nearly 60 dB has been demonstrated, and this appears consistent with operation over a range of several kilometers.[3]

An example of a nonlinear process that possesses the ability to create directly the wave whose field is the complex conjugate of a signal wave is stimulated Brillouin scattering (SBS). It was first noticed in 1965[4] that the backscatter from SBS possessed the peculiar property that, if the incident laser beam was diverging, the backscattered light formed a converging beam of matching cone angle. Zel'dovich *et al.*[5] and Nosach *et al.*[6] have reported the ability of SBS to compensate for aberrations in a ruby laser beam. Zel'dovich[5] and recently several other Soviet researchers[7] have given semiquantitative arguments that the backscattered light of SBS can everywhere retrace the path of the incident light and is equivalent to the spatial phase conjugate wavefront of the incident light. The conjugate field can be viewed as equivalent to the incident field traveling backward in time.[8,9] Nosach[6] used this effect to compensate for aberrations in a ruby amplifier rod.

In view of the importance this process might have to adaptive optics and because of theoretical uncertainties accompanying our present understanding of this process, we have prepared the experiment shown in Fig. 2, following closely the work of Nosach *et al.*,[6] especially in the design of the highly multimode waveguide CS_2 cell. A TEM_{00} single longitudinal-mode ruby oscillator passively Q switched by a dye cell provides an output pulse of 17-nsec duration. This is amplified and then controlled by an adjustable attenuator to deliver about 25 mJ to the SBS cell.

An aberration can be purposely introduced into the beam at position 2 or 3 in Fig. 2 to test the corrective properties of SBS backscatter. The aberrator is a microscope slide etched in HF. The original beam quality is monitored by placing a partially reflecting mirror in position 2 and reflecting a portion of the light back into the 1-m focal-length camera through the beam splitter. The degree of aberration is measured by placing the aberration in front of the reference reflector at position 2, causing the light to double-pass the aberrator. The SBS-corrected process is accomplished by passing the light through the amplifier and attenuator, through the aberrator now at position 3, and into the focusing lens and CS_2 waveguide. The lens is used to focus the beam to a waist just in front on the cell entrance window giving a divergent entrance beam. Since the index of CS_2 is higher than the glass, this diverging beam is completely internally reflected in the 2.5-mm-i.d. 1-m-long capillary. The waveguide SBS cell serves to increase

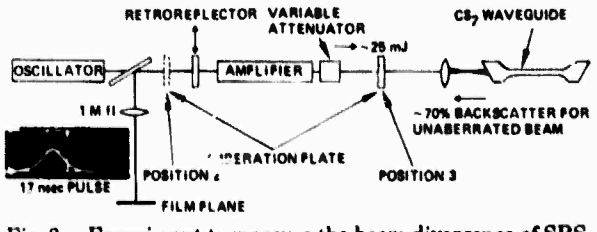

Fig. 2. Experiment to measure the beam divergence of SBS backscatter at 0.69 μm.

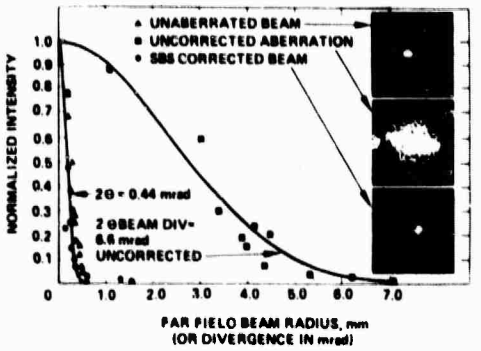

Fig. 3. Measured full-angle beam divergences of original, aberrated, and corrected beams and their appearance in the far field.

the interaction length and percentage of light backscattered without increasing power density to the point where laser-induced breakdown of CS_2 can occur and without increasing the total power input to the point of self-focusing. The slightly redshifted SBS backscatter retraces the path of the original beam through the multiple bounces in the waveguide and through the aberrator and the amplifier. A portion is sampled by the beam splitter and the 1-m camera.

Divergence of these beams is measured by a technique using a series of exposures at differing attenuations at the focal point of a 1-m lens.[10] In this way the actual profile of the original aberrated and corrected beams can be determined independently of film linearity. In a plot of the log of the relative intensity versus spot diameter squared, as recorded on film of sharp threshold, a Gaussian beam will result in a straight line plot, with slope proportional to the $1/e$ Gaussian-beam diameter.

Beam profile plots were taken for the reference, aberrated, and SBS-corrected beams, and all were approximately Gaussian. The full-angle beam divergences obtained from the slope of these plots are 0.57 ± 0.06, 6.6 ± 0.9, and 0.44 ± 0.06 mrad. The SBS process provides a corrected beam that has a divergence almost indistinguishable from the original beam and substantiates earlier results.[5,6] In fact, the SBS beam divergence, 0.44 mrad, is the calculated diffraction-limited divergence of this laser beam. (The slight improvement over the reference beam is unexplained but could result from the reference retroreflector's being out of flat by $\lambda/6$ across the beam.) In Fig. 3 the normalized beam intensity is plotted versus divergence or radius at the focal plane of the camera. Also shown are photographs of the reference, aberrated, and corrected beams. The corrected beam has horizontal sidelobes not present in the reference. The presence of these sidelobes makes a negligible contribution to the overall beam divergence since their intensity is very low (the outermost two data points in the plot of the corrected beam divergence are the result of these sidelobes).

There is some theoretical justification for concern that other wavefronts in addition to the desired phase conjugate wavefront may exist in the backscattered beam. For example, a plane wavefront backscattered by the SBS might go undetected after passing through

the aberrator if the resultant diffused beam gave a maximum intensity below the film's threshold of sensitivity. Locating the source of aberration ahead of the beam splitter and adjacent to the oscillator did not result in a bright focused spot at the camera focal plane, which would be the result of a collimated return wave. We are now in the process of exploring the effect of power and interaction length upon the efficiency of the correction.

We have also found that an optical waveguide appears necessary to the phase conjugation process. When the beam was focused within a conventional cell with comparable total input power and comparable percentage backscatter, the backscattered light was not capable of correcting the divergence introduced by our aberrator but returned a reflection with divergence similar to an ordinary reflection. Thus the selection process that allows ascendency of the phase conjugate phasefront over all other possible phasefronts seems to be dependent on propagation of confined modes within a waveguide.

An oversimplified but intuitively satisfying physical picture of this process is illustrated in Fig. 4. The phase aberrated beam is represented by a wavefront with a simple step. An ordinary reflection results in the doubly aberrated wavefront shown as Fig. 4. As a result of the SBS interaction, the aberrated pump wave creates aberrated hypersonic waves with identical phasefronts (as in Fig. 4, bottom) which act as a moving "deformable" dielectric reflector that yields the conjugate scattered wave.

Other phase conjugating processes that have been proposed include parametric down-conversion[11] and four-wave mixing.[9,12] At this time SBS appears to be quite efficient, yielding from 10 to 70% backscatter, depending on the degree of aberration introduced.

Other promising applications of this class of corrective techniques include correction of large-diameter laser resonator cavities as well as large optical trains, such as those proposed for laser fusion or space optics.

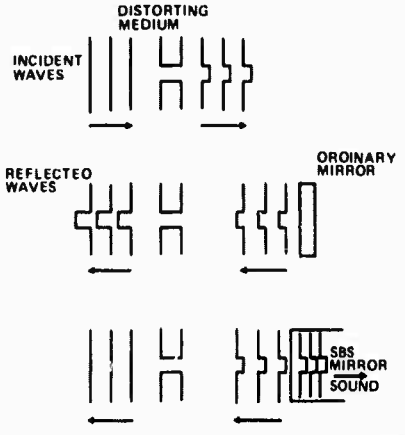

Fig. 4. A simplified view of the SBS phase conjugating process as a moving multilayer reflector.

In summary, we have presented the first report of a quantitative evaluation of SBS phase conjugation and suggested a means by which phase conjugation can be used for adaptive optics.

We wish to acknowledge fruitful discussions with V. Evtuhov, R. W. Hellwarth, D. M. Pepper, and A. Yariv and thank T. Horne for his technical assistance.

References

1. J. E. Pearson, "Atmospheric turbulence compensation using coherent optical adaptive techniques," Appl. Opt. **15**, 662 (1976).
2. J. Opt. Soc. Am. **67** (1977) (special issue on adaptive optics).
3. V. Wang, "Nonlinear optical phase conjugation for laser systems" Opt. Eng. (to be published).
4. T. A. Wiggins, R. V. Wick, and D. H. Rank, "Stimulated effects in N_2 and CH_4 gases," Appl. Opt. **5**, 1069 (1966).
5. B. Ya. Zel'dovich, V. I. Popovichev, V. V. Ragul'skii, and F. S. Faizullov, "Connection between the wavefronts of the reflected and exciting light in stimulated Mandel'shtam–Brillouin scattering," Zh. Eksp. Teor. Fiz. Pis. Red. **15**, 160–164 (1972).
6. O. Yu. Nosach, V. I. Popovichev, V. V. Ragul'skii, and F. S. Faizullov, "Cancellation of phase distortions in an amplifying medium with a Brillouin mirror," Zh. Eksp. Teor. Fix. Pis. Red. **16**, 617–621, (1972); translated in Sov. Phys. JETP **16**, 435 (1972).
7. M. Bel'dyugin, M. G. Galushkin, E. M. Zemskov, and V. I. Mandrosov, "Complex conjugation of fields in stimulated Brillouin scattering," Sov. J. Quantum Electron. **6**, 1349 (1976); V. G. Sidorovich, "Theory of the 'Brillouin mirror,' " Sov. Phys. Tech. Phys. **21**, 1270 (1976); G. G. Kochemasox and V. D. Nikolaev, "Reproduction of the spatial amplitude and phase distributions of a pump beam in stimulated Brillouin scattering," Sov. J. Quantum Electron. **7**, 60 (1977).
8. W. Lukosz, "Equivalent-lens theory of holographic imaging," J. Opt. Soc. Am. **58**, 1084 (1968).
9. R. W. Hellwarth, "Generation of time-reversed wavefronts by nonlinear refraction," J. Opt. Soc. Am., **67**, 1 (1977); A. Yariv, "Compensation for atmospheric degradation of optical beam transmission by nonlinear optical mixing," Opt. Commun. **21**, 49 (1977).
10. C. R. Giuliano and D. Y. Tseng, "Damage in lithium iodate with and without second harmonic generation," presented at the Symposium on Damage in Laser Materials, Boulder, Colorado, May 1973.
11. A. Yariv, "On transmission and recovery of three-dimensional image information in optical waveguides," J. Opt. Soc. Am. **66**, 301 (1976).
12. A. Yariv and D. M. Pepper, "Amplified reflection, phase conjugation, and oscillation in degenerate four-wave mixing," Opt. Lett. **1**, 16 (1977).

APPENDIX B

Theory of phase conjugation by stimulated scattering in a waveguide*

R. W. Hellwarth

Electronic Sciences Laboratory, University of Southern California, University Park, Los Angeles, California 90007

(Received 13 February 1978)

We consider the backward optical wave stimulated by a multimode, monochromatic, incident optical wave in a waveguide filled with a transparent nonlinear medium, when the incident wave is negligibly perturbed by the nonlinear processes. We derive the conditions on guide length, area, mode number, and Stokes shift in order that a given high percentage of the power in the backscattered field be the "phase conjugate" of the incident field, i.e., be proportional to its complex conjugate in the entrance plane of the waveguide.

I. INTRODUCTION

When a strong monochromatic wave (at ν) is incident on a transparent medium it causes waves at lower frequencies ω to experience exponential gain if their frequency offset corresponds to the frequency of some excitation in the medium. If this excitation is an acoustic wave, the effect is called stimulated Brillouin scattering (SBS), otherwise it is called stimulated Raman scattering (SRS). It has long been known that laser sources may produce stimulated gain that is large enough ($\sim 10^{12}$) so that spontaneously scattered light experiences sufficient amplification, in a single pass out of the incident-beam region, to emerge with a power approaching that of the incident beam. More recently, it has been observed that, when the incident beam is multimode (i.e., has a complex wave front), the high intensity backscattered SBS or SRS waves generated in this single-pass process may be nearly the "phase conjugate" to the incident wave.[1-6] That is, in the entrance plane, the complex amplitude $\mathbf{E}_\omega(\mathbf{r})$ of the stimulated wave is nearly equal to the complex conjugate $\mathbf{E}_\nu^*(\mathbf{r})$ of the incident wave times a constant. When the incident and scattered frequencies, ν and ω, are nearly equal, phase conjugation makes the scattered wave appear to be nearly a time-reversed replica of the incident wave in a large region of space. Zel'dovich *et al.*[1] suggested that, when $\omega \sim \nu$, this effect should come from the solution of the nonlinear Maxwell equations after they were linearized with respect to the scattered fields. They pointed out that the resulting complicated set of coupled linear equations for the spatial amplitudes would have various solutions which exhibited spatial gain, and that one solution should: (a) have $\mathbf{E}_\omega \sim \mathbf{E}_\nu^*$ in some plane, and (b) have significantly ("2 to 3 times") higher gain than the others. As the SBS phase-conjugation experiments had been performed in an optical waveguide, Sidorovich[3] examined the equations appropriate to an optical waveguide, and agreed with these conclusions, however, surmising some "necessary" conditions for this effect for which we will show counter examples here. Zel'dovich and Shkunov pointed out that, when the beams interact in free space (rather than in a waveguide), phase conjugation can occur even when the frequency separation between the beams was large, as in SRS.[4] However, the conditions they find differ from those we will find here. Subsequently, Zel'dovich *et al.*[5] observed SRS from the 656 cm^{-1} Raman line of CS_2 to be largely a phase conjugate to an incident beam comprising about 300 transverse modes. Wang and Giuliano verified the high degree of phase conjugation present in SBS.[6]

In this paper we will analyze the degree of phase conjugation present in waves which are stimulated (from noise) in a waveguide by a strong multimode beam, whose propagation is assumed to be negligibly disturbed by the stimulated processes and negligibly attenuated by linear losses. Phase conjugation by stimulated scattering from an unguided beam (which requires more power and may be spoiled by self-focusing, breakdown, etc.) may be approximated by considering a waveguide whose length equals the diffraction length of the incident beam. We find that, even when a gap exists between the gain of one solution, or wave pattern, and that of the others, the maximum-gain solution is never a perfect phase conjugate to the pump (input) wave pattern. However, a very large fraction (>90%) of this maximum-gain solution is phase conjugate to the pump under conditions which are much less restrictive than those suggested by previous workers.[3,4] First, the waveguide must have a finite number of modes that can be excited and the transverse field patterns of the pump and

 0030-3941/78/6808-1050$00.50

stimulated modes must be essentially the same. This constitutes very little restriction in practice. More importantly, the product of the waveguide length, the Stokes wavelength shift, and the number of excited waveguide modes divided by their cross-sectional area must be less than a number that is of the order of the square root of the maximum acceptable fraction that is *not* phase conjugate.

Unlike Ref. 3, we find (a) that large differences in the amplitudes of the excited incident modes do *not* spoil phase conjugation; (b) the waveguide does *not* have to be much longer than a diffraction length; (c) the incident beam solid angle does *not* have to exceed the nonlinear index change. The free-space (no guide) theory of Ref. 4 also produces somewhat different conditions that depend on the value of the stimulated gain.

Unlike previous analyses, our conclusions are based on a general perturbation theory for the non-phase-conjugate fraction in the wave of maximum gain, valid for any distribution of incident-wave amplitudes and phases. We apply this theory to several models in a rectangular waveguide which have arbitrary distribution of phase and arbitrary distribution among four possible arbitrary amplitudes. What seems truly remarkable is that the many extraneous terms in the original coupled-mode equations fail to spoil the phase-conjugate nature of the guided wave with maximum gain, at least in the quite representative classes of input waves in a rectangular waveguide which we considered. A general proof of the conditions for phase conjugation of all possible inputs into all possible guide shapes is still lacking. However, we feel that our conditions are accurate for cases of interest in the laboratory.

II. FORM OF THE NONLINEAR POLARIZATION

We will consider the interaction in a straight waveguide of a multimode "pump" wave or input wave with stimulated backscattered "Brillouin" waves, i.e., waves generated by interactions with backward acoustic waves. The pump waves will be assumed to be monochromatic at angular frequency ν and to be Fourier analyzable inside the guide in terms of plane waves whose wave vectors lie mainly in a small cone of half-angle θ about the waveguide axis z. We will look for solutions of the nonlinear Maxwell equations which are backward-scattered waves of a single (Brillouin-shifted) frequency ω; solutions at different frequencies superpose. However, stimulated gain will make those solutions predominate which lie in a narrow range about frequency

$$\omega = \nu - \omega_B, \tag{1}$$

where

$$\omega_B \cong 2nv_s\nu/c \tag{2}$$

is the acoustic frequency. Here v_s is the sound velocity, n is the (linear) refractive index, and c is the velocity of light in vacuum.

We will find that the backscattered waves will have wave vectors lying mainly inside a cone whose half-angle is also θ, the angle containing the pump waves. (In fact, the backscattered waves will often be nearly the time-reversed replica, or "phase conjugate," of the pump wave.) Here we will consider only the case

$$\theta < Q^{-1/2}, \tag{3}$$

where $Q = \omega_B/\Delta\omega_B$ is the "Q value" of the backward acoustic waves and $\Delta\omega_B$ is the linewidth of the resonant acoustic response (and of the spontaneous backward Brillouin-scattered light). When Eq. (3) holds, it is readily verified that the magnitudes of the sound wave vectors, excited by pump and scattered light waves, lie within the bandwidth $\Delta\omega_B/v_s$ in which the acoustic response is nearly constant—the same as at exact resonance. The independence of Brillouin response to wave vector in this case implies that the amplitude at ω of the nonlinear optical polarization density $\mathbf{P}_\omega^{\rm nl}(\mathbf{r})$ depends only on the optical field at the same position $\mathbf{r}$. That is, we can neglect spatial dispersion when Eq. (3) holds. It is well known that on resonance, the nonlinear Brillouin polarization at $\mathbf{r}$ has the form

$$\mathbf{P}_\omega^{\rm nl} = -iG\,\mathbf{E}_\nu\,\mathbf{E}_\nu^*\cdot\mathbf{E}_\omega, \tag{4}$$

where $\mathbf{E}_\nu$ and $\mathbf{E}_\omega$ are the (complex) amplitudes of the pump and backscattered waves. On resonance, G is a real constant which we will relate later to the usual plane-wave Brillouin gain coefficient. [When ω deviates from the resonance condition (1), G becomes complex and of smaller magnitude.] Other nonlinear effects, such as SRS, give a third-order polarization density that is largely imaginary and spatially local as in Eq. (4), and our theory here will apply to these also, after possible minor modification of the tensorial character of Eq. (4).

Although Eq. (3) has been well-satisfied in all experiments to date, we note that it need not be if the waveguide-acceptance angle is larger than $Q^{-1/2}$. In this case phase-conjugation properties can be predicted by considering subsets of excited incident modes, each of which interacts with a different subset of phonon waves, the results of each subset of interactions being treated essentially as we will treat the case obeying Eq. (3).

III. FORMULATION IN A CYLINDRICAL WAVEGUIDE

We will assume that the nonlinear polarization density does not disturb the incident pump waves so that their complex amplitude $\mathbf{E}_\nu(\mathbf{r})$ can be written inside the waveguide as

$$\mathbf{E}_\nu = \sum_m A_m\hat{e}_m(x,y)e^{ik_{m\nu}z}. \tag{5}$$

Here the A_m are complex amplitudes for the pump wave to be in various normal modes of the guide, whose transverse mode patterns $\hat{e}_m(x,y)$ are normalized so that

$$\int dx\,dy\,\hat{e}_m^*\cdot\hat{e}_n = \delta_{mn}. \tag{6}$$

We will assume that the transverse refractive index variations or metallic walls, etc., forming the guide are such that the transverse functions $\hat{e}_m$ do not differ significantly for the various temporal frequencies (pump and Stokes-shifted) that are propagating in the guide. However, the propagation constants $k_{m\nu}$ are frequency-dependent and obey

$$k_{m\nu}^2 + u_m^2 = n_\nu^2\nu^2/c^2, \tag{7}$$

where u_m^2 is the (frequency-independent) eigenvalue associated with the function $\hat{e}_m$. Here, n_ν, the refractive index at

the guide axis, is assumed to be real, i.e., linear attenuation in the interaction regions is assumed to be negligible.

We will not need to digress here on the characteristics of waveguide modes; our results will be largely independent of the detailed nature of the waveguide, provided that it propagates a number of modes at ν and ω whose transverse mode patterns $\hat{e}$ are congruent.

IV. NONLINEAR MAXWELL EQUATIONS FOR MODE AMPLITUDES

We now consider Maxwell's equations for the complex amplitude $\mathbf{E}_\omega$ of the waves generated in the guide, at frequency ω, under the influence of the nonlinear polarization density (4). We will try a solution of the nonlinear Maxwell equations of the form

$$\mathbf{E}_\omega = \sum_n B_n \hat{e}_n(x,y) e^{-ik_{n\omega}z - \gamma z/2} \tag{8}$$

which is similar to Eq. (5) except that the waves are both traveling and growing in the backwards direction $(-z)$. When there is no nonlinear term (4) and $\gamma = 0$, Eq. (8) satisfies Maxwell's equations identically. When the nonlinear term (4) is added as a small perturbation, Maxwell's equations are satisfied in a length L of guide provided that

$$\gamma k B_m = 4\pi\omega^2 c^{-2} G \sum_{ijn} \int\int dx\, dy\, \hat{e}_m^* \cdot \hat{e}_i\, \hat{e}_j^* \cdot \hat{e}_n \times K_{mijn} A_i A_j^* B_n, \tag{9}$$

where

$$K_{mijn} \equiv \int_0^L e^{i\Delta kz}\, dz/L \tag{10a}$$

and $\Delta k \equiv k_{m\omega} + k_{i\nu} - k_{j\nu} - k_{n\omega}$. It is useful to note that

$$|K_{mijn}| = x^{-1} \sin x, \tag{10b}$$

where $x \equiv \Delta kL/2$ equals zero when $i = j$ and $m = n$.

In Eq. (9), as in the following formulas, repeated space indices are assumed to be summed unless otherwise stated. We have approximated a factor $k_{m\omega}$ on the left-hand side of (9) by its average k; the small difference is negligible, as will be seen by an obvious extension of the perturbation theory which we will apply to more important terms below.

From Eq. (9) it is seen that the nonlinear Maxwell equations lead to a coupled set of linear equations for the backward-scattered-wave mode amplitudes B_n, when these are too small to affect the incident-wave amplitudes A_m. We have not established the properties of B_n for all possible sets of A_m, but we have solved for B_n for some nontrivial A_m. We have also derived a perturbation expression for the non-phase-conjugated fraction f of that solution $\{B_n\}$ of Eq. (9) having the largest value γ_0 of gain γ. We also calculate γ_0, showing that, when $f \ll 1$, γ_0 is larger enough than the γ for any other solution so that the near-conjugate solution can dominate in practice. The perturbation theory needed to accomplish these tasks takes a form that is familiar to quantum mechanics if we rewrite Eq. (9) in the form of an eigenvalue equation, with eigenvalue Y, in a Hilbert space of dimension N equal to the number of transverse mode patterns that are excitable in the guide. This reexpression of Eq. (9) is

$$\sum_n (H_{mn} + V_{mn} + U_{mn})\, B_n = Y B_m, \tag{11}$$

where the "effective unperturbed Hamiltonian" is

$$H_{mn} \equiv \bar{\alpha}\, \delta_{mn} + \bar{\beta}\, a_m^* a_n \tag{12}$$

and the first perturbation Hamiltonian is (no implied summations)

$$V_{mn} \equiv \sum_l (\alpha_{nl} - \bar{\alpha})\, a_l^* a_l\, \delta_{nm} + (\beta_{mn} - \bar{\beta}) a_m^* a_n. \tag{13}$$

Here the a_n are normalized dimensionless pump-beam amplitudes

$$a_n = A_n \left(\sum_m A_m^* A_m \right)^{-1/2}. \tag{14}$$

The α_{mn} and β_{mn} matrices are derived from mode-overlap integrals according to

$$\alpha_{mn} \equiv \int\int dx\, dy\, |\hat{e}_m^* \cdot \hat{e}_n|^2 \tag{15}$$

and (no implied summation)

$$\beta_{mn} \equiv \int\int dx\, dy\, (\hat{e}_m^* \cdot \hat{e}_n)^2 K_{mnmn}. \tag{16}$$

Their averages $\bar{\alpha}$ and $\bar{\beta}$ are defined by

$$\bar{\alpha} \equiv \sum_{mn} \alpha_{mn} |a_m|^2 |a_n|^2 \tag{17}$$

and similarly for $\bar{\beta}$. One sees that the α terms in Eqs. (12) and (13) are from the terms in (9) for which $i = j$ and $m = n$; the β terms are from the terms in (9) for which $i = n$ and $j = m$. Note that H_{mn} and V_{mn} are Hermitian.

The second perturbation Hamiltonian is (no implied summation)

$$U_{mn} \equiv \sum_{ij}{}' a_i a_j^* \int\int dx\, dy\, \hat{e}_m^* \cdot \hat{e}_i\, \hat{e}_j^* \cdot \hat{e}_n K_{mijn}, \tag{18}$$

where the prime on the summation signifies the inclusion of only those terms not included in Eqs. (12) and (13). The K_{mijn} in Eq. (18) have $\Delta k \neq 0$ except when degeneracies occur which make either $k_{i\nu} = k_{j\nu}$ and $k_{n\omega} = k_{m\omega}$ simultaneously, or $k_{i\nu} = k_{n\omega}$ and $k_{j\nu} = k_{m\omega}$ simultaneously.[7] In practice, the K_{mijn} in Eq. (18) for which $\Delta k \simeq 0$ can be omitted from consideration for the following reasons. First, the component of $\mathbf{E}_\nu$ in any degenerate manifold of guide modes can be taken as one of the basis vectors in this manifold. Then, no terms will exist in (18) with $k_{i\nu} = k_{j\nu}$. The second case is possible when $\omega \simeq \nu$, $u_i^2 = u_n^2$, and $u_j^2 = u_m^2$. However, then it is usual that $\hat{e}_n^* \cdot \hat{e}_i = \hat{e}_j^* \cdot \hat{e}_m = 0$. In a guide with high symmetry, the latter may not be the case, but then the x-y overlap integral in (18) seems to be greatly reduced over that in (16) arising from $i = n$ and $j = m$; in fact it reduces to zero for a rectangular waveguide. Thus we will neglect the terms in (18) for which Δk is accidently near zero, considering next the effects of the remaining terms.

If the difference between ΔkL values for various mode indices is larger than π, expressions (10) show K_{mijn} to oscillate randomly and cause a great deal of cancellation among terms. If the area of the guide is S, and there are N excitable modes, then $u_n^2 \sim N^2/S$, $|K_{mijn}| \ll 1$, and ΔkL changes by at least π

for most changes in (i, j, n, m) when

$$NL > Sk. \tag{19}$$

We expect therefore that U_{mn} can be neglected compared to H_{mn} when $L > L_d/N^{1/2}$, where L_d is a diffraction length ($\sim Sk/N^{1/2}$). This condition is met by free-space interactions and all practical guides. Therefore we proceed to solve Eq. (11) with $U_{mn} = 0$.

Before proceeding it is useful to relate the eigenvalue Y for any N-dimensional vector solution $|B_n|$ of Eq. (11) to its gain γ and the commonly defined stimulated gain coefficient g (Np cm/MW) for plane pump and scattered waves. The "free-space" coefficient g is the same as that (γS + total pump power P) in a guide that is excited in a single mode e_n having a uniform intensity profile ($e_n = \text{const}$), and for which Eqs. (6), (15), and (16) give $\bar{\alpha} = \bar{\beta} = 1/S$. In this case $V_{nm} = U_{nm} = 0$ and $B_m = a_m^*$ is the solution of (11) with eigenvalue

$$Y_{pw} = 2/S. \tag{20}$$

Since $\Sigma_n |A_n|^2$ is proportional to the power P in the guide, a comparison of Eqs. (9) and (11) shows $Y \propto \gamma/P$ in all cases. Therefore the power gain γ for any solution of (11) with eigenvalue Y is related to g by

$$\gamma(\text{cm}^{-1}) = \tfrac{1}{2}\, Y(\text{cm}^{-2})\, g(\text{cm/MW})\, P(\text{MW}), \tag{21}$$

where the most common units used are indicated. We proceed now to find solutions of Eq. (11) and their gains γ for multimode pump beams.

V. FIRST APPROXIMATE SOLUTION FOR ARBITRARY INPUT

The "unperturbed" matrix H_{mn} in (11) is of the particularly simple form of a unit matrix plus a projection operator P_a onto the conjugate a_n^* of that vector whose components a_n are the complex mode-amplitudes of the incident wave in the guide. Therefore, the eigenstates and eigenvalues $G^{(\nu)}$ of H_{mn} are easily seen to be a_n^*, with eigenvalue

$$G^{(0)} = \bar{\alpha} + \bar{\beta} \tag{22}$$

and any set of vectors $b_n^{(\nu)}$ orthogonal to a_n^* and to each other, which complete the space of guide modes. The latter have eigenvalues

$$G^{(\nu)} = \bar{\alpha}. \tag{23}$$

Note that when all guide modes have the same linear (or elliptical) polarization, and when $\omega \to \nu$, so that by Eq. (10) $K_{mnmn} \to 1$, as in practical SBS experiments, then

$$\bar{\alpha} \to \bar{\beta} \tag{24}$$

and

$$G^0 \to 2G^\nu. \tag{25}$$

That is, the conjugate backscattered wave, whose mode amplitudes are a_n^*, would experience twice the gain as any other mode, provided that V_{mn} can be neglected.

We will find that whenever the scattered-wave's energy is mostly in the phase conjugate to the incident wave, its gain is nearly twice that of any other wave. Furthermore this condition occurs whenever the elements K_{mnmn} of (10) are always near unity, as they are for practical configurations producing SBS. To see this we consider first a class of pump waves for which Eq. (11) can be solved exactly, and then apply general perturbation theory to an even wider class of pump waves.

VI. SET OF EXACT SCATTERED SOLUTIONS AND THEIR GAINS

There is an important class of incident-mode patterns in a rectangular waveguide for which the eigenvectors of both H_{nm} and V_{nm} are the same set, provided $K_{mnmn} \sim 1$ (as for SBS) which we assume here. This is the class of waves for which all N excitable modes of one polarization of the guide are excited with equal energy but with arbitrary phases ϕ_n:

$$a_n = N^{-1/2} e^{-i\phi_n}. \tag{26}$$

For simplicity, assume the first M modes in both x and y directions are excited ($N = M^2$) and label the modes by x and y indices, $(n_x, n_y) \leftrightarrow n$, such that

$$n_x, n_y = 0, 1, 2, \ldots, M\text{-}1 \tag{27}$$

in order of increasing numbers of nodes. The integrals in (15) and (16) are then easily approximated (assume the mode functions are sine waves vanishing at the boundary) to obtain

$$\alpha_{nl} = \beta_{nl} = [2 + \delta(n_x,l_x)]\,[2 + \delta(n_y,l_y)]/4S, \tag{28}$$

where the δ function is 1 if its arguments are equal, and zero otherwise. It is easily verified by substitution in Eq. (11) that the $N = M^2$ eigenvectors have components (mode amplitudes)

$$B_n(l_x, l_y) = M^{-1} \exp[i\phi_n + 2\pi i(n_x l_x + n_y l_y)/M], \tag{29}$$

where pairs of the integers

$$l_x, l_y = 0, 1, \ldots, M\text{-}1 \tag{30}$$

are convenient labels for the N vectors. The eigenvector with $l_x = l_y = 0$ is the desired phase-conjugate state ($B_n = a_n^*$), and it has the largest eigenvalue:

$$Y_{00} = \bar{\alpha} + \bar{\beta}. \tag{31}$$

Then there are $2M$-2 eigenvectors having either $l_x = 0$ or $l_y = 0$ (but not both) which all have the eigenvalue

$$Y_{0\nu} = \bar{\alpha} + (1 + 2M)/4SM^2. \tag{32}$$

Finally the $(M\text{-}1)^2$ states for which $l_x \neq 0$ and $l_y \neq 0$ have the eigenvalues

$$Y_{\mu\nu} = \bar{\alpha} + 1/4SM^2. \tag{33}$$

For the sine-wave modes,

$$\bar{\alpha} = \bar{\beta} = (1 + M^{-1} + M^{-2}/4)/S. \tag{34}$$

Therefore the "gap" in gain between Y_{00} of the conjugate wave and $Y_{0\nu}$ the next nearest gain is

$$Y_{00} - Y_{0\nu} = (1 - \tfrac{1}{2} N^{-1/2})/S \tag{35}$$

which, for a large number N of modes, approaches the gap between Eqs. (22) and (23) for $V_{mn} = 0$. Also, for large N, we see from (21) that the gain of the conjugate wave is the same as for a plane-wave pump of intensity P/S in free space.

Studies of pump beams that do not have equal power in all modes have led us to believe that the gap between the highest and next-highest mode gains is quite generally $\bar{\alpha}$ less a term

of order $N^{-1/2}$ smaller. This gap is usually enough in practice to make a single stimulated solution dominate in experiments where the backscattered wave grows from noise. It remains to be seen in Sec. VII how closely this single solution approximates a phase conjugate to the incident wave.

VII. PERTURBATION SOLUTIONS FOR SCATTERING FROM ARBITRARY PUMP WAVES

Having seen from the exact solutions for B_n in the special case of the previous section that the effect of V_{mn} in Eq. (11) was small when the number N of pump-wave modes excited was large, we are encouraged to treat V_{mn} as a small perturbation on H_{mn} in solving the eigenvalue equation (11) (in which we continue to assume $U_{mn} = 0$ for reasons argued previously). Let us denote the exact eigenvector of $H_{mn} + V_{mn}$ having largest eigenvalue Y_0 by B_{0n}. Since we have already shown in (22) that the eigenvector $b_n^{(0)}$ of H_{mn} having highest eigenvalue $G^{(0)} = (\bar{\alpha} + \bar{\beta})$ was a_n^*, let us write the exact solution as

$$B_{0n} = a_n^* + c_n. \tag{36}$$

Then standard perturbation theory gives for the correction c_n (repeated mode indices are to be summed henceforth)

$$c_n = \sum_{\nu \neq 0} b_n^{(\nu)} b_l^{(\nu)*} V_{lm} a_m^* / (G^{(0)} - G^{(\nu)}) \tag{37}$$

to lowest order in the perturbation V_{lm}. Recall that the $b_n^{(\nu)}$ is the eigenvector of H_{mn} with eigenvalue $G^{(\nu)}$. From Eqs. (22) and (23) we recall that the energy denominator $G^{(0)} - G^{(\nu)}$ in Eq. (37) is a constant $\bar{\beta}$. Since, from its definition in Eqs. (13)–(17), V_{mn} has the property

$$a_m V_{mn} a_n^* = 0, \tag{38}$$

the sum in (37) may be extended over all ν (with constant denominator), and closure invoked to obtain the expression

$$c_n \approx V_{nm} a_m^* / \bar{\beta}, \tag{39}$$

which is simpler for calculation. The most important quantity to calculate for our purposes is the fraction f of power in the highest gain solution B_{0n} that is *not* in the phase-conjugate wave a_n^*. Since $a_n^* a_n = 1$ by (14),

$$f = r/(1-r), \tag{40}$$

where $r \equiv c_n^* c_n$. From Eqs. (39) and (13) we have

$$r = |a_l|^2 \theta_{lm} |a_m|^2 \theta_{mn} |a_n|^2 / \bar{\beta}^2, \tag{41}$$

where $\theta_{lm} \equiv \alpha_{lm} + \beta_{lm} - \bar{\alpha} - \bar{\beta}$. This is the most important result of perturbation theory for assessing the fraction f of stimulated backward scattering that is not phase conjugate to the pump wave. If r is not much less than 1, the process is useless and it is pointless to calculate further corrections to Eq. (39). If $r \ll 1$ then (39) and (40) are accurate enough. It is of minor interest to note that the gain Y_0 of the important wave is somewhat larger than $G^{(0)}$. From nondegenerate perturbation theory for eigenvalues,

$$Y_0 = G^{(0)} + r\bar{\beta} \tag{42}$$

to second order in V_{mn}. [The correction linear in V_{mn} vanishes because of Eq. (38).] That is, the gain is increased by the fraction r of the gain "gap" $\bar{\beta}$.

We next use (41) to calculate r for a fairly general class of pump beams.

VIII. MODEL CALCULATION OF NONCONJUGATED POWER FRACTION

We calculate here the nonconjugated power ratio r of Eq. (41) for a realistic set of complex pump-beam amplitudes a_n, each member having arbitrary phase and one of four possible magnitudes, in the ideal rectangular waveguide considered in Sec. VI. Expressing the mode label n in terms of the x and y mode-integers l_x and l_y of Eq. (30), we take for the square magnitudes required in Eq. (41)

$$|a_n|^2 = g_x(l_x) g_y(l_y). \tag{43}$$

The real positive functions g_x and g_y are defined to have the value g_+ for a number N_+ of the M values of their integer argument, to have the value g_- (less than g_+) for N_- of these M values, and to have the value zero for the remainder. The particular members of each of these three sets need not be the same for g_x and g_y. This results in four possible values for $|a_n|^2$:

$$g_+g_+, \quad g_-g_-, \quad g_+g_-, \quad \text{or } 0$$

depending on $n \leftrightarrow (l_x, l_y)$. The total number N of excitable modes equals $M^2 (\geq N_+N_-)$.

Again we assume all modes to have the same linear polarization $\hat{e}_n$ parallel to $\hat{x}$ or $\hat{y}$ so that $\alpha_{nm} = \beta_{nm}$ in θ_{nm} are given by Eq. (28). The required sums in (41) are then easily done to yield

$$r = 4[(u_\pm^2)^2/(u_\pm)^4 - 1], \tag{44}$$

where the average $\langle\ \rangle$ is to be performed over the two-valued function

$$u_\pm \equiv 1 + \tfrac{1}{2} g_\pm/(N_+g_+ + N_-g_-) \tag{45}$$

with the two-valued, normalized probability

$$w_\pm \equiv g_\pm N_\pm/(N_+g_+ + N_-g_-). \tag{46}$$

Clearly r in Eq. (44) is a function of three independent parameters, which we choose as N_+, N_-, and g_-/g_+, whose ranges are

$$0 \leq N_+ \leq M, \quad 0 \leq N_- \leq M, \quad 0 \leq g_-/g_+ \leq 1. \tag{47}$$

Let us consider r for various possible parameter sets representing various possible classes of pump beams.

A. N_- (or g_-) $= 0$; $1 < N_+ \leq M$. This is a pump beam with N_+^2 modes excited with equal amplitude and arbitrary phase. In this case Eq. (44) reduces immediately to $r = 0$. To this order in perturbation theory, the phase-conjugate wave with $B_{0m} = a_m^*$ is exact. We saw above that when $N_+ = M$, this solution is exact to all orders in V_{nm}. In any event we expect this case to yield maximum gain for a wave that is indistinguishable in practice from the phase conjugate.

B. $g_- = g_+$. This is obviously equivalent to case A and gives $r = 0$.

C. $N_- = 0, N_+ = 1$. This is the single-mode pump, which we saw above had the conjugate wave as an exact solution to Eq. (11); and Eq. (47) gives $r = 0$ as expected.

D. $N_+ = N_- = 1$. This is the worst case in the model (four

modes with three amplitudes), giving the largest nonconjugate ratio r for given g_-/g_+. Simple numerical analysis shows that the maximum of r is

$$r_{max} \sim 0.0669 \text{ at } g_- \sim 0.20 g_+. \tag{48}$$

That is, in the worst case, less than 8% of the backscattered energy should be different from the pure phase-conjugate wave.

E. $N_+ = N_- \gg 1$. For many modes excited among three amplitudes this way, $r \propto N_+^{-2}$. Plots of Eq. (44) show that the maximum r is

$$r_{max} \sim 0.1 N_+^{-2} \tag{49}$$

with little change in the range $0.1 < g_-/g_+ < 0.2$ and rapid drop off when this ratio is smaller than 0.05 or larger than 0.5. A more exact treatment is not useful as clearly the nonconjugate fraction $f \sim r$ becomes insignificant when the number of excited modes is large.

F. $N_+ \neq N_-$, $N_+ \gg 1$. Then $r \propto N_+^{-2}$ as in Eq. (49).

In conclusion, we see that for any pump wave that is distributed among guide modes with arbitrary phase and any distribution among four amplitudes obeying (43), there is never more than 8% nonconjugated power in the stimulated wave with maximum gain and generally much less. We are led to conclude (contrary to Ref. 4) that the stimulated backscattering wave with the highest gain has an order-of-magnitude more power in the phase conjugate than in the useless background, for any distribution of pump-mode amplitudes whatever, provided that, as in SBS, $\nu - \omega \ll \omega$ so that $K_{mnmn} \to 1$. We consider next the relaxation of this condition.

IX. PHASE-CONJUGATION IN STIMULATED RAMAN SCATTERING (SRS)

When the scattered frequency ω is significantly different from ν, then K_{mnmn} in Eq. (16) may not be nearly unity, as we have assumed. We will find that phase conjugation disappears as $|K_{mnmn}|$ declines, but this need not happen, even at sizable Stokes shifts, provided that the guide interaction length L is short enough. Before deriving the conditions ω, ν, and L must satisfy, we consider the possibility of stimulated forward scattering (which does not occur in SBS).

If the B_n in Eq. (11) were to represent amplitudes of forward traveling waves (i.e., $k_{n\omega} \to -k_{n\omega}$), then one sees immediately that there is again often one solution having about twice the gain of any other (when $K_{mmnn} \sim 1$), but that solution has $B_n \sim a_n$. That is, this solution is a sort of replica of the incident wave, but not time reversed or phase conjugated. This possibility may be of interest but we shall not consider it further here.

To consider the effect of reduced K_{mnmn} on backward scattering, we consider again the model of Sec. VI in which the first M modes along both the x and y axes of a rectangular guide are excited with arbitrary phases. Inasmuch as this model produced results close to that of the variable-amplitude model when $K_{mnmn} \sim 1$, we expect it to do so here also. We specialize to a square waveguide for which the transverse eigenvalues u_n of Eq. (7) are

$$u_n^2 = \pi^2 (n_x^2 + n_y^2)/S \tag{50}$$

with the mode integers as in Eq. (27). It is sufficiently accurate to expand Δk of Eq. (10) to lowest order in the u_n^2 to obtain for the (m,n) element

$$\Delta k = q\,(m_x^2 - n_x^2 + m_y^2 - n_y^2), \tag{51}$$

where

$$q = \pi \Delta\lambda / 4S \tag{52}$$

and $\Delta\lambda$ is the difference between the wavelengths in the medium at ω and ν:

$$\Delta\lambda = (c/2\pi)\,(1/n_\omega \omega - 1/n_\nu \nu). \tag{53}$$

Here n_ω and n_ν are the refractive indices at ω and ν.

We use these specific forms now to calculate the nonconjugated fraction r, using the perturbation expression (41), and to find the conditions necessary to keep this below some desired maximum value r_0. With Eqs. (50)–(53) in (10) and (16), the β_{mn} matrix we will need in this calculation is given by

$$4S\beta_{mn} = \int_0^L dz\,[2e^{iqz(m_x^2 - n_x^2)} + \delta(m_x, n_x)] \times [2e^{iqz(m_y^2 - n_y^2)} + \delta(m_y, n_y)]/L, \tag{54}$$

which is seen to reduce to the previous form (28) when $q \to 0$. The α_{mn} terms in (41) for r cancel exactly as before, leaving only the β_{mn} terms to be estimated. This we do by calculating the correction Δr that is lowest order in qL, by expanding (54) in powers of q. Higher-order corrections are not interesting as they only tell more precisely what happens after the phase-conjugated fraction has become uninterestingly small. We will also approximate the sums over integers in the resulting expressions by integrals, since the accuracy of this is quite good, especially at large M. This gives directly for the increase Δr in r from its value when $K_{mnmn} \sim 1$:

$$\Delta r = \frac{2}{45}\left(\frac{\pi \Delta\lambda M^2 L}{4S}\right)^2 (1 + O\,|q^2 L^2| + O\,|M^{-1}|), \tag{55}$$

leading to the condition on the interaction length L

$$L \lesssim 6 r_0^{1/2}\, S/N\Delta\lambda \tag{56}$$

in order that the nonconjugated fraction be kept less than r_0 for N equally excited modes in a rectangular waveguide of area S. We feel that Eq. (56) can be applied usefully when there are N unequally excited modes of arbitrary phase, provided that the required nonconjugated fraction r_0 is small.

As Δr increases by (55), so does the gap in gain between the nearly-phase-conjugate wave and its nearest competitor decrease. An estimate of this can be made from Eqs. (22) and (23). However, it is not very interesting to calculate this gap when the waves are already degraded.

In the SRS phase-conjugation experiment of Zel'dovich *et al.*,[5] the incident beam was focused into an "infinite" medium of CS_2. This was roughly equivalent to employing a waveguide whose length was a diffraction length $\sim S\lambda^{-1} N^{-1/2}$.[8] We may use Eq. (55) then to estimate the nonconjugate fraction Δr arising from this finite length, obtaining $\Delta r \sim 0.7\%$, in agreement with the qualitative report of excellent conjugation. (See parameter summary above.)

In conclusion, stimulated backward scattering at ω in a waveguide can be an efficient generator of the phase conjugate of an incident wave at ν, irregardless of the distribution of the N mode amplitudes of the incident wave, provided that the frequency ω is not so different from ν for given guide length as to violate Eq. (56). For some incident beams the nonconjugate fraction contained in the backward wave with highest stimulated gain may be of order 10^{-1} but is generally much smaller, decreasing as N^{-1} as the number of modes N increases. Scattering without a waveguide may be approximated by considering a waveguide one diffraction length long. However, when a waveguide will satisfy the above criteria for phase conjugation, it has the advantage of greatly reducing power requirements and the competition from other nonlinear effects, such as self-focusing.

ACKNOWLEDGMENT

The author wishes to thank V. Wang for many helpful discussions.

*This work was supported in part by the Defense Advanced Projects Agency and monitored through the ONR, and in part by the Joint Services Electronics Project, monitored by the AFOSR under Contract No. F44620-76-C-0061.

[1]B. Y. Zel'dovich, V. I. Popovichev, V. V. Ragul'skii, and F. S. Faisullov, "Connection between the wavefronts of the reflected and exciting light in stimulated Mandel'stam-Brillouin scattering," Pisma Zh. Eksp. Teor. Fiz. 15, 160–164 (1972) [JETP Lett. 15, 109–113 (1972)].

[2]O. Y. Nosach, V. I. Popovichev, V. V. Ragul'skii, and F. S. Faisullov, "Cancellation of phase distortions in an amplifying medium with a 'Brillouin mirror,'" Pisma Zh. Eksp. Teor. Fiz. 16, 617–621 (1972) [JETP Lett. 16, 435–438 (1972)].

[3]V. G. Sidorovich, "Theory of the 'Brillouin mirror,'" Zh. Tekh. Fiz. 46, 2168–2174 (1976) [Sov. Phys. Tech. Phsy. 21, 1270–1274 (1976)].

[4]B. Ya. Zel'dovich and V. V. Shkunov, "Wavefront reproduction in stimulated Raman scattering," Kvantovaya Elektron. (Moscow) 4, 1090–1098 (1977) [Sov. J. Quantum Electron. 7, 610–615 (1977)].

[5]B. Ya. Zel'dovich, N. A. Mel'nikov, N. F. Pilipetskii, and V. V. Ragul'skii, "Observation of wave-front inversion in stimulated Raman scattering of light," Pisma Zh. Eksp. Fiz. 25, 41–44 (1977) [JETP Lett. 25, 36–38 (1977)].

[6]Wang and C. R. Giuliano, "Correction of phase aberrations via stimulated Brillouin scattering," Opt. Lett. 2, 4–6 (1978).

[7]The degeneracies referred to here are those arising from symmetry, such as occur for similar right- and left-circularly polarized modes in a cylindrical waveguide. That Δk cannot approach zero (to within less than L^{-1}) for any other cases is because otherwise $u_m^2 + u_l^2$ cannot come within S^{-1} of $u_n^2 + u_j^2$ without, at the same time, there being a drastic reduction in the x-y integral in (9). This may be appreciated by studying the example of Eq. (50) for u_n^2. Here, without the aforementioned degeneracies occuring, one sees that $\Delta kL \gtrsim L/Sk$, and L/Sk is never much less than unity when guiding occurs.

[8]A waveguide which imitates well the interaction of focused unguided waves may be imagined as follows. Construct that complete orthonormal set of free-space Guassian-beam modes whose parameters are such that the smallest number N of modes need be superposed to give a good representation of the (focused) incident beam. Then let the waveguide axis coincide with the z axis of these modes and let it barely encompass the beam waist over the length where the waist size does not change appreciably. This length is generally of order $S\lambda^{-1}N^{-1/2}$. Calculate the backscattered wave using the mode decompositions in Eqs. (5) and (8) as we have prescribed. The field patterns calculated at the entrance to the waveguide should approximate those in the same plane in free space, since guiding is minimal.

APPENDIX C

EFFECTS OF ATOMIC MOTION ON WAVEFRONT CONJUGATION BY RESONANTLY ENHANCED DEGENERATE FOUR WAVE MIXING

S. M. Wandzura†

Hughes Research Laboratories

Malibu, California 90265

ABSTRACT

In current experiments studying CW optical wavefront conjugation by degenerate four wave mixing, the effects of atomic motion are not negligible. I summarize a calculation, that includes such effects from the beginning, of the small signal phase conjugate reflection coefficient for both Doppler broadened and homogeneously broadened resonant transitions.

†Present address: NOAA Environmental Research Laboratories
Wave Propagation Lab
Boulder, Colorado 80303
(303) 499-1000

In wavefront conjugation experiments employing degenerate four wave mixing in an atomic vapor, atomic motion can have a non-negligible effect even in a homogeneously broadened medium if the longitudinal (population difference) relaxation time, T_1, is longer than the characteristic Doppler time (optical wavelength/thermal speed). The form of the solution given in the analyses of previous authors[1,2] depends only on the homogeneity and isotropy of the medium and the validity of the WKB approximation (slowly varying amplitudes); therefore the effects of the atomic motion are totally contained in the coupling parameters α and κ, that respectively express the polarizability and the coupling of the forward and backward waves, in the presence of counterpropagating pump beams. Because the phase conjugate reflection coefficient R is proportional to the fourth power of the pump field[2], a lowest (third) order perturbation theory calculation need only consider the coupling constant κ. In this order we thus have

$$R = \frac{|\kappa|^2}{4\alpha_r^2} [1 - \exp(-2\alpha_r L)]^2 \quad , \tag{1}$$

where α_r is the linear absorption coefficient and L is the length of the interaction region along the direction of the signal beam.

In order to calculate κ, including the effects of atomic motion, go back to the Bloch equations[3,4] for the two-by-two density matrix, written "symbolically" as

$$\frac{\partial}{\partial t} \rho(t) = -\frac{i}{\hbar} [H(t), \rho(t)] + \text{relaxation } (T_1, T_2) \text{ terms} \tag{2}$$

where

$$H = \frac{\hbar\omega_0}{2} \begin{pmatrix} 1 & 0 \\ 0 & -1 \end{pmatrix} - \mu E(t) \begin{pmatrix} 0 & 1 \\ 1 & 0 \end{pmatrix}. \tag{3}$$

(ω_0 is the resonant frequency of the transition, μ the dipole matrix element and E the electric field.) The position and velocity dependence of the density matrix can then be taken into account by making the replacements

$$\rho(t) \rightarrow \rho(\vec{x},\vec{v},\vec{t})$$

$$E(t) \rightarrow E(\vec{x},t)$$

$$\frac{\partial}{\partial t} \rightarrow \frac{d}{dt} \equiv \frac{\partial}{\partial t} + \vec{v}\cdot\vec{\nabla} \ .$$

I have found it convenient to employ the vector representation of Feynman, Vernon and Hellwarth,[5] in which the resultant equations are

$$\left(\frac{\partial}{\partial t} + \vec{v}\cdot\vec{\nabla} + \frac{1}{T_1} \right) \left\{ \rho_3(\vec{x},\vec{v},t) - \rho_3^{(0)}(\vec{v}) \right\} = \frac{2\mu}{h} E(\vec{x},t)\rho_2 \qquad (4)$$

$$\left(\frac{\partial}{\partial t} + \vec{v}\cdot\vec{\nabla} + \frac{1}{T_2} \right) \rho_1(\vec{x},\vec{v},t) = - \omega_0 \rho_2 \qquad (5)$$

$$\left(\frac{\partial}{\partial t} + \vec{v}\cdot\vec{\nabla} + \frac{1}{T_2} \right) \rho_2(\vec{x},\vec{v},t) = \omega_0 \rho_1 + \frac{2\mu}{h} E(\vec{x},t)\rho_3 \qquad (6)$$

I take

$$\rho_3^{(0)}(\vec{v}) = \frac{\rho_0}{(\pi u^2)^{3/2}} \exp\left(- \frac{v^2}{u^2} \right) \ , \qquad (7)$$

where u is the thermal speed.

These equations can be derived somewhat more rigorously by considering the "quasi-classical" ($\hbar \rightarrow 0$) limit of the equation obeyed by the Wigner function. An additional benefit of the latter approach is the presence of terms which describe velocity changing (recoil) effects, corresponding to the $\vec{F}\cdot\frac{\partial}{\partial \vec{v}}$ terms in the classical Boltzmann equation. The inclusion of these terms will necessitate the

introduction of yet another phenomenological relaxation time for the trace of the density matrix (number density).[6] The full equations could be used to quantitatively explore the recently proposed[7] idea to use density changing effects to enhance nonlinear couplings in atomic vapors.

The polarization is given by

$$P(\vec{x},t) = \mu \int d^3 \vec{v} \quad \rho_1(\vec{x},\vec{v},t) \quad . \tag{8}$$

The third order perturbation theory result for ρ_1 is most easily obtained by first going to an interaction representation (in which $\frac{\partial \rho}{\partial t}$ vanishes in the absence of an electric field), Fourier transforming in both space and time (giving integral equations) and finally dropping non-resonant terms (the "rotating wave" approximation). In order to perform the velocity integration in the above expression for $\rho(\vec{x},t)$, Feynman's trick[8] of combining the perturbation theory denominators is invaluable. The phase conjugate coupling amplitude κ is then identified by picking out the part of $P(\vec{q})$ proportional to $E^*(\vec{q})$, where $\vec{q}$ is the wave vector of the signal wave. The result is

$$\kappa^* = \alpha_0 \frac{E_1 E_2}{E_s^2} \frac{\gamma_1 \gamma_2}{2} \int_0^1 dx \int_0^1 dy \left[\left\{ - \frac{i}{\delta \gamma_2} \frac{1}{d^2(x,0)} \, Im \, Z' \left(\frac{(1-x)(i+\delta)\gamma_2 + ix\gamma_1}{d(x,0)} \right) \right.\right.$$

$$\left.\left. - \frac{1-x}{f^3(x,y,0)} \, Z'' \left(\frac{(1-x)(i+\delta)\gamma_2 + ix\gamma_1}{f(x,y,0)} \right) \right\} + \{0 \to \pi - 0\} \right] \tag{9}$$

where

$$\gamma_{1,2} \equiv \frac{1}{T_{1,2}} \frac{1}{ku} \tag{10}$$

$$d(x,\theta) \equiv \sqrt{1-2x\cos\theta+x^2} \tag{11}$$

$$f(x,y,\theta) \equiv \sqrt{(1-x)^2(1-2y)^2\cos^2\frac{\theta}{2} + (1+x)^2\sin^2\frac{\theta}{2}} \quad , \tag{12}$$

θ is the angle between the signal and the pump beams, δ is the normalized (to $1/T_2$) detuning from resonance, and Z' and Z'' are the first and second derivatives of the plasma dispersion function.[9] In order to proceed further, approximations to the remaining (Feynman parameter) integrations are used appropriate to either the homogeneously broadened regime ($\gamma_2 \gg 1$) or the Doppler broadened regime ($\gamma_2 \ll 1$).

In the homogeneously-broadened regime, the important region of integration is $x \approx 1$. Approximating

$$d(x,\theta) \cong d(1,\theta) \tag{13}$$

$$f(x,y,\theta) \cong f(1,y,\theta) \tag{14}$$

and integrating by parts, one obtains

$$\kappa = -\frac{2\alpha_0}{(1+\delta^2)(1+\delta)} \frac{E_1 E_2}{E_0^2} m(\gamma_1,\theta) \quad , \tag{15}$$

where

$$m(\gamma_1,\theta) = \frac{\sqrt{\pi}}{2} \left[s_+ \exp(s_+)\operatorname{erfc}(s_+^2) + s_- \exp(s_-^2) \operatorname{erfc}(s_-) \right] \tag{16}$$

$$s_+ = \frac{\gamma_1}{2 \sin \theta/2} \tag{17}$$

$$s_- = \frac{\gamma_1}{2 \cos \theta/2} \tag{18}$$

Thus the κ of reference 1 is multiplied by the attenuation factor m, and R by its square. This factor is plotted in Figure 1 as a function of angle for constant γ_1. The asymtotic value $m(\theta=0) \to \frac{1}{2}$ for infinite thermal speed ($\gamma_1 \to 0$) is a reflection of the fact that only one of the two possible holographic gratings formed by the signal and one pump beam (the infinite wavelength grating) survives the "washing out" by the atomic motion.

In the Doppler broadened regime ($\gamma_2 \ll 1$), the derivatives of the Z function can be replaced by their small argument limits, as long as θ does not become so small as to makde $\gamma_{1,2}/f$ or $\gamma_{1,2}/d$ large. The result under these circumstances is

$$\kappa \cong 2i \sqrt{\pi}\ \alpha_0\ \frac{E_1 E_2}{E_s^2}\ \frac{\gamma_1 \gamma_2^2}{\sin^2 \theta}\ ; \ \theta \neq 0 \tag{19}$$

(This is only valid if the detuning does not exceed the Doppler line width, $\delta\gamma_2 \ll 1$.) In order to estimate the behavior for small angles, κ can be calculated for $\theta = 0$:

$$\kappa \cong -\frac{\alpha_0}{2}\ \frac{E_1 E_2}{E_s^2}\ \frac{\sqrt{\pi}\ \gamma_2}{i+\delta}\ ; \quad \theta = 0 \tag{20}$$

Comparing these two, we see that the small angle behavior sets in at an angle θ_0, given by

$$\sin^4 \theta_0 \cong 16 \gamma_1^2 \gamma_2^2 (1+\delta^2) \quad . \tag{21}$$

For fixed θ, the reflection coefficient will exhibit a linewidth

$$(\Delta\omega)^2 \cong \min(\Gamma_d^2, \frac{\sin^4 \theta}{\lambda_1^2} \Gamma_d^2) \quad , \tag{22}$$

where $\Gamma_d \equiv ku$. A simple interpolating formula for the Doppler-broadened reflection coefficient that agrees with the above small and large angle results is

$$R \cong \frac{\gamma_1^2 \gamma_2^2}{\sin^4 \theta + 16 \gamma_1^2 \gamma_2^2 (1+\delta^2)} \left(\frac{E_1 E_2}{E_s^2}\right)^2 [1-\exp(-2\alpha_r L)]^2. \tag{23}$$

This is plotted for fixed detuning parameter δ in Figure 2 and for fixed angle in Figure 3. The angular dependence is qualitatively similar to the homogeneously broadened case, the main new feature arising being the quasi Doppler-free nature of the frequency dependence at small angles, consistent with the observations of Liao, Bloom and Economou.[10]

I would like to acknowledge conversations with R. L. Abrams and R. W. Hellwarth and lectures on Quantum Electronics by R. P. Feynman, given under the auspices of the Hughes Aircraft Company's Advanced Technical Education Program, all of which stimulated my interest in this problem. I thank J. F. Lam for helping check some of the calculations. This work was supported in part by DARPA (Order No. 3427), and was completed while I held a NRC Resident Research Associate.

1. A. Yariv and D. M. Pepper, Opt. Lett. 1, 16 (1977).

2. R. L. Abrams and R. C. Lind, Opt. Lett. 2, 94 (1978); 3, 205 (1978).

3. F. W. Bloch, Phys. Rev. 70, 460 (1946).

4. A. Yariv, Quantum Electronics, Second edition (Wiley, New York, 1975).

5. R. P. Feynman, F. L. Vernon and R. W. Hellwarth, J. Appl. Phys. 28, 49 (1957).

6. This procedure seems to be justifiable only when the lower of the two resonant states is the true ground state. I am indebted to M. Sargent for clarification of this point.

7. A. J. Palmer, "Radiatively Coooled Vapors as Media for Low Power Nonlinear Optics" (to be published).

8. R. P. Feynman, Phys. Rev. 76, 769 (1949).

9. B. D. Fried and S. D. Conte, The Plasma Dispersion Function (Academic Press, New York, 1961).

10. P. F. Liao, D. M. Bloom and N. P. Economou, Appl. Phys. Lett. 32, 813 (1978).

Figure Captions

Figure 1. Amplitude reduction factor $m(\gamma_1,\theta)$ versus angle (for homogeneously broadened system).

Figure 2. Interpolated reflectivity versus angle (normalized to $\theta=\delta=0$) for Doppler broadened system. $\gamma_1 \gamma_2 = 10^{-2}$.

Figure 3. Reflectivity lineshapes (Doppler broadened system) for various angles.

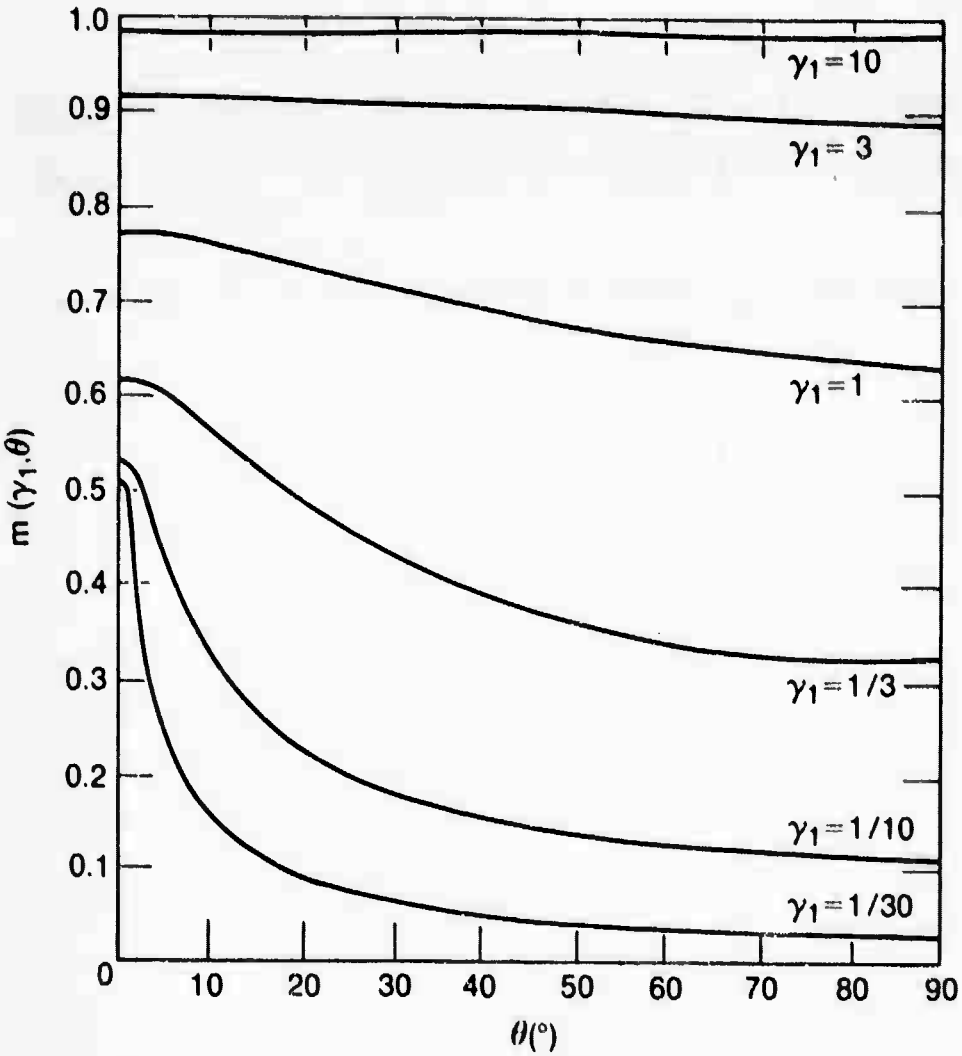

Figure 1. Amplitude reduction factor m (γ_1,θ) versus angle (for homogeneously broadened system).

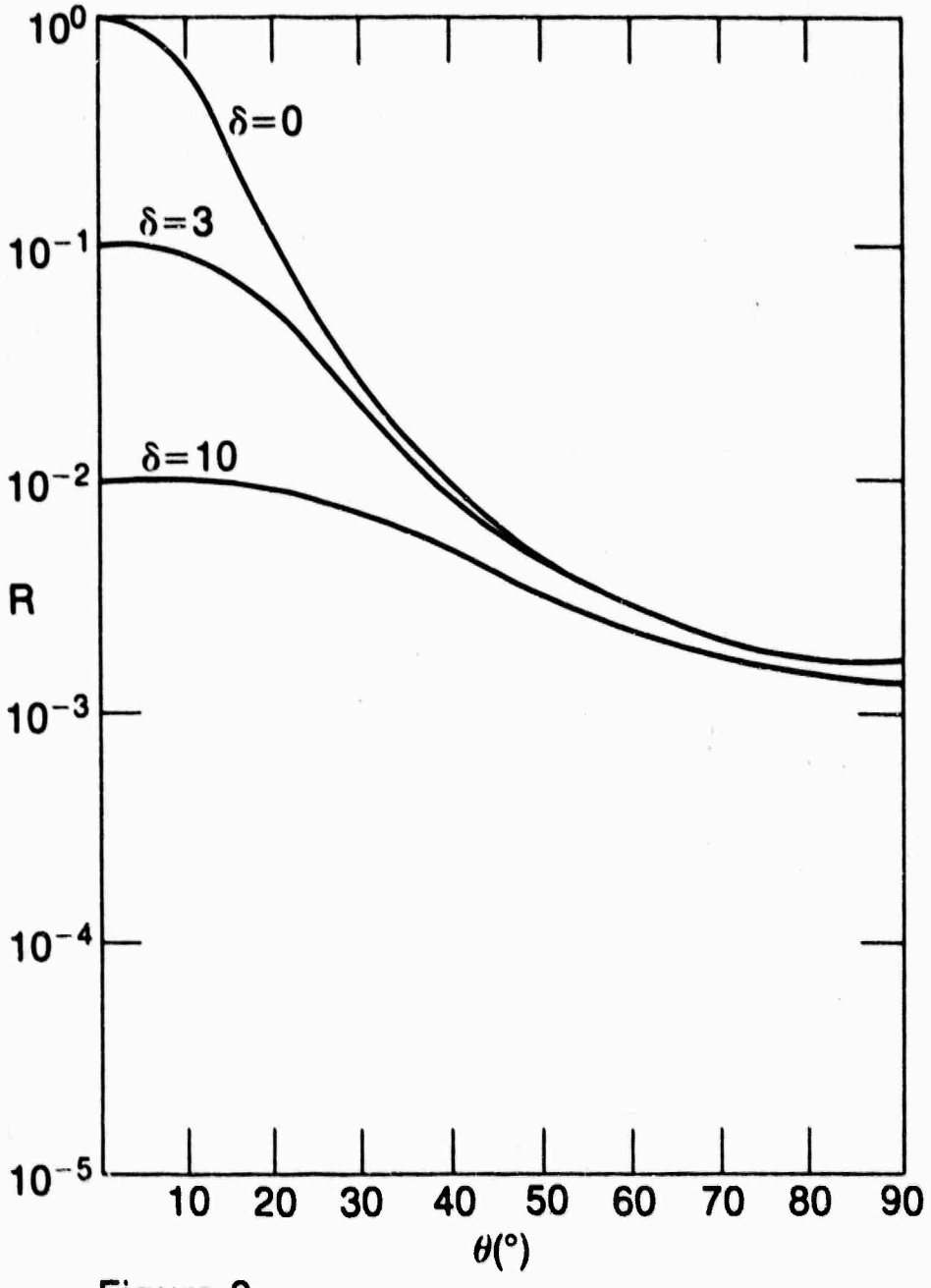

Figure 2

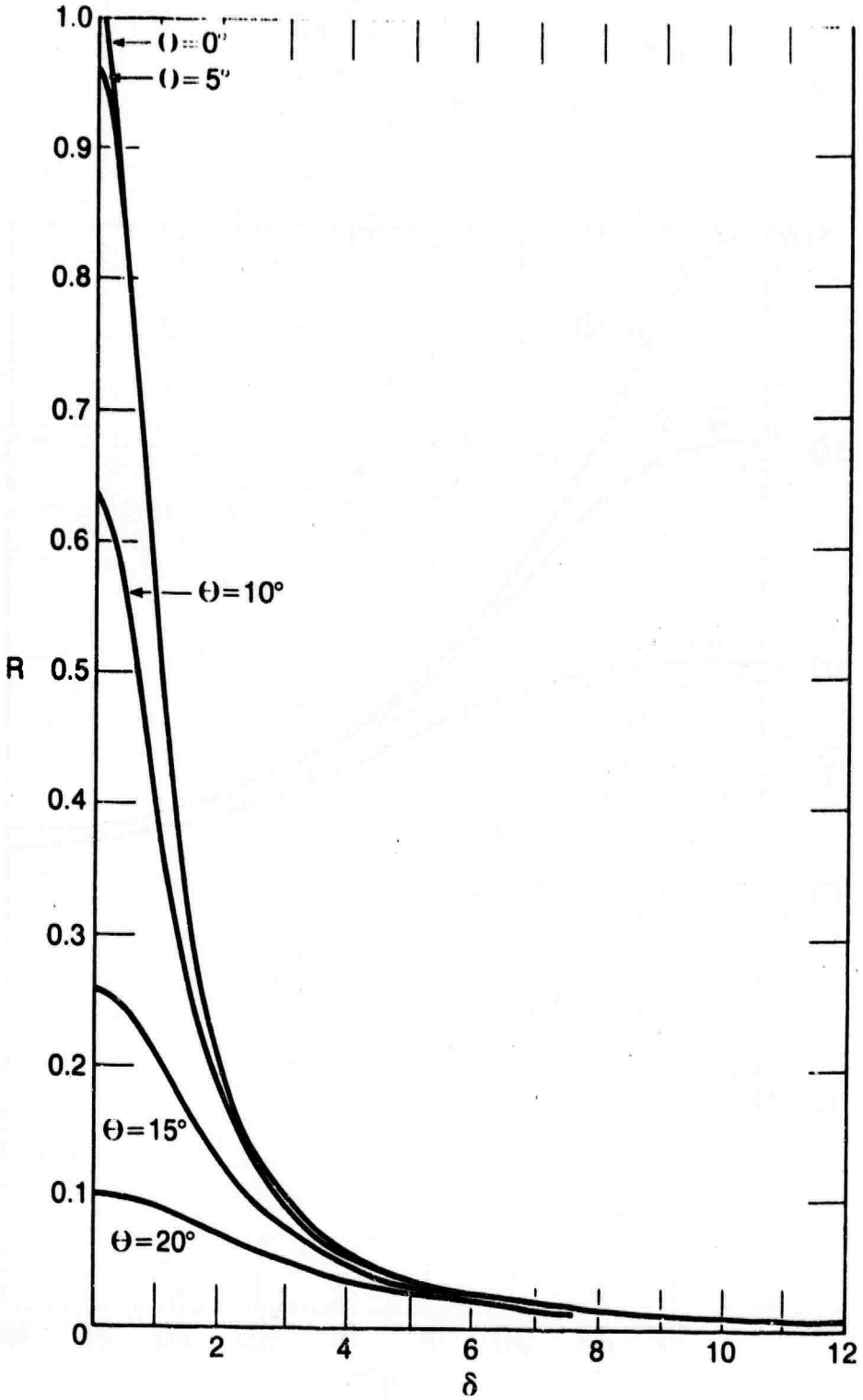

Figure 3. Reflectivity lineshapes (doppler broadened system) for various angles.

APPENDIX D

THE IMPACT OF ISOPLANATIC EFFECTS ON TARGET REFERENCING SYSTEMS AT VISIBLE WAVELENGTH*

In this class of problem the transmitted laser radiation is to be focused to a spot on the target. The reference information is from laser reflection off of a glint or highlight located at or near this spot. Specifically with orbiting targets, as illustrated in Figure D-1, the target emits or reflects a reference wave at position A on its orbital path and then moves to position B during the round trip propagation time. That is, it is required to point the transmitted laser beam along a path which intercepts the target at a point slightly ahead of its position at the time the laser energy leaves the transmitter aperture. Thus the laser must be fired ahead of the target in order to intercept it. For this application, the reference beam and the laser beam are essentially similar cones with axes inclined at the point-ahead angle defined by the angular distance between the positions A and B. For low orbits the required point-ahead angle is

$$\theta_p = \frac{2v_0}{c} \cos \phi, \tag{D.1}$$

where v_c is the orbital velocity (typically of the order 7 km/sec for low altitude satellites), c is the velocity of light and ϕ is the azimuthal angle. At zenith, a typical point-ahead angle is

$$\theta_p \sim \frac{2x7x10^3}{3x10^8} \sim 50 \text{ μrad.} \tag{D.2}$$

*The work described in this appendix was performed under IR&D and not in the course of the contract. It is included because of its relevance to atmospheric phase compensation with nonlinear phase conjugation.

In spite of the fact that a synchronous satellite remains essentially fixed at a given point above the surface of the earth, there is still a point-ahead requirement in this case also. The earth and the satellite rotate in unison at the rate of 2π radians per 24 hours. Thus, the reference (transmitter) aperture must be pointed at the position where the transmitter (target) aperture will have moved to during the time it takes the light to propagate through the intervening space. For synchronous orbits, the relation in Eq. D.1 remains valid if we replace the cosine factor by unity and use the value ΩR for the orbital velicity where Ω is the rotation of the earth and R is the altitude of the orbit. This yields

$$\theta_p = \frac{2\Omega R}{c}$$

$$= \frac{2X(2\pi/3600)\ X\ 4\ X\ 10^7}{3\ X\ 10^8}$$

$$= 20\ \mu rad. \qquad (D.3)$$

The conventional isoplanatic problem in which the reference and transmitter beams have similar geometries has been widely studied with two different approaches. The problem was first studied by Fried[6] using a Huygens-Fresnel type of calculation. Fried's theory requires the evaluation of some fairly complicated integrals which have been coded for numerical evaluation by personnel at the Air Force Weapons Laboratory (AFWL). Using the AFWL code, we have recently obtained results from the Fried theory for isoplanatic effects at 3.8 microns as a part of a ground-based beam control study presently being performed for the Air Force. In addition, we have modified our propagation and adaptive optics simulation software to allow us to model the isoplanatic problem without making the simplifying assumptions inherent in the Fried theory. In each of these approaches we have assumed an

index structure constant variation with altitude with a similar to the model proposed by Hufnagel[7] in 1974. It consists of the 1974 Hufnagel model plus an additional ground layer term which is used to adjust the strength of this layer. Hufnagel's model has the form

$$C_N^2 = 2.7[2.2(10^{2.3}h)^{10} \exp(-h)(\frac{v_w}{27})^2 + 10^{-16} \exp(-h/1.5)], \ m^{-2/3} \quad , \qquad (D.4)$$

where h is the altitude in km and v_w is the rms wind speed between 5 and 20 km. In our studies we have used three different values of v_w (15,27 and 40 m/sec).

Figure 3-2 shows a comparison of results obtained from the Hughes propagation code and from the Fried theory. These results apply to propagation at 3.8 microns and assume perfect adaptive optics; i.e., infinite temporal and spatial bandwidth. In these calculations we used the Hufnagel model given in Eq. D.4 (v_w = 40 m/sec) augmented by a ground layer of the form

$$(C_n^2)_{\text{ground}} = 10^{-14} \exp(-10h), \ m^{-2/3} \quad . \qquad (D.5)$$

The solid curve in Figure D-2 is the Fried theory result. The circles indicate the average result obtained from the propagation code and the bars indicate the variation observed about this average (recall, that the propagation code generates results for typical sample media from the ensemble of possible media and thus yields results which inherently fluctuate). The agreement between the results in this case is strikingly good, which implies that the assumptions inherent in the Field theory are valid under these conditions. Moreover, these results indicate that the isoplanatic effects at 3.8 microns, although bothersome, can probably be tolerated for the typical point-ahead angles cited in Eqs. D.2 and D.3.

In contrast to the relatively benign nature of the isoplanatic problem at 3.8 microns, the decrease in Strehl ratio caused by the point-ahead angles given in Eqs. D.2 and D.3 is quite significant at visible wavelengths. An indication of the severity of the isoplanatic problem at .5 microns is given in Figure D-3. These results were obtained from results given by Fried in his 1977 report. They are replotted from the data given in Figures 3a and 3b of that report and apply to two different structure constant profiles. One of these profiles is based on the data of Miller and Zieske[1] and the other on the data of Barletti.[2] As shown in Figure D-4, these two models are similar below an altitude of 5 km but differ significantly above that altitude. The Barletti model fits the Hufnagel model used in our 3.8 micron work reasonably well for a rms wind velocity of 27 m/sec. We believe that the Barletti data are probably more representative of the type of turbulence profile that will be encountered but this question must be explored experimentally to verify this conslusion. For either profile, however, the key conclusion is that the isoplanatic effects range from severe to overwhelming. In order to obtain a compensated Strehl ratio greater than .8, it will be necessary to limit the angle between the reference and transmitter beams to less than 2 microradians, if the Barletti data apply, and to less than 6 microradians if the more benign data of Miller and Zieske apply. To our knowledge, the only way to achieve this will be to use a reference which is located on a "stick" or on another satellite, which leads the relay satellite in orbit.

We would like to emphasize that the above conclusions relative to the magnitude of the isoplanatic effects at visible wavelengths are based entirely on results obtained from Fried's theory. We have not used the Hughes adaptive optics simulation to check these conclusions. Unfortunately, this software must be modified before we can obtain results pertinent to the extremely large transmitter apertures contemplated in the systems of interest.

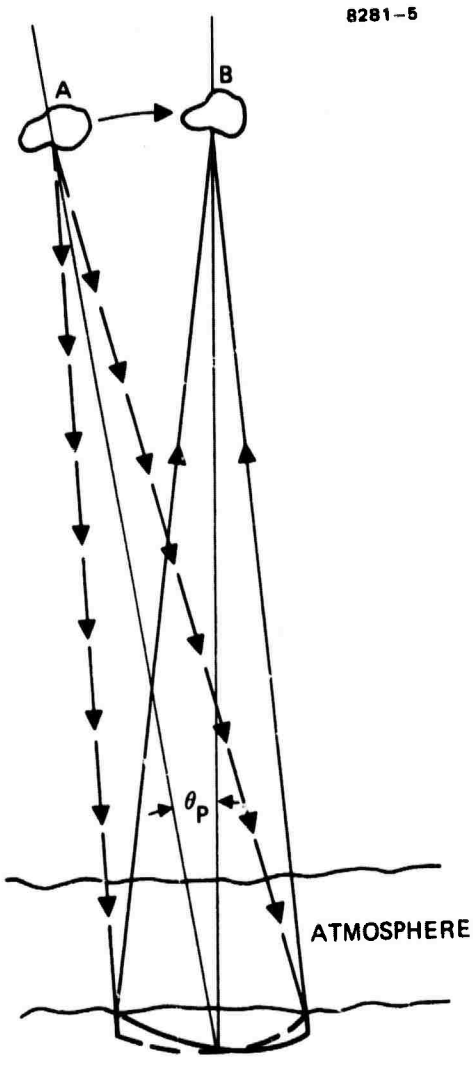

Figure D-1. The basic isoplanatic problem. The target emits or reflects a reference wave (dashed) at position A and moves ahead to position B during a round-trip propagation time.

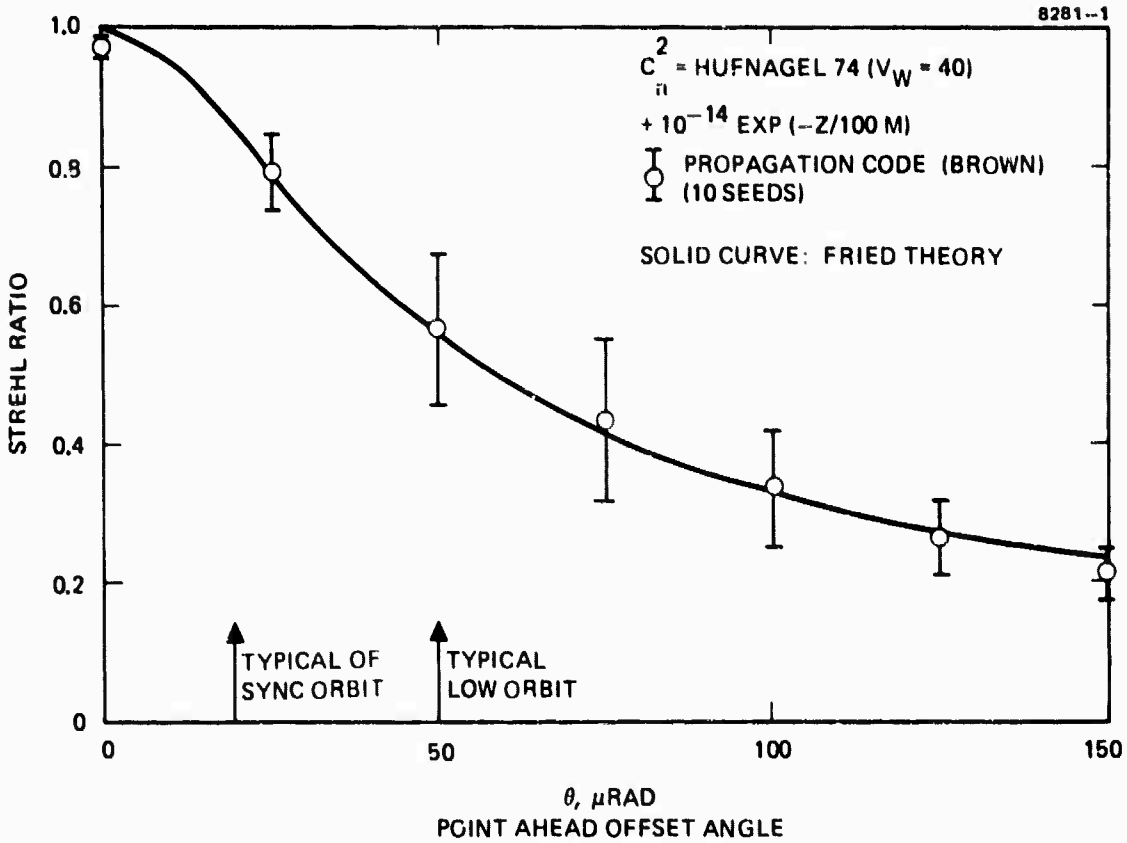

Figure D-2. The conventional isoplanatic degradation experienced at 3.8 μm with a 2.5 meter aperture. Comparison results obtained using two basically different classes of calculation are used to compute the strehl ratio associated with a given offset angle.

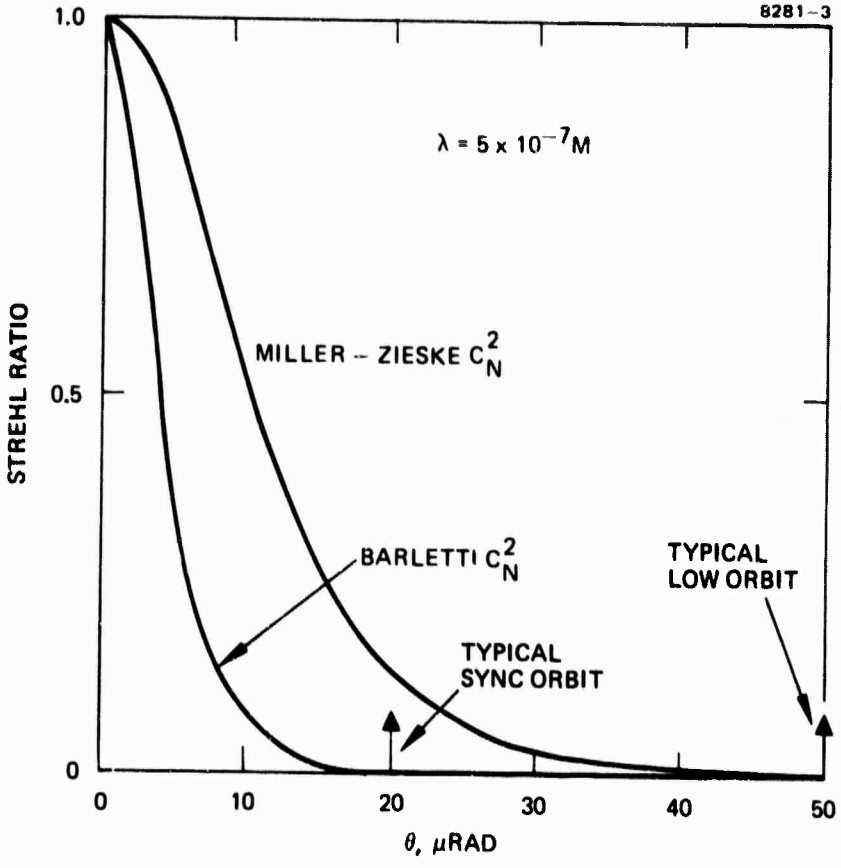

Figure D-3. The conventional isoplanatic degradation for λ = .5 μm for a 4.0 meter aperture after Fried with ideal adaptive optics.

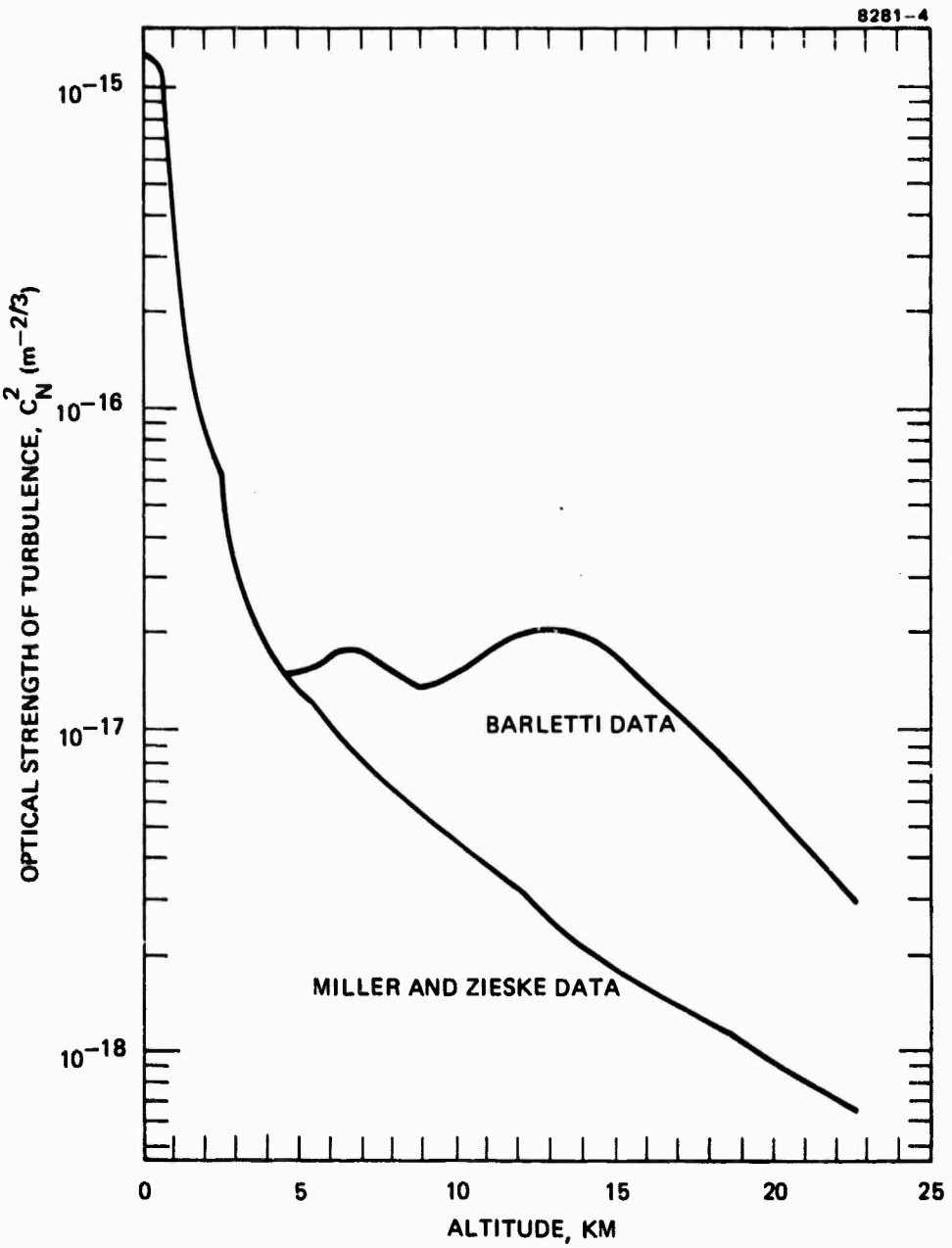

Figure D-4. Measurement of the vertical distribution of the optical strength of turbulence. The Barletti model was obtained by thermosonde baloon. The Miller & Zieske data only apply above 4 km.

APPENDIX E

DOPPLER AND POINT-AHEAD OVERRIDE TECHNIQUES IN FOUR-WAVE-MIXER PHASE CONJUGATION

For an orbiting retroreflector with orbital velocity v and line-of-sight angle* θ, as illustrated in Figure E-1(a), the required point-ahead angle, as seen at the conjugation subsystem, is†

$$\alpha_{pa} = \frac{\pm 2v}{c} M \cos \theta \quad , \tag{E-1}$$

whre M is the optical magnification** of the beam director (M will typically fall in the range $40 < M < 400$). The fractional Doppler shift is

$$\delta_D = \frac{2v}{c} \sin \theta \quad , \tag{E-2}$$

where v is the orbital tangential velocity, and C is the velocity of light. Clearly α_{pa} and δ_D differ only in scale (the M multiplier) and in their θ dependence. The raw ($M = 1$) point-ahead angle typically is in the range of 40 to 60 μrad.

The normal k-vector phase-matching relations are given in Figure E-1(b), while the k vector diagram for an equal frequency (degenerate) four-wave phase conjugator is illustrated in Figure E-1(c). Since the system is degenerate, the angle β between pumps and signal is arbitrary.

---

*For low orbits, θ is approximately the zenith angle.

†The sign ambiguity reflects the possibility that there may be one or more image inversions in the optical train. We can include a K mirror to invert the position of the conjugation beam relative to the input beam.

**For the "carrot-on-the-stick" approach, where full point-ahead compensation is not employed, the residual point-ahead/-behind compensation will be absorbed within the M factor.

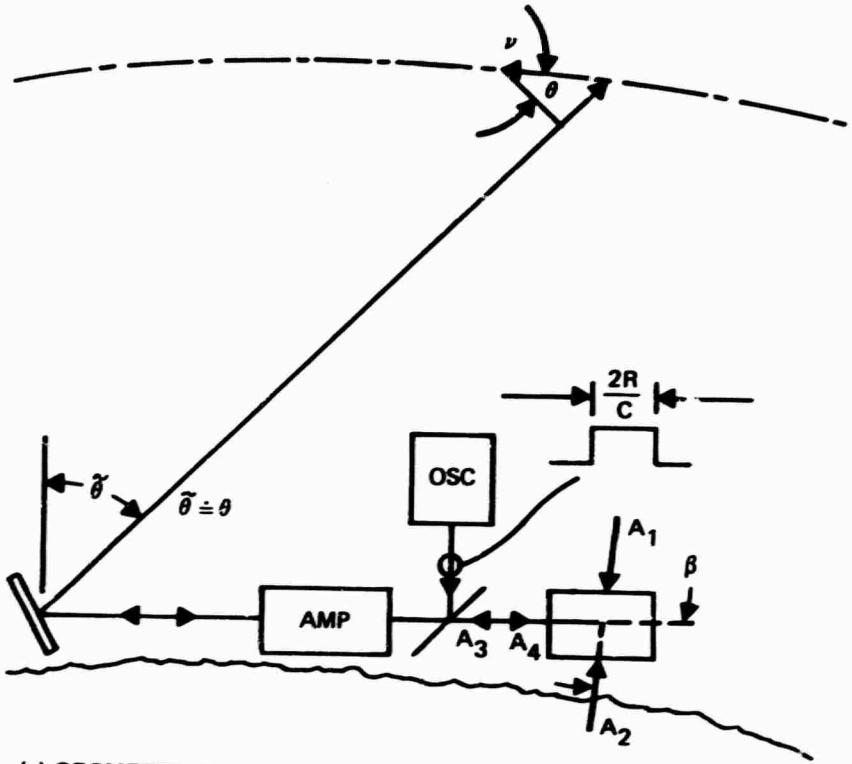

(a) GEOMETRY OF THE GROUND-BASED OSCILLATOR SYSTEM. THIS IS A CW SYSTEM WHICH ITERATES ON AN INITIAL OSCILLATOR INJECTED PULSE. M = 0 FOR THIS SYSTEM

(b) RELATIONSHIPS FOR PHASE CONJUGATION

$$\omega_1 + \omega_2 = \omega_3 + \omega_4$$

$$\overline{k_1} + \overline{k_2} = \overline{k_3} + \overline{k_4}$$

(c) NORMAL (DEGENERATE) PHASE CONJUGATION κ VECTOR DIAGRAM. THE ANGLE β IS ARBITRARY AND

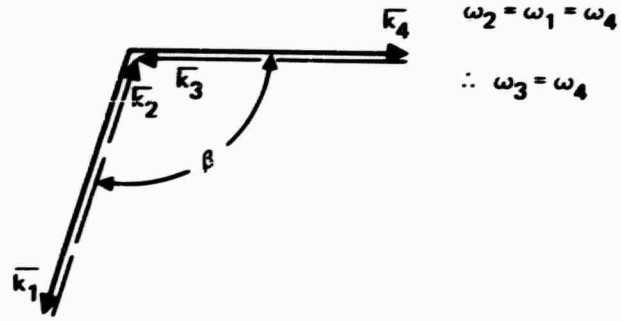

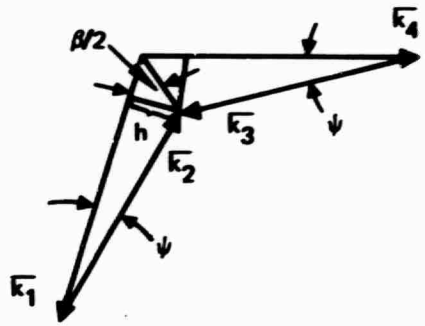

(d) DOPPLER AND POINT-AHEAD COMPENSATION, THE ANGLE β IS DETERMINED BY θ. ψ IS THE POINT-AHEAD ANGLE AND

$$\omega_2 = \omega_1 (1-\delta_{p2})$$

$$\omega_1 = \omega_4$$

$$\therefore \omega_3 = \omega_4 (1-\delta_{p2})$$

Figure E-1. Simultaneous Doppler and point-ahead compensation with a four-wave phase conjugator.

However, if the output must be shifted (slightly) in frequency to compensate δ_D above, the degeneracy is formally broken, and the angle β is not arbitrary.

Figure E-1(d) illustrates a k-matched system in which the frequency of pump A_2 is shifted upward by a small fraction δ_{p2}, causing a corresponding fractional shift in the conjugated output A_3 (the original frequencies are normalized to unity and the sizes of δ_{p2} and ψ are greatly exaggerated in the figure). For small δ and ψ, the geometry gives

$$h \doteq \psi \doteq \delta_{p2} \tan \frac{\beta}{2} \quad . \tag{E-3}$$

To compensate for Doppler and point-ahead simultaneously, we can let

$$\psi = \pm\alpha_{pa} \tag{E-4a}$$

$$\delta_{p2} = \delta_D \tag{E-4b}$$

Dividing Eq. E-4a by Eq. E-4b and substituting from Eqs. E-3, E-3, and E-1 gives

$$\tan \frac{\beta}{2} = \pm M \cot \theta \tag{E-5a}$$

or

$$\beta = \pi \pm 2 \tan^{-1} \left(\frac{\tan \theta}{M}\right). \tag{E-5b}$$

Typically, operating ranges of θ will fall in the range $-\pi/4 \leq \theta \leq \pi/4$; for typical M values ($40 < M < 400$), Eq. E-5b can be well approximated by

$$\beta \doteq \pi \pm \frac{2\theta}{M} \quad . \tag{E-5c}$$

With M = 1, even a modest range of $(-45 \leq \theta \leq 45°)$ requires a wide swing in pump orientation, and the pumps become nearly collinear with the input-output waves at $\theta = 0$ causing a separability problem. However, with modest magnifications (M = 40), the required swing in pump orientation is greatly reduced, although the separability problem remains.

At the overhead condition ($\theta = 90°$), point ahead is required but not Doppler compensation. However, a second-order fractional frequency shift δ_{p2} in pump A_2 is required to produce the desired point-ahead angle ψ. This shift is given to an excellent approximation (with an exact k vector match) as

$$\delta_{p2} = \frac{\psi^2}{2} = \frac{1}{2}\left(\frac{2v}{C} M\right)^2 . \qquad \text{(E-6)}$$

For $v = 7 \times 10^3$ km/sec, M = 40, and $\theta = 0$:

$$\delta_{p2} = \frac{1}{2}\left(\frac{7 \times 10^3 \times 40}{3 \times 10^8}\right)^2 = 4.4 \times 10^{-7} . \qquad \text{(E-7)}$$

At a wavelength of 3 μm, for example, this corresponds to only a modest frequency shift in pump 2 of about 44 MHz. Another possible approach for this overhead regime (which avoids the frequency shift requirement* entirely) is to let

$$\bar{k}_2 = \bar{k}_4 \qquad \text{(E-8a)}$$

$$\bar{k}_1 = \bar{k}_3 , \qquad \text{(E-8b)}$$

as illustrated in Figure E-2.

*Actually, this is only a formal requirement. Practically speaking, the k vector mismatch resulting from no frequency shift in tolerable.

Up to this point, we have assumed that the probe wavefront A_4 is a plane wave. Of course, for applications of real interest, it is not. How does the tilt/frequency offset affect the phase conjugation process? As shown below, we effectively repoint the conjugated wavefront much as a tilt mirror would do.

For purposes of analysis, we have defined the somewhat simplified system illustrated in Figure E-3 in which the return wave front is essentially propagating in the negative z direction and has picked up a phase distortion $\phi(x,y)$ from a phase screen reasonably near the primary optics. Thus, we assume the incident field through the collecting aperture to be*

$$U_4 = A_4 F(x,y)\, e^{i\phi(x,y)}\, e^{i(-k_z z-\omega_4 t)}, \qquad \text{(E-9)}$$

where $F(x,y)$ is the collecting aperture. After demagnification, the incident field on the conjugator is approximately

$$U_4' = A_4'\, e^{i\phi(Mx,My)}\, e^{i(-k_z z-\omega_4 t)}, \qquad \text{(E-10a)}$$

where

$$A_4' = MF(Mx,My)A_4 \qquad \text{(E-10b)}$$

and where we have assumed that the propagation-diffraction effects through the telescope are minor. The pump waves are assumed to be plane waves:

*It will be understood that the real fields are the real parts of the given expressions.

7757-22R1

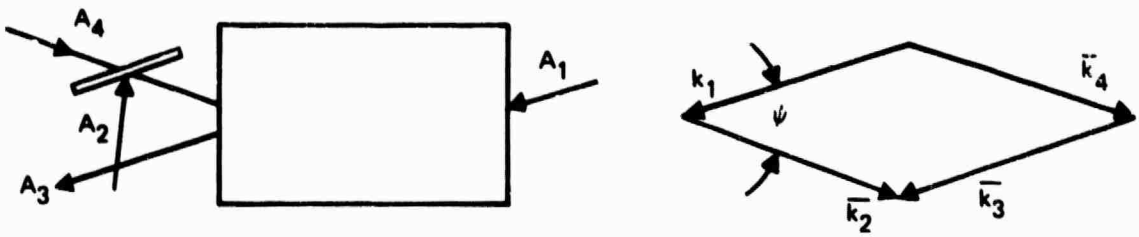

Figure E-2. Point-ahead and κ vector matching without a requirement for pump frequency perturbations.

7757-23

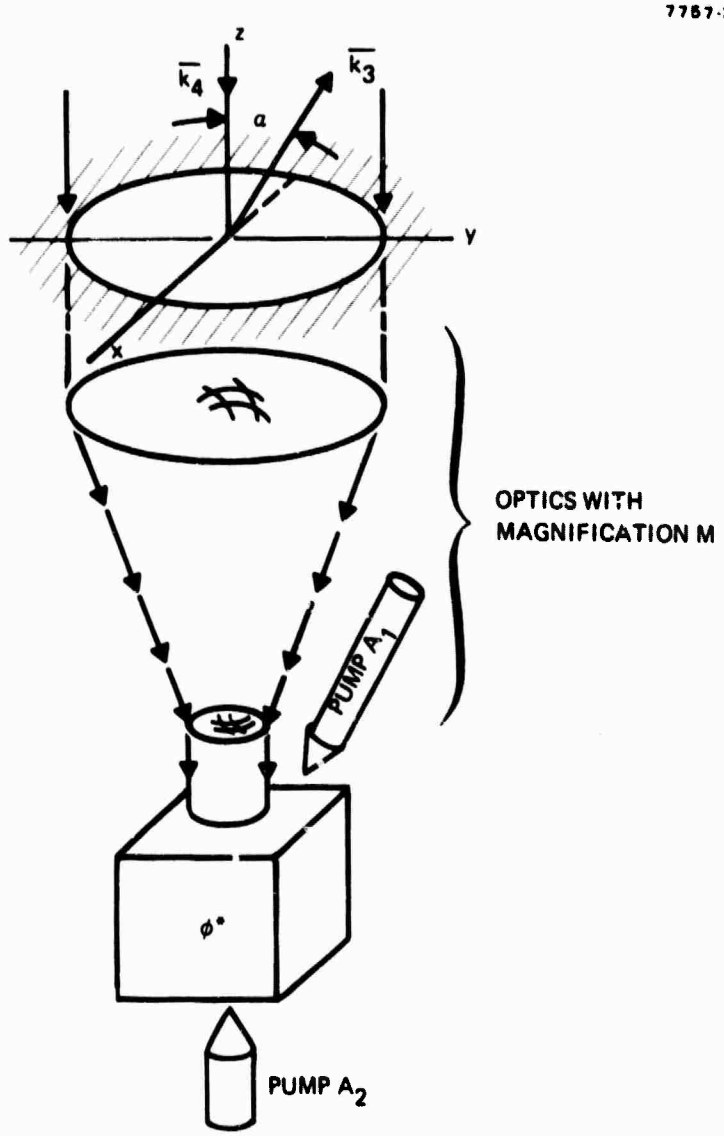

Figure E-3. Geometry and coordinate system for analysis of the perturbed system.

$$U_1 = A_1 e^{i(\bar{k}_1 \cdot \bar{r} - \omega_1 t)} \qquad \text{(E-11)}$$

$$U_2 = A_2 e^{i(\bar{k}_2 \cdot \bar{r} - \omega_3 t)} \qquad \text{(E-12)}$$

The nonlinear outputs of present interest result from the third order expansion in the total field:

$$U_o = C\,(U_1 + U_2 + U_4 + \text{c.c.})^3 \quad , \qquad \text{(E-13)}$$

where c.c. represents the complex conjugate, and C is a conversion efficiency parameter. In particular, the conjugated output of interest will be a component called U_3':

$$U_3' = C[U_4 * U_2 U_1 + \text{c.c.}]$$

$$= CA_1 A_4 A_4' \exp[-i\phi(Mx,My)] \exp i[\bar{k}_3 \cdot \bar{r} - \omega_e t] \quad , \qquad \text{(E-14a)}$$

where

$$\bar{k}_3 = \bar{k}_1 + \bar{k}_2 - \bar{k}_4 \qquad \text{(E-14b)}$$

and

$$\bar{k}_4 = k_z \cdot \bar{a}_z \qquad \text{(E-14b)}$$

$$\omega_3 = \omega_2 + \omega_1 - \omega_4 \qquad \text{(E-14c)}$$

and where $\bar{a}_z$ is a unit vector in the z direction. In the offset designs, we have arranged that $\bar{\kappa}_3$ be offset from $\bar{\kappa}_4$ by $\pi - \psi$ such that

$$\bar{\kappa}_3 \cdot \bar{r} = z\kappa_z (1 - \delta) \cos \psi + y\kappa_z (1 - \delta) \sin \psi \ . \qquad \text{(E-15a)}$$

Further, it has been proposed that the frequency of pump one equal that of the return wavefront and that the frequency of pump two be perturbed from the return wavefront such that

$$\omega_1 = \omega_4 \qquad \text{(E-15b)}$$

and

$$\omega_2 = \omega_4 (1 - \delta) \qquad \text{(E-15c)}$$

giving

$$\omega_3 = \omega_4 (1 - \delta) \ . \qquad \text{(E-15d)}$$

Under these circumstances, it follows that

$$U_3' = CA_1A_2A_4' \exp [-i\phi(Mx,My)] \exp i[z\kappa_z \cos \psi + y\kappa_z \sin \psi - \omega_4 t](1-\delta). \text{(D-16)}$$

This is, to a first approximation, a pseudo plane wavefront of frequency ω_4 propagating at a small offset angle ψ from the z axis and having superimposed on it the demagnified wavefront error. We assume that the reverse propagation distances to the primary are relatively short such that his field propagates like a plane wave to the main aperture, retaining its phase distortions. However, the demagnifications are stripped off, giving an aperture field at $z = z_a$ which is

$$U_3 = C_1A_1A_2A_4F(x,y) \exp [-i\phi(x,y)] \exp i[\phi_a + \frac{y}{M}\kappa_z \sin \psi - \omega_4 t](1-\delta) \ , \ \text{(E-17a)}$$

where ϕ_a, a constant of no importance here, is

$$\phi_a = D\kappa_z \cos \psi \ . \tag{E-17b}$$

The U_3 field is effectively an aperture excitation field which reradiates at the off-axis angle

$$\alpha = \alpha_{pa} = \frac{\sin \psi}{M} \doteq \frac{\psi}{M}. \tag{E-18}$$

However, this tilted wavefront reradiates with the wavefront error distribution $-\phi(x,y)$ superimposed on it. Functionally, the resulting radiating source could be replaced with a thin phase screen $[-\phi(x,y)]$ in front of the aperture. Small changes in the exit angle by which the exit wave passes through this screen do not change its effect on the radiating field. Thus, for small angles ψ, the radiated fields are equivalent to what the reradiated (conjugated) wavefront would have been without the pump perturbations, except that the entire radiation pattern is tiled by an angle α_{pa}, and the reradiated frequency ω_4 is changed with a fractional decrease δ.

Of course, if the offset angle is appreciable, an isoplanatic problem exists, as discussed in Appendix D. If the frequency offset is too great, large optical path differences may not be well compensated.